

Sensitivity analysis–guided model reduction of a mathematical model of pembrolizumab therapy for de novo metastatic MSI-H/dMMR colorectal cancer

Georgio Hawi^{1, *}, Peter S. Kim^{1, †}, and Peter P. Lee^{2, †}

¹School of Mathematics and Statistics, University of Sydney, Sydney, Australia

²Department of Immuno-Oncology, Beckman Research Institute, City of Hope, Duarte, California, USA

*Corresponding author: georgio.hawi@sydney.edu.au

[†]These authors contributed comparably to this work

Abstract

Colorectal cancer (CRC) is the third most commonly diagnosed cancer worldwide and the leading cause of cancer-related deaths in adults under 55, involving a complex interplay of biological processes such as dendritic cell (DC) maturation and migration, T cell activation and proliferation, cytokine production, and T cell and natural killer (NK) cell-mediated cancer cell killing. Microsatellite instability-high (MSI-H) CRC and deficient mismatch repair (dMMR) CRC constitute 15% of all CRC, and 4% of metastatic CRC, and exhibit remarkable responsiveness to immunotherapy, especially with PD-1 inhibitors such as pembrolizumab. Mathematical models of the underlying immunobiology and the interactions underpinning immune checkpoint blockade offer mechanistic insights into tumour–immune dynamics and provide avenues for treatment optimisation and the identification of novel therapeutic targets. We used our data-driven model of de novo metastatic MSI-H/dMMR CRC (dnmMCRC) and performed sensitivity analysis–guided model reduction using the FAST and EFAST methods. In this work, we constructed two simplified models of dnmMCRC: one that faithfully reproduces all of the original model’s trajectories, and a second, minimal model that accurately replicates the original dynamics while being highly extensible for future inclusion of additional components to explore various aspects of the anti-tumour immune response.

Keywords: sensitivity analysis, model reduction, de novo metastatic MSI-H/dMMR colorectal cancer, pembrolizumab, delay integro-differential equations, mechanistic model.

1 Introduction

Colorectal cancer (CRC) is the third most common cancer worldwide, with more than 1.85 million cases and 850,000 deaths annually [1]. Despite CRC being diagnosed mostly in adults 65 and older, there has been an increase in the incidence rate of CRC amongst younger populations [2–4] since the mid-1990s, with CRC being the leading cause of cancer-related deaths in adults under 55 [4]. In the United States, the 5-year survival rates for stage IIIA, stage IIIB, and Stage IIIC colon cancer are

90%, 72%, and 53%, respectively, whilst stage IV CRC has a 5-year survival of only 12% [5]. Of new CRC diagnoses, 20% of patients present with de novo metastatic disease, with an estimated 75%–90% of these patients presenting with unresectable metastatic lesions [6]. However, patients with the hypermutant microsatellite instability-high (MSI-H) or deficient mismatch repair (dMMR) phenotype, hereby referred to as the MSI-H/dMMR phenotype, who have reached metastasis are less responsive to conventional chemotherapy and have a poorer prognosis compared to patients with microsatellite stable (MSS) CRC [7].

That being said, patients with MSI-H/dMMR CRC have a much better prognosis with immunotherapy, in particular with immune checkpoint inhibitors (ICIs). Immune checkpoints, such as programmed cell death-1 (PD-1), normally downregulate immune responses after antigen activation [8]. PD-1, a cell membrane receptor that is expressed on a variety of cell types, including activated T cells, activated B cells and monocytes, has been extensively researched in the context of cancer such as MSI-H/dMMR CRC [9, 10]. When PD-1 interacts with its ligands (PD-L1 and PD-L2), effector T cell activity is inhibited, resulting in the downregulation of pro-inflammatory cytokine secretion and the upregulation of immunosuppressive regulatory T cells (Tregs) [11, 12]. Cancers can exploit this by expressing PD-L1 themselves, evading immunosurveillance, and impairing the proliferation and activity of cytotoxic T lymphocytes (CTLs) [13]. Blockade of PD-1/PD-L1 complex formation reinvigorates effector T cell activity, resulting in enhanced anti-tumour immunity and responses, leading to improved clinical outcomes in cancer patients [14, 15]. In particular, we refer to the FDA-approved regimen for the first-line treatment of metastatic MSI-H/dMMR CRC (mMCRC) in adults—200 mg of pembrolizumab, an anti-PD-1 antibody, administered by intravenous infusion over 30 minutes every 3 weeks until disease progression or unacceptable toxicity [16]—as the standard regimen for the remainder of this work.

Mathematical models provide a powerful framework for analysing the immunobiology underpinning diseases, which can then be used to investigate the dynamics of relevant biological components—improving theoretical understanding—especially when approached from a mechanistic perspective. Additionally, such modelling provides avenues for comparing and optimising treatment regimens, whilst avoiding the significant time and financial costs associated with human clinical trials. However, to effectively model complex biological systems, one must master the balance between model complexity and model accuracy. Traditional models incorporate multiple biological processes and usually result in models containing many input variables and model parameters [17]. In addition to the challenge of properly estimating and calibrating these parameters, one must also consider the resources and computational costs needed to repeatedly run the model [18]. As such, it is ideal to reduce models such that their key dynamics are maintained, but parameters and inputs with minimal influence on the outputs are identified and appropriately removed. There are numerous ways to do this reduction, including multiple timescale methods [19], singular value decomposition [20], and sensitivity analysis (SA).

SA aims to determine the robustness of a system to fluctuations in its input variables, and can be used to eliminate the least significant components in a model [21]. One can classify SA techniques into two categories: local and global. Local SA concerns slightly perturbing a model’s parameters in a predetermined region in parameter space and exploring the model outputs. As such, the results attained by local SA are only valid in a small neighbourhood of the perturbed region [22]. The main drawback of local SA is its inapplicability to nonlinear models, as it fails to consider interaction effects between variables, resulting in an underestimation of variables’ true significance [23]. Nonetheless, due to their transparency, ease of understanding and computational speed, local SA methods such as the partial rank correlation coefficient (PRCC) [24], and derivative-based local methods have been widely used in analysing the sensitivity of parameters in mathematical models of CRC and ICI therapy

[25–30]. On the other hand, global SA methods allow for exploration of the entire parameter space and can examine the effects of large changes of model inputs on the model output - even in non-linear models [31]. Whilst being computationally intensive, these methods account for higher-order interactions between variables, unlike local SA methods. There exist many types of global SA methods, such as the elementary effects methods [18, 32], high-dimensional model representation [33], and metamodel-based analyses [34]. We focus on variance-based SA, which features model-independent methods that have been used to analyse models in immunology, biophysics, and engineering [23, 35–37].

In this work, we consider our two-compartmental model of pembrolizumab therapy in de novo metastatic MSI-H/dMMR CRC (dnmMCRC) [38], which, to the authors’ knowledge, is the only immunobiological model of ICI therapy in metastatic CRC, and extends [39] to the metastatic setting. We perform global variance-based SA on this model to evaluate the sensitivity of individual parameters to the model and use this to guide model reduction and facilitate the development of two simplified models: one that faithfully replicates all model trajectories, and a minimal model that accurately replicates trajectories of its state variables.

2 Variance-Based Sensitivity Analysis Background

It is prudent for us to detail the mathematical background for variance-based sensitivity analysis, beginning with the Sobol’ method. The rationale behind the Sobol’ method, and variance-based sensitivity analysis in general, is to quantify the impact of each input parameter of a model on the total variance of its output [40]. For simplicity, we consider a model $Y = f(\mathbf{X})$, where Y is a scalar and $\mathbf{X} = (X_1, X_2, \dots, X_n)$ are the n model input parameters. Via rescaling and appropriate transformations, we can consider each X_i as a random variable to be independently and uniformly distributed on $[0, 1]$. Furthermore, we assume that $f \in L^2([0, 1]^n)$. The key idea is that $f(\mathbf{X})$ can be uniquely decomposed via an Sobol-Hoeffding decomposition [41, 42] given by

$$f(\mathbf{X}) = f_0 + \sum_{i=1}^n f_i(X_i) + \sum_{i=1}^n \sum_{j=1}^{i-1} f_{ij}(X_i, X_j) + \dots + f_{1,2,\dots,n}(X_1, X_2, \dots, X_n), \quad (2.1)$$

where

$$f_0 = \mathbb{E}[f(\mathbf{X})] = \int_{[0,1]^n} f(\mathbf{X}) \, d\mathbf{X}, \quad (2.2)$$

$$f_i(X_i) = \mathbb{E}[f(\mathbf{X})|X_i] - f_0 = \int_{[0,1]^{n-1}} f(\mathbf{X}) \prod_{\substack{k=1 \\ k \neq i}}^n dX_k - f_0, \quad (2.3)$$

$$f_{ij}(X_i, X_j) = \mathbb{E}[f(\mathbf{X})|X_i, X_j] - f_0 - f_i - f_j = \int_{[0,1]^{n-2}} f(\mathbf{X}) \prod_{\substack{k=1 \\ k \neq i,j}}^n dX_k - f_0 - f_i - f_j, \quad (2.4)$$

and so forth. From this, it is easy to see that f_i represents the effect of varying just X_i , denoted the main effect of X_i , f_{ij} represents the effect of varying X_i and X_j simultaneously, etc. We note that this decomposition is only unique when all terms in (2.1) are orthogonal, i.e.

$$\mathbb{E}[f_I(X_I)|X_J] = 0. \quad (2.5)$$

for all $I \subseteq \{1, 2, \dots, n\}$ and all $J \subseteq \{1, 2, \dots, n\}$ where $J \cap I = \{\emptyset\}$. If $I = \{i_1, \dots, i_s\}$ for $i_1, \dots, i_s \in \{1, 2, \dots, n\}$, then we define X_I as the set $\{X_{i_1}, \dots, X_{i_s}\}$ and f_I as f_{i_1, \dots, i_s} and analogously for X_J . Squaring (2.1) and integrating, with multiple applications of the orthogonality condition, render

$$\int_{[0,1]^n} f^2(\mathbf{X}) \, d\mathbf{X} - f_0^2 = \sum_{s=1}^n \sum_{i_1 < \dots < i_s} f_{i_1 \dots i_s}^2(X_{i_1}, X_{i_2}, \dots, X_{i_s}). \quad (2.6)$$

By definition, the left-hand side of (2.6) is $\text{Var}(Y) = \text{Var}(f(\mathbf{X}))$ and the right-hand side is a sum of partial variances over all subsets of $\{X_1, X_2, \dots, X_n\}$. Thus, this leads to the ANOVA decomposition

$$\text{Var}(f(\mathbf{X})) = \sum_{i=1}^n V_i + \sum_{i=1}^n \sum_{j=1}^{i-1} V_{ij} + \dots V_{12\dots n}, \quad (2.7)$$

where

$$V_I = \int_{[0,1]^{|I|}} f_I^2(X_I) \prod_{k=1}^{|I|} dX_{I_k}, \quad (2.8)$$

for all $I \subseteq \{1, 2, \dots, n\}$. We consider the first-order sensitivity index, S_i , as the main contribution of a single parameter to the output variance, neglecting interactions with other input parameters. This is given by [41]

$$S_i = \frac{V_i}{\text{Var}(Y)}. \quad (2.9)$$

In addition to S_i being a way to measure the importance of X_i via determining the sensitivity of the model output to X_i , it also represents the expected percentage reduction in $\text{Var}(Y)$ when X_i has zero uncertainty [40, 43]. Second-order sensitivity indices incorporate the main and second-order contributions - the extent of $\text{Var}(Y)$ due to two input parameters that cannot be explained by the individual effects of the parameters alone and are given by

$$S_{ij} = \frac{V_{ij}}{\text{Var}(Y)}. \quad (2.10)$$

This notion continues for higher-order indices and is similarly notated. By (2.7), one has that

$$\sum_{i=1}^n S_i + \sum_{i=1}^n \sum_{j=1}^{i-1} S_{ij} + \dots S_{12\dots n} = 1. \quad (2.11)$$

One particularly useful index is the total-order sensitivity index for an input parameter, S_{Ti} , which is the proportion of the total output variance that is caused by an input variable and its interactions with any of the other input variables [44]. One can express this as

$$S_{Ti} = S_i + \sum_{\substack{j=1 \\ j \neq i}}^n S_{ij} + \dots + S_{1\dots i\dots n}. \quad (2.12)$$

We note that the sum of all the total-order indices is greater than or equal to 1, with equality if and only if the model is purely additive. Since each sensitivity index must clearly be non-negative, it is

easy to see that the closer an index is to 1, the more important the corresponding variables are to the model output and vice versa.

Whilst calculating each S_i only involves n integrals, to calculate all sensitivity indices (including the total-order indices), one needs $\sum_{k=0}^n \binom{n}{k} = 2^n$ integral evaluations. For low-dimensional models, this does not pose an issue, but for larger ones, this is computationally expensive.

To remedy this, one can calculate the first-order Sobol' indices via optimisations such as Fourier amplitude sensitivity testing (FAST) [45, 46]. As before, we consider the model $Y = f(\mathbf{X})$, where, after the necessary transformations, we can consider \mathbf{X} as a random variable independently and uniformly distributed on the n -dimensional unit cube, $[0, 1]^n$. Since the complex exponentials of multidimensional Fourier series form an orthonormal basis, there exist unique C_{k_1, k_2, \dots, k_n} such that $f(\mathbf{X})$ can be represented as

$$f(\mathbf{X}) = \sum_{k_1=-\infty}^{\infty} \sum_{k_2=-\infty}^{\infty} \dots \sum_{k_n=-\infty}^{\infty} C_{k_1 k_2 \dots k_n} \exp[2\pi i (k_1 X_1 + k_2 X_2 + \dots + k_n X_n)], \quad (2.13)$$

where the Fourier coefficients $C_{k_1 k_2 \dots k_n}$ are given by

$$C_{k_1 k_2 \dots k_n} = \int_{[0,1]^n} f(\mathbf{X}) \exp[-2\pi i (k_1 X_1 + k_2 X_2 + \dots + k_n X_n)] d\mathbf{X}. \quad (2.14)$$

This immediately gives the decomposition in (2.1), where

$$\begin{aligned} f_0 &= C_{00\dots 0}, \\ f_i(X_i) &= \sum_{\substack{k_i=-\infty \\ k_i \neq 0}}^{k_i=\infty} C_{0\dots k_i \dots 0} \exp[2\pi i (k_i X_i)], \\ f_{ij}(X_i, X_j) &= \sum_{\substack{k_i=-\infty \\ k_i \neq 0}}^{k_i=\infty} \sum_{\substack{k_j=-\infty \\ k_j \neq 0}}^{k_j=\infty} C_{0\dots k_i \dots k_j \dots 0} \exp[2\pi i (k_i X_i + k_j X_j)], \end{aligned}$$

and so forth. We thus see that

$$V_i = \int_0^1 f_i^2(X_i) dX_i = \sum_{\substack{k_i=-\infty \\ k_i \neq 0}}^{k_i=\infty} |C_{0\dots k_i \dots 0}|^2 = 2 \sum_{k_i=1}^{\infty} (A_{k_i}^2 + B_{k_i}^2), \quad (2.15)$$

where A_{k_i} , and B_{k_i} are the Fourier cosine and sine coefficients, respectively, given by

$$A_{k_i} = \int_{[0,1]^n} f(\mathbf{X}) \cos(2\pi k_i X_i) d\mathbf{X}, \quad B_{k_i} = \int_{[0,1]^n} f(\mathbf{X}) \sin(2\pi k_i X_i) d\mathbf{X}, \quad (2.16)$$

where we have used Parseval's identity. We immediately see a major problem - the computation of the Fourier coefficients requires an infinite number of multi-dimensional integrals to be calculated, which

is very computationally expensive. To remedy this, we consider the set of transformations

$$X_i(s) = \frac{1}{2} + \frac{1}{\pi} \arcsin(\sin(\omega_i s)), \quad (2.17)$$

from [47], where s is a new independent variable. The key idea is to choose the set of frequencies $\{\omega_i\}$ such that the n -dimensional Fourier integrals are converted to 1-dimensional integrals with respect to s [40]. If $\{\omega_i\}$ are chosen to be incommensurate, so that each ω_i cannot be expressed as a linear combination of the other frequencies with integer coefficients, then as s varies from $-\infty$ to ∞ , $\mathbf{X}(s) = (X_1(s), X_2(s), \dots, X_n(s))$ passes through every point in $[0, 1]^n$. As such, the curve is space-filling, and by Weyl's ergodic theorem [48] we can replace the n -dimensional integrals with the appropriate 1-dimensional counterparts. For example, we have that

$$\mathbb{E}[f(\mathbf{X})] = \lim_{T \rightarrow \infty} \frac{1}{2T} \int_{-T}^T f(\mathbf{X}(s)) ds, \quad (2.18)$$

$$A_{k_i} = \lim_{T \rightarrow \infty} \frac{1}{2T} \int_{-T}^T f(\mathbf{X}(s)) \cos(2\pi k_i X_i(s)) ds, \quad (2.19)$$

$$B_{k_i} = \lim_{T \rightarrow \infty} \frac{1}{2T} \int_{-T}^T f(\mathbf{X}(s)) \sin(2\pi k_i X_i(s)) ds, \quad (2.20)$$

and similarly for other integrals. Recalling that

$$\text{Var}(f(\mathbf{X})) = \mathbb{E}[f(\mathbf{X})^2] - \mathbb{E}[f(\mathbf{X})]^2, \quad (2.21)$$

in conjunction with (2.9), (2.15), (2.18), (2.19), and (2.20) gives a means to calculate the first-order sensitivity indices.

However, it is obvious that at most one of the ω_i can be rational, whilst the others must be irrational. Due to the finite precision of computers, irrational numbers cannot be stored exactly on computers, and so $\{\omega_i\}$ can only be incommensurate up to some level of precision. Thus, the resultant search curve is not truly space-filling, and a rational approximation of $\{\omega_i\}$ is needed. Without loss of generality, one can assume that each frequency is integral, and choose $\{\omega_i\}$ to be incommensurate to the order M , so that each ω_i cannot be expressed as a linear combination of the other frequencies with integer coefficients when the sums of the absolute values of those coefficients are less than or equal to $M + 1$. M is known as the interference number [45], and is usually set to 4 or higher [47], with $\{\omega_i\}$ becoming exactly incommensurate as $M \rightarrow \infty$. Since $\{\omega_i\}$ is not truly incommensurate for finite M , there exists some positive rational number T , such that $f(\mathbf{X}(s)) = f(\mathbf{X}(s+T))$. In the case of integral ω_i , it was shown in [45] that $T = 2\pi$, and so we can approximate the improper integrals using proper ones. Thus, if we consider $f(\mathbf{X}(s))$ for $s \in [-\pi, \pi]$, we have that (2.19), (2.20), and (2.21) become

$$A_{k_i} \approx \frac{1}{2\pi} \int_{-\pi}^{\pi} f(\mathbf{X}(s)) \cos(2\pi k_i X_i(s)) ds, \quad (2.22)$$

$$B_{k_i} \approx \frac{1}{2\pi} \int_{-\pi}^{\pi} f(\mathbf{X}(s)) \sin(2\pi k_i X_i(s)) ds, \quad (2.23)$$

$$\text{Var}(f(\mathbf{X})) \approx \frac{1}{2\pi} \int_{-\pi}^{\pi} f^2(\mathbf{X}(s)) ds - \left(\frac{1}{2\pi} \int_{-\pi}^{\pi} f(\mathbf{X}(s)) ds \right)^2. \quad (2.24)$$

If we express $f(\mathbf{X}(s))$ as a 1-dimensional Fourier series in s , via the expansion

$$f(\mathbf{X}(s)) = \sum_{k=-\infty}^{\infty} (A_k \cos(ks) + B_k \sin(ks)), \quad (2.25)$$

then by Parseval's identity, we have that

$$\text{Var}(f(\mathbf{X})) \approx 2 \sum_{k=1}^{\infty} (A_k^2 + B_k^2), \quad (2.26)$$

where

$$A_k = \frac{1}{2\pi} \int_{-\pi}^{\pi} f(\mathbf{X}(s)) \cos(ks) \, ds, \quad B_k = \frac{1}{2\pi} \int_{-\pi}^{\pi} f(\mathbf{X}(s)) \sin(ks) \, ds. \quad (2.27)$$

Thus, analogous to (2.9), one has that the first-order FAST sensitivity indices are given by

$$S_i^{\text{FAST}} = \frac{\sum_{k_i=1}^{\infty} (A_{k_i}^2 + B_{k_i}^2)}{\sum_{k=1}^{\infty} (A_k^2 + B_k^2)}. \quad (2.28)$$

These integrals can be numerically determined using N sampling points, uniformly chosen on $[-\pi, \pi]$, in conjunction with predetermined sets of frequencies (which have been calculated up to $n = 50$) [49].

There are a few important things to note. One important thing to consider is that since a finite number of sampling points are used, N must be chosen so that aliasing is avoided, and that it is not possible for more than one frequency to contribute to each Fourier coefficient [45]. By the Nyquist–Shannon sampling theorem, this is equivalent to choosing N such that

$$N \geq 2M\omega_{\max} + 1, \quad (2.29)$$

where ω_{\max} is the maximum value of $\{\omega_i\}$. Furthermore, S_i^{FAST} is independent of the choice of $\{\omega_i\}$ [50], and it was shown in [46] that $S_i^{\text{FAST}} \rightarrow S_i$ as $N \rightarrow \infty$. There exist optimisations that can be made to FAST, such as that due to [51], in which if $\{\omega_i\}$ are all chosen to be odd, then $f(\mathbf{X}(s))$ is symmetric about $s = \pm\pi/2$, so that one can restrict the interval of integration from $[-\pi, \pi]$ to $[-\pi/2, \pi/2]$, and half the number of model evaluation. Furthermore, this methodology can be extended to estimate total-order sensitivity indices using the extended Fourier amplitude sensitivity test (EFAST) algorithm, with further details in [47]. One point of comparison between FAST-based and Sobol' methods is that, in general, the Sobol' method requires N times more model evaluations than FAST for a given N [46]. As such, FAST-based methods are computationally less expensive, with faster convergence to the true sensitivity indices.

3 Mathematical Models

3.1 Model Assumptions

For simplicity, we ignore spatial effects in the models, ignoring the effects of diffusion, advection, and chemotaxis by all species. We assume the system has two compartments: one at the TS, located in the colon or rectum, and one at the tumour-draining lymph node (TDLN). This is a simplification since metastatic CRC typically involves multiple tumour-draining lymph nodes [52]; however, for simplicity, we focus on the sentinel node and refer to it as the TDLN for the purposes of the model. In a similar fashion to nearly all models of de novo metastatic cancer, we primarily focus on the growth of the primary tumour, using it as a proxy to infer the progression of lymph node and distant metastases. We assume that cytokines in the TS are produced only by effector or activated cells and that damage-associated molecular patterns (DAMPs) in the TS are only produced by necrotic cancer cells. We assume that all mature DCs in the TDLN are cancer-antigen-bearing and that all T cells in the TS are primed with cancer antigens. Furthermore, we assume that all activated T cells in the TDLN are activated with cancer antigens and that T cell proliferation/division follows a deterministic program. We ignore CD4+ and CD8+ memory T cells and assume that naive CD4+ T cells differentiate immediately upon activation. We also assume that all Tregs in the TS are natural Tregs (nTregs), ignoring induced Tregs (iTregs). We assume, for simplicity, that activated macrophages polarise into the M1/M2 dichotomy. We also assume that the duration of pembrolizumab infusion is negligible compared to the timescale of the model. Therefore, we treat their infusions as an intravenous bolus so that drug absorption occurs immediately after infusion. Finally, we assume a constant solution history, where the history for each species is set to its respective initial condition.

We assume that all species, X_i , degrade/die at a rate proportional to their concentration, with decay constant d_{X_i} . We assume that the rate of activation/polarisation of a species X_i by a species X_j follows the Michaelis-Menten kinetic law $\lambda_{X_i X_j} X_i \frac{X_j}{K_{X_i X_j} + X_j}$, for rate constant $\lambda_{X_i X_j}$, and half-saturation constant $K_{X_i X_j}$. Similarly, we model the rate of inhibition of a species X_i by a species X_j using a term with form $\lambda_{X_i X_j} \frac{X_i}{1 + X_j/K_{X_i X_j}}$ for rate constant $\lambda_{X_i X_j}$, and half-saturation constant $K_{X_i X_j}$. Production of X_i by X_j is modelled using mass-action kinetics unless otherwise specified, so that the rate at which X_i is formed is given by $\lambda_{X_i X_j} X_j$ for some positive constant $\lambda_{X_i X_j}$. Finally, we assume that the rate of lysis of X_i by X_j follows mass-action kinetics in the case where X_j is a cell and follows Michaelis-Menten kinetics in the case where X_j is a cytokine.

3.2 Model Summary

We also outline some of the main processes accounted for in the models.

1. Effector CD8+ T cells and NK cells induce apoptosis of cancer cells, with this being inhibited by TGF- β and the PD-1/PD-L1 complex. However, TNF and IFN- γ induce necroptosis of cancer cells, causing them to become necrotic before they are removed.
2. Necrotic cancer cells release DAMPs such as HMGB1 and calreticulin, which stimulate immature DCs to mature.
3. Some mature DCs migrate to the T cell zone of the TDLN and activate naive CD8+ and CD4+ T cells (including Tregs), with CD8+ T cell and Th1 cell activation being inhibited by Tregs and the PD-1/PD-L1 complex.

4. Activated T cells undergo clonal expansion and proliferate rapidly in the TDLN, with CD8+ T cell and Th1 cell proliferation being inhibited by Tregs and the PD-1/PD-L1 complex.
5. T cells that have completed proliferation migrate to the TS and perform effector functions including the production of pro-inflammatory (IL-2, IFN- γ , TNF) and immunosuppressive (TGF- β , IL-10) cytokines. Extended exposure to the cancer antigen can lead CD8+ T cells to become exhausted, however, this exhaustion can be reversed by pembrolizumab.
6. In addition, mature DCs, NK cells and macrophages secrete cytokines that can activate NK cells and polarise and repolarise macrophages into pro-inflammatory and immunosuppressive phenotypes.
7. Pembrolizumab infusion promotes the binding of unbound PD-1 receptors to pembrolizumab, forming the PD-1/pembrolizumab complex instead of the PD-1/PD-L1 complex. This reduces the inhibition of pro-inflammatory CD8+ and Th1 cell activation and proliferation while also reducing the inhibition of cancer cell lysis.

3.3 Full Model

3.3.1 Model Variables

The variables and their units in the full model are shown in [Table 1](#).

Table 1: Variables used in the full model. Quantities in the top box are in units of cell/cm^3 , quantities in the second box are in units of g/cm^3 , and all other quantities are in units of molec/cm^3 . All quantities pertain to the tumour site unless otherwise specified. TDLN denotes the tumour-draining lymph node, whilst TS denotes the tumour site.

Var	Description	Var	Description
V_{TS}	Primary tumour volume		
C	Viable cancer cell density	N_c	Necrotic cell density
D_0	Immature DC density	D	Mature DC density in the TS
D^{LN}	Mature DC density at TDLN	T_0^8	Naive CD8+ T cell density in the TDLN
T_A^8	Effector CD8+ T cell density in the TDLN	T_8	Effector CD8+ T cell density in the TS
T_{ex}	Exhausted CD8+ T cell density in the TS	T_0^4	Naive CD4+ T cell density in the TDLN
T_A^1	Effector Th1 cell density in the TDLN	T_1	Effector Th1 cell density in the TS
T_0^r	Naive Treg density in the TDLN	T_A^r	Effector Treg density in the TDLN
T_r	Effector Treg density in the TS	M_0	Naive macrophage density
M_1	M1 macrophage density	M_2	M2 macrophage density
K_0	Naive NK cell density	K	Activated NK cell density
H	HMGB1 concentration	S	Calreticulin concentration
I_2	IL-2 concentration	I_γ	IFN- γ concentration
I_α	TNF concentration	I_β	TGF- β concentration
I_{10}	IL-10 concentration		
$P_D^{T_8}$	Unbound PD-1 receptor concentration on effector CD8+ T cells in the TS	$P_D^{T_1}$	Unbound PD-1 receptor concentration on effector Th1 cells in the TS
P_D^K	Unbound PD-1 receptor concentration on activated NK cells	$Q_A^{T_8}$	PD-1/pembrolizumab complex concentration on effector CD8+ T cells in the TS
$Q_A^{T_1}$	PD-1/pembrolizumab complex concentration on effector Th1 cells in the TS	Q_A^K	PD-1/pembrolizumab complex concentration on activated NK cells
P_L	Unbound PD-L1 concentration in the TS	Q^{T_8}	PD-1/PD-L1 complex concentration on effector CD8+ T cells in the TS
Q^{T_1}	PD-1/PD-L1 complex concentration on effector Th1 cells in the TS	Q^K	PD-1/PD-L1 complex concentration on activated NK cells
A_1	Concentration of pembrolizumab in the TS		
$P_D^{8\text{LN}}$	Unbound PD-1 receptor concentration on effector CD8+ T cells in the TDLN	$P_D^{1\text{LN}}$	Unbound PD-1 receptor concentration on effector Th1 cells in the TDLN
$Q_A^{8\text{LN}}$	PD-1/pembrolizumab complex concentration on effector CD8+ T cells in the TDLN	$Q_A^{1\text{LN}}$	PD-1/pembrolizumab complex concentration on effector Th1 cells in the TDLN
P_L^{LN}	Unbound PD-L1 concentration in the TDLN	$Q^{8\text{LN}}$	PD-1/PD-L1 complex concentration on effector CD8+ T cells in the TDLN
$Q^{1\text{LN}}$	PD-1/PD-L1 complex concentration on effector Th1 cells in the TDLN	A_1^{LN}	Concentration of pembrolizumab in the TDLN

3.3.2 Model Equations

The model equations are identical to those from [38]; however, for completeness, we provide the mathematical model below. A full derivation of the model is available in [38], and the parameter values used—listed in Table A.1—are estimated as described therein.

3.3.2.1 Equations for Cancer Cells, DAMPs, and DCs

$$\begin{aligned} \frac{dC}{dt} = & \underbrace{\lambda_C C \left(1 - \frac{C}{C_0}\right)}_{\text{growth}} - \underbrace{\lambda_{CT_8} T_8 \frac{1}{1 + I_\beta / K_{CI_\beta}} \frac{1}{1 + Q^{T_8} / K_{CQ^{T_8}}} C}_{\text{elimination by } T_8 \text{ inhibited by } I_\beta \text{ and } Q^{T_8}} - \underbrace{\lambda_{CK} K \frac{1}{1 + I_\beta / K_{CI_\beta}} \frac{1}{1 + Q^K / K_{CQ^K}} C}_{\text{elimination by } K \text{ inhibited by } I_\beta \text{ and } Q^K} \\ & - \underbrace{\lambda_{CI_\alpha} \frac{I_\alpha}{K_{CI_\alpha} + I_\alpha} C}_{\text{elimination by } I_\alpha} - \underbrace{\lambda_{CI_\gamma} \frac{I_\gamma}{K_{CI_\gamma} + I_\gamma} C}_{\text{elimination by } I_\gamma}, \end{aligned} \quad (3.3.1)$$

$$\frac{dN_c}{dt} = \underbrace{\lambda_{CI_\alpha} \frac{I_\alpha}{K_{CI_\alpha} + I_\alpha} C}_{\text{Elimination by } I_\alpha} + \underbrace{\lambda_{CI_\gamma} \frac{I_\gamma}{K_{CI_\gamma} + I_\gamma} C}_{\text{Elimination by } I_\gamma} - \underbrace{d_{N_c} N_c}_{\text{Removal}}. \quad (3.3.2)$$

$$\begin{aligned} \frac{dV_{TS}}{dt} = & \frac{1}{f_C + f_{N_c}} \left[\lambda_C f_C V_{TS} \left(1 - \frac{f_C V_{TS}}{C_0}\right) - \lambda_{CT_8} T_8 \frac{1}{1 + I_\beta / K_{CI_\beta}} \frac{1}{1 + Q^{T_8} / K_{CQ^{T_8}}} f_C V_{TS} \right. \\ & \left. - \lambda_{CK} K \frac{1}{1 + I_\beta / K_{CI_\beta}} \frac{1}{1 + Q^K / K_{CQ^K}} f_C V_{TS} - d_{N_c} f_{N_c} V_{TS} \right], \end{aligned} \quad (3.3.3)$$

where $C(t) = f_C V_{TS}(t)$ and $N_c(t) = f_{N_c} V_{TS}(t)$.

$$\frac{dH}{dt} = \underbrace{\lambda_{HN_c} N_c}_{\text{production by } N_c} - \underbrace{d_H H}_{\text{degradation}}, \quad (3.3.4)$$

$$\frac{dS}{dt} = \underbrace{\lambda_{SN_c} N_c}_{\text{production by } N_c} - \underbrace{d_S S}_{\text{degradation}}, \quad (3.3.5)$$

$$\begin{aligned} \frac{dD_0}{dt} = & \underbrace{\mathcal{A}_{D_0}}_{\text{source}} - \underbrace{\lambda_{DH} D_0 \frac{H}{K_{DH} + H}}_{D_0 \rightarrow D \text{ by } H} - \underbrace{\lambda_{DS} D_0 \frac{S}{K_{DS} + S}}_{D_0 \rightarrow D \text{ by } S} - \underbrace{\lambda_{D_0 K} D_0 K \frac{1}{1 + I_\beta / K_{D_0 I_\beta}}}_{\text{elimination by } K \text{ inhibited by } I_\beta} - \underbrace{d_{D_0} D_0}_{\text{death}}, \end{aligned} \quad (3.3.6)$$

$$\begin{aligned} \frac{dD}{dt} = & \underbrace{\lambda_{DH} D_0 \frac{H}{K_{DH} + H}}_{D_0 \rightarrow D \text{ by } H} + \underbrace{\lambda_{DS} D_0 \frac{S}{K_{DS} + S}}_{D_0 \rightarrow D \text{ by } S} - \underbrace{\lambda_{DD^{\text{LN}}} D}_{D \text{ migration to TDLN}} - \underbrace{d_D D}_{\text{death}}, \end{aligned} \quad (3.3.7)$$

$$\frac{dD^{\text{LN}}}{dt} = \frac{V_{TS}}{V_{\text{LN}}} \underbrace{\lambda_{DD^{\text{LN}}} e^{-d_D \tau_m} D(t - \tau_m)}_{D \text{ migration to TDLN}} - \underbrace{d_D D^{\text{LN}}}_{\text{death}}. \quad (3.3.8)$$

A diagram encompassing the interactions of these components is shown in [Figure 1](#).

3.3.2.2 Equations for T Cells

$$\frac{dT_0^8}{dt} = \underbrace{\mathcal{A}_{T_0^8}}_{\text{source}} - \underbrace{R^8(t)}_{\text{CD8+ T cell activation}} - \underbrace{d_{T_0^8} T_0^8}_{\text{death}}, \quad (3.3.9)$$

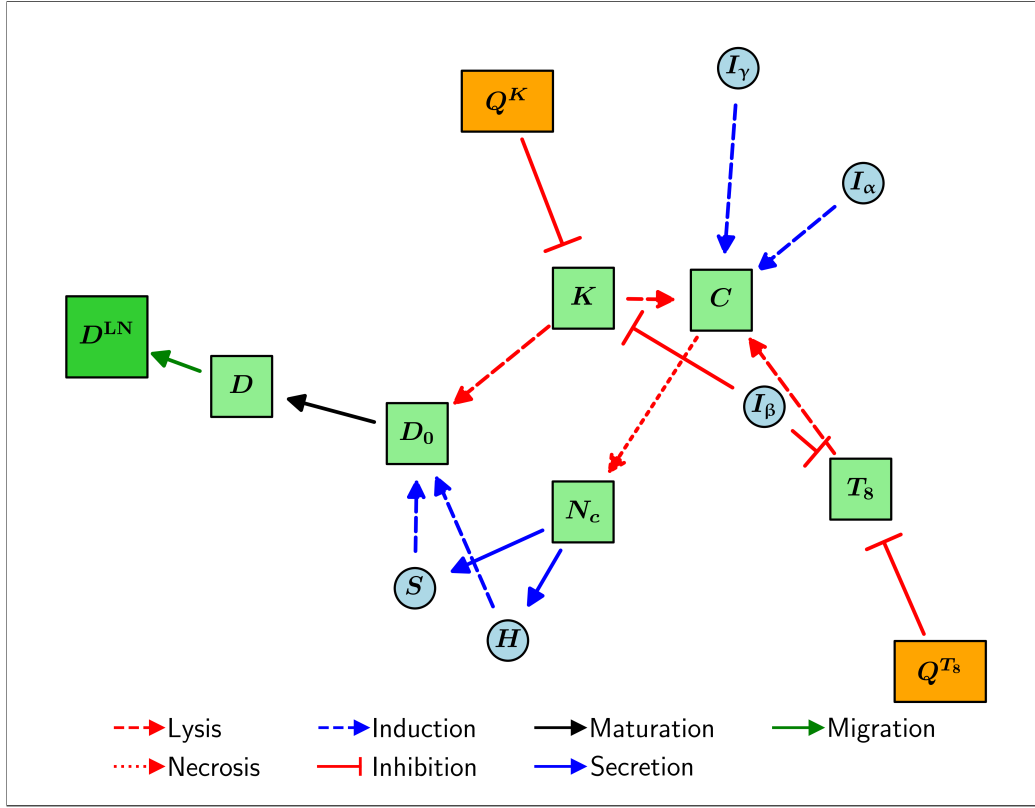


Figure 1: Schematic diagram of the interactions of cancer cells, DAMPs, and DCs in the full model.

where $R^8(t)$ is defined as

$$R^8(t) := \frac{\lambda_{T_0^8 T_A^8} e^{-d_{T_0^8} \tau_8^{\text{act}}} D^{\text{LN}}(t - \tau_8^{\text{act}}) T_0^8(t - \tau_8^{\text{act}})}{\underbrace{\left(1 + \int_{t-\tau_8^{\text{act}}}^t T_A^r(s) ds / K_{T_0^8 T_A^r}\right) \left(1 + \int_{t-\tau_8^{\text{act}}}^t Q^{\text{SLN}}(s) ds / K_{T_0^8 Q^{\text{SLN}}}\right)}_{\text{CD8+ T cell activation inhibited by } T_A^r \text{ and } Q^{\text{SLN}}}}. \quad (3.3.10)$$

$$\frac{dT_A^8}{dt} = \frac{2^{n_{\text{max}}^8} e^{-d_{T_0^8} \tau_{T_A^8}} R^8(t - \tau_{T_A^8})}{\underbrace{\left(1 + \int_{t-\tau_{T_A^8}}^t T_A^r(s) ds / K_{T_A^8 T_A^r}\right) \left(1 + \int_{t-\tau_{T_A^8}}^t Q^{\text{SLN}}(s) ds / K_{T_A^8 Q^{\text{SLN}}}\right)}_{\text{CD8+ T cell proliferation inhibited by } T_A^r \text{ and } Q^{\text{SLN}}}} - \underbrace{\lambda_{T_A^8 T_8} T_A^8}_{T_A^8 \text{ migration to the TS}} - \underbrace{d_{T_8} T_A^8}_{\text{death}}, \quad (3.3.11)$$

where $\tau_{T_A^8}$ is defined as

$$\tau_{T_A^8} := \Delta_8^0 + (n_{\text{max}}^8 - 1) \Delta_8. \quad (3.3.12)$$

$$\begin{aligned} \frac{dT_8}{dt} = & \underbrace{\frac{V_{\text{LN}}}{V_{\text{TS}}} \lambda_{T_A^8 T_8} e^{-d_{T_8} \tau_a} T_A^8(t - \tau_a)}_{T_A^8 \text{ migration to the TS}} + \underbrace{\lambda_{T_8 I_2} \frac{T_8 I_2}{K_{T_8 I_2} + I_2} \frac{1}{1 + T_r / K_{T_8 T_r}}}_{\text{growth by } I_2 \text{ inhibited by } T_r} \\ & - \underbrace{\lambda_{T_8 C} \frac{T_8 \int_{t-\tau_l}^t C(s) ds}{K_{T_8 C} + \int_{t-\tau_l}^t C(s) ds}}_{T_8 \rightarrow T_{\text{ex}} \text{ from } C \text{ exposure}} + \underbrace{\lambda_{T_{\text{ex}} A_1} \frac{T_{\text{ex}} A_1}{K_{T_{\text{ex}} A_1} + A_1}}_{T_{\text{ex}} \rightarrow T_8 \text{ by } A_1} - \underbrace{\frac{d_{T_8} T_8}{1 + I_{10} / K_{T_8 I_{10}}}}_{\text{death inhibited by } I_{10}}, \end{aligned} \quad (3.3.13)$$

$$\frac{dT_{\text{ex}}}{dt} = \underbrace{\lambda_{T_8 C} \frac{T_8 \int_{t-\tau_l}^t C(s) ds}{K_{T_8 C} + \int_{t-\tau_l}^t C(s) ds}}_{T_8 \rightarrow T_{\text{ex}} \text{ from } C \text{ exposure}} - \underbrace{\lambda_{T_{\text{ex}} A_1} \frac{T_{\text{ex}} A_1}{K_{T_{\text{ex}} A_1} + A_1}}_{T_{\text{ex}} \rightarrow T_8 \text{ by } A_1} - \underbrace{\frac{d_{T_{\text{ex}}} T_{\text{ex}}}{1 + I_{10}/K_{T_{\text{ex}} I_{10}}}}_{\text{death inhibited by } I_{10}}. \quad (3.3.14)$$

$$\frac{dT_0^4}{dt} = \underbrace{\mathcal{A}_{T_0^4}}_{\text{source}} - \underbrace{R^1(t)}_{\text{Th1 cell activation}} - \underbrace{d_{T_0^4} T_0^4}_{\text{death}}, \quad (3.3.15)$$

where $R^1(t)$ is defined as

$$R^1(t) := \frac{\lambda_{T_0^4 T_A^1} e^{-d_{T_0^4} \tau_{\text{act}}^4} D^{\text{LN}}(t - \tau_{\text{act}}^4) T_0^4(t - \tau_{\text{act}}^4)}{\underbrace{\left(1 + \int_{t-\tau_{\text{act}}^4}^t T_r^A(s) ds / K_{T_0^4 T_A^1}\right) \left(1 + \int_{t-\tau_{\text{act}}^4}^t Q^{\text{1LN}}(s) ds / K_{T_0^4 Q^{\text{1LN}}}\right)}_{\text{Th1 cell activation inhibited by } T_A^r \text{ and } Q^{\text{1LN}}}}. \quad (3.3.16)$$

$$\frac{dT_A^1}{dt} = \frac{2^{n_{\text{max}}^1} e^{-d_{T_0^4} \tau_{T_A^1}^1} R^1(t - \tau_{T_A^1}^1)}{\underbrace{\left(1 + \int_{t-\tau_{T_A^1}^1}^t Q^{\text{1LN}}(s) ds / K_{T_A^1 Q^{\text{1LN}}}\right) \left(1 + \int_{t-\tau_{T_A^1}^1}^t T_A^r(s) ds / K_{T_A^1 T_A^r}\right)}_{\text{Th1 cell proliferation inhibited by } T_A^r \text{ and } Q^{\text{1LN}}}} - \underbrace{\lambda_{T_A^1 T_1} T_A^1}_{T_A^1 \text{ migration to the TS}} - \underbrace{d_{T_1} T_A^1}_{\text{death}}, \quad (3.3.17)$$

where $\tau_{T_A^1}$ is defined as

$$\tau_{T_A^1} := \Delta_1^0 + (n_{\text{max}}^1 - 1) \Delta_1. \quad (3.3.18)$$

$$\frac{dT_1}{dt} = \frac{V_{\text{LN}}}{V_{\text{TS}}} \underbrace{\lambda_{T_A^1 T_1} e^{-d_{T_1} \tau_a} T_A^1(t - \tau_a)}_{T_A^1 \text{ migration to the TS}} + \underbrace{\lambda_{T_1 I_2} \frac{T_1 I_2}{K_{T_1 I_2} + I_2} \frac{1}{1 + T_r / K_{T_1 T_r}}}_{\text{growth by } I_2 \text{ inhibited by } T_r} - \underbrace{\lambda_{T_1 T_r} T_1 \frac{Q^{T_1}}{K_{T_1 T_r} + Q^{T_1}}}_{T_1 \rightarrow T_r \text{ by } Q^{T_1}} - \underbrace{d_{T_1} T_1}_{\text{death}}, \quad (3.3.19)$$

$$\frac{dT_0^r}{dt} = \underbrace{\mathcal{A}_{T_0^r}}_{\text{source}} - \underbrace{R^r(t)}_{\text{Treg activation}} - \underbrace{d_{T_0^r} T_0^r}_{\text{death}}, \quad (3.3.20)$$

where $R^r(t)$ is defined as

$$R^r(t) := \underbrace{\lambda_{T_0^r T_A^r} e^{-d_{T_0^r} \tau_{\text{act}}^r} D^{\text{LN}}(t - \tau_{\text{act}}^r) T_0^r(t - \tau_{\text{act}}^r)}_{\text{Treg activation}}. \quad (3.3.21)$$

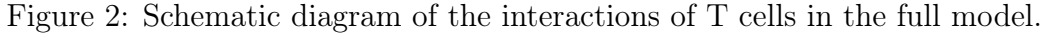
$$\frac{dT_A^r}{dt} = \underbrace{2^{n_{\text{max}}^r} e^{-d_{T_0^r} \tau_{T_A^r}^r} R^r(t - \tau_{T_A^r}^r)}_{\text{Treg proliferation}} - \underbrace{\lambda_{T_A^r T_r} T_A^r}_{T_A^r \text{ migration to the TS}} - \underbrace{d_{T_r} T_A^r}_{\text{death}}, \quad (3.3.22)$$

where $\tau_{T_A^r}$ is defined as

$$\tau_{T_A^r} := \Delta_r^0 + (n_{\text{max}}^r - 1) \Delta_r. \quad (3.3.23)$$

$$\frac{dT_r}{dt} = \frac{V_{\text{LN}}}{V_{\text{TS}}} \underbrace{\lambda_{T_A^r T_r} e^{-d_{T_r} \tau_a} T_A^r(t - \tau_a)}_{T_A^r \text{ migration to the TS}} + \underbrace{\lambda_{T_1 T_r} T_1 \frac{Q^{T_1}}{K_{T_1 T_r} + Q^{T_1}}}_{T_1 \rightarrow T_r \text{ by } Q^{T_1}} - \underbrace{d_{T_r} T_r}_{\text{death}}. \quad (3.3.24)$$

A diagram encompassing the interactions of these components is shown in [Figure 2](#).


$$\begin{aligned}
\frac{dM_0}{dt} &= \underbrace{\mathcal{A}_{M_0}}_{\text{source}} - \underbrace{\lambda_{M_1 I_\alpha} M_0 \frac{I_\alpha}{K_{M_1 I_\alpha} + I_\alpha}}_{M_0 \rightarrow M_1 \text{ by } I_\alpha} - \underbrace{\lambda_{M_1 I_\gamma} M_0 \frac{I_\gamma}{K_{M_1 I_\gamma} + I_\gamma}}_{M_0 \rightarrow M_1 \text{ by } I_\gamma} - \underbrace{\lambda_{M_2 I_{10}} M_0 \frac{I_{10}}{K_{M_2 I_{10}} + I_{10}}}_{M_0 \rightarrow M_2 \text{ by } I_{10}} \\
&\quad - \underbrace{\lambda_{M_2 I_\beta} M_0 \frac{I_\beta}{K_{M_2 I_\beta} + I_\beta}}_{M_0 \rightarrow M_2 \text{ by } I_\beta} - \underbrace{d_{M_0} M_0}_{\text{degradation}}, \\
\frac{dM_1}{dt} &= \underbrace{\lambda_{M_1 I_\alpha} M_0 \frac{I_\alpha}{K_{M_1 I_\alpha} + I_\alpha}}_{M_0 \rightarrow M_1 \text{ by } I_\alpha} + \underbrace{\lambda_{M_1 I_\gamma} M_0 \frac{I_\gamma}{K_{M_1 I_\gamma} + I_\gamma}}_{M_0 \rightarrow M_1 \text{ by } I_\gamma} + \underbrace{\lambda_{M I_\gamma} M_2 \frac{I_\gamma}{K_{M I_\gamma} + I_\gamma}}_{M_2 \rightarrow M_1 \text{ by } I_\gamma} + \underbrace{\lambda_{M I_\alpha} M_2 \frac{I_\alpha}{K_{M I_\alpha} + I_\alpha}}_{M_2 \rightarrow M_1 \text{ by } I_\alpha} \\
&\quad - \underbrace{\lambda_{M I_\beta} M_1 \frac{I_\beta}{K_{M I_\beta} + I_\beta}}_{M_1 \rightarrow M_2 \text{ by } I_\beta} - \underbrace{d_{M_1} M_1}_{\text{degradation}}, \\
\frac{dM_2}{dt} &= \underbrace{\lambda_{M_2 I_{10}} M_0 \frac{I_{10}}{K_{M_2 I_{10}} + I_{10}}}_{M_0 \rightarrow M_2 \text{ by } I_{10}} + \underbrace{\lambda_{M_2 I_\beta} M_0 \frac{I_\beta}{K_{M_2 I_\beta} + I_\beta}}_{M_0 \rightarrow M_2 \text{ by } I_\beta} - \underbrace{\lambda_{M I_\gamma} M_2 \frac{I_\gamma}{K_{M I_\gamma} + I_\gamma}}_{M_2 \rightarrow M_1 \text{ by } I_\gamma} - \underbrace{\lambda_{M I_\alpha} M_2 \frac{I_\alpha}{K_{M I_\alpha} + I_\alpha}}_{M_2 \rightarrow M_1 \text{ by } I_\alpha} \\
&\quad + \underbrace{\lambda_{M I_\beta} M_1 \frac{I_\beta}{K_{M I_\beta} + I_\beta}}_{M_1 \rightarrow M_2 \text{ by } I_\beta} - \underbrace{d_{M_2} M_2}_{\text{degradation}},
\end{aligned}$$

$$\frac{dK_0}{dt} = \underbrace{\mathcal{A}_{K_0}}_{\text{source}} - \left(\underbrace{\lambda_{KI_2} K_0 \frac{I_2}{K_{KI_2} + I_2}}_{K_0 \rightarrow K \text{ by } I_2} + \underbrace{\lambda_{KD_0} K_0 \frac{D_0}{K_{KD_0} + D_0}}_{K_0 \rightarrow K \text{ by } D_0} + \underbrace{\lambda_{KD} K_0 \frac{D}{K_{KD} + D}}_{K_0 \rightarrow K \text{ by } D} \right) \underbrace{\frac{1}{1 + I_\beta / K_{KI_\beta}}}_{\text{activation inhibited by } I_\beta} - \underbrace{d_{K_0} K_0}_{\text{degradation}}, \quad (3.3.28)$$

$$\frac{dK}{dt} = \left(\underbrace{\lambda_{KI_2} K_0 \frac{I_2}{K_{KI_2} + I_2}}_{K_0 \rightarrow K \text{ by } I_2} + \underbrace{\lambda_{KD_0} K_0 \frac{D_0}{K_{KD_0} + D_0}}_{K_0 \rightarrow K \text{ by } D_0} + \underbrace{\lambda_{KD} K_0 \frac{D}{K_{KD} + D}}_{K_0 \rightarrow K \text{ by } D} \right) \underbrace{\frac{1}{1 + I_\beta / K_{KI_\beta}}}_{\text{activation inhibited by } I_\beta} - \underbrace{d_K K}_{\text{degradation}}. \quad (3.3.29)$$

A diagram encompassing the interactions of these components is shown in [Figure 3](#).

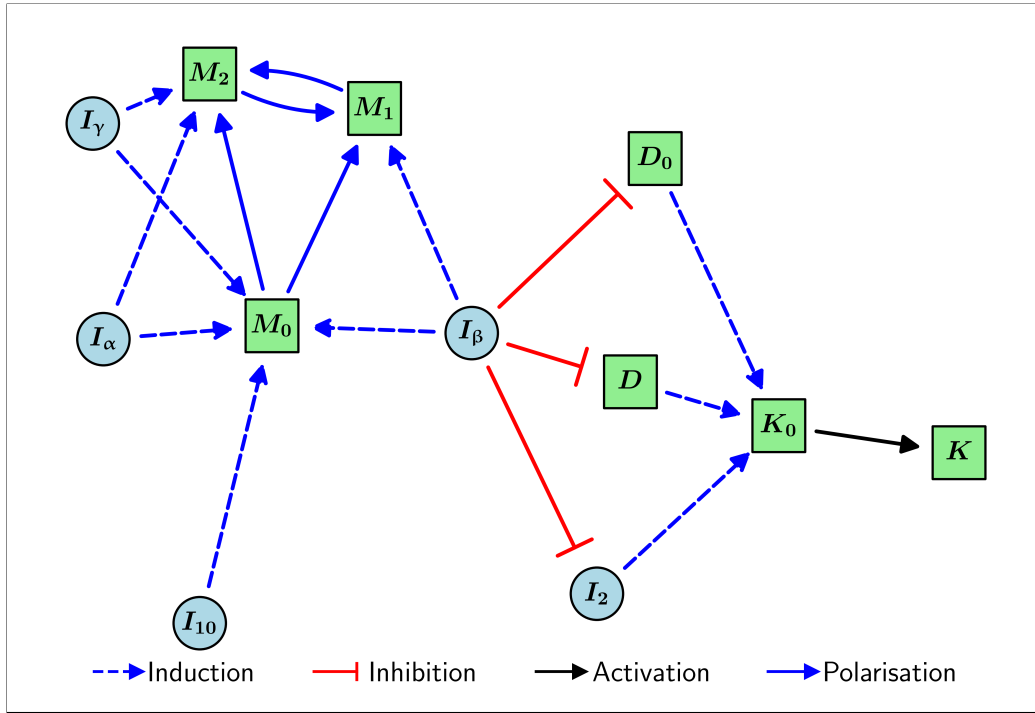


Figure 3: Schematic diagram of the interactions of macrophages and NK cells in the full model.

3.3.2.4 Equations for Cytokines

$$\frac{dI_2}{dt} = \underbrace{\lambda_{I_2 T_8} T_8}_{\text{production by } T_8} + \underbrace{\lambda_{I_2 T_1} T_1}_{\text{production by } T_1} - \underbrace{d_{I_2} I_2}_{\text{degradation}}. \quad (3.3.30)$$

After applying a quasi-steady-state approximation (QSSA), this becomes

$$I_2 = \frac{1}{d_{I_2}} (\lambda_{I_2 T_8} T_8 + \lambda_{I_2 T_1} T_1). \quad (3.3.31)$$

$$\frac{dI_\gamma}{dt} = \left(\underbrace{\lambda_{I_\gamma T_8} T_8}_{\text{production by } T_8} + \underbrace{\lambda_{I_\gamma T_1} T_1}_{\text{production by } T_1} \right) \underbrace{\frac{1}{1 + T_r/K_{I_\gamma T_r}}}_{\text{inhibition by } T_r} + \underbrace{\lambda_{I_\gamma K} K}_{\text{production by } K} - \underbrace{d_{I_\gamma} I_\gamma}_{\text{degradation}} . \quad (3.3.32)$$

After applying a QSSA, this becomes

$$I_\gamma = \frac{1}{d_{I_\gamma}} \left[(\lambda_{I_\gamma T_8} T_8 + \lambda_{I_\gamma T_1} T_1) \frac{1}{1 + T_r/K_{I_\gamma T_r}} + \lambda_{I_\gamma K} K \right] . \quad (3.3.33)$$

$$\frac{dI_\alpha}{dt} = \underbrace{\lambda_{I_\alpha T_8} T_8}_{\text{production by } T_8} + \underbrace{\lambda_{I_\alpha T_1} T_1}_{\text{production by } T_1} + \underbrace{\lambda_{I_\alpha M_1} M_1}_{\text{production by } M_1} + \underbrace{\lambda_{I_\alpha K} K}_{\text{production by } K} - \underbrace{d_{I_\alpha} I_\alpha}_{\text{degradation}} . \quad (3.3.34)$$

After applying a QSSA, this becomes

$$I_\alpha = \frac{1}{d_{I_\alpha}} (\lambda_{I_\alpha T_8} T_8 + \lambda_{I_\alpha T_1} T_1 + \lambda_{I_\alpha M_1} M_1 + \lambda_{I_\alpha K} K) . \quad (3.3.35)$$

$$\frac{dI_\beta}{dt} = \underbrace{\lambda_{I_\beta C} C}_{\text{production by } C} + \underbrace{\lambda_{I_\beta T_r} T_r}_{\text{production by } T_r} + \underbrace{\lambda_{I_\beta M_2} M_2}_{\text{production by } M_2} - \underbrace{d_{I_\beta} I_\beta}_{\text{degradation}} . \quad (3.3.36)$$

After applying a QSSA, this becomes

$$I_\beta = \frac{1}{d_{I_\beta}} (\lambda_{I_\beta C} C + \lambda_{I_\beta T_r} T_r + \lambda_{I_\beta M_2} M_2) . \quad (3.3.37)$$

$$\frac{dI_{10}}{dt} = \underbrace{\lambda_{I_{10} C} C}_{\text{production by } C} + \underbrace{\lambda_{I_{10} M_2} M_2}_{\text{production by } M_2} + \underbrace{\lambda_{I_{10} T_r} T_r \left(1 + \lambda_{I_{10} I_2} \frac{I_2}{K_{I_{10} I_2} + I_2} \right)}_{\text{production by } T_r \text{ enhanced by } I_2} - \underbrace{d_{I_{10}} I_{10}}_{\text{degradation}} . \quad (3.3.38)$$

A diagram encompassing the interactions of cytokines is shown in [Figure 4](#).

3.3.2.5 Equations for Immune Checkpoint-Associated Components in the TS

$$\frac{dP_D^{T_8}}{dt} = \underbrace{\lambda_{P_D^{T_8}} T_8}_{\text{synthesis}} + \underbrace{\lambda_{Q_A} Q_A^{T_8}}_{\text{dissociation of } Q_A^{T_8}} - \underbrace{\lambda_{P_D A_1} P_D^{T_8} A_1}_{\text{binding to } A_1} - \underbrace{d_{P_D} P_D^{T_8}}_{\text{degradation}} , \quad (3.3.39)$$

$$\frac{dP_D^{T_1}}{dt} = \underbrace{\lambda_{P_D^{T_1}} T_1}_{\text{synthesis}} + \underbrace{\lambda_{Q_A} Q_A^{T_1}}_{\text{dissociation of } Q_A^{T_1}} - \underbrace{\lambda_{P_D A_1} P_D^{T_1} A_1}_{\text{binding to } A_1} - \underbrace{d_{P_D} P_D^{T_1}}_{\text{degradation}} , \quad (3.3.40)$$

$$\frac{dP_D^K}{dt} = \underbrace{\lambda_{P_D^K} K}_{\text{synthesis}} + \underbrace{\lambda_{Q_A} Q_A^K}_{\text{dissociation of } Q_A^K} - \underbrace{\lambda_{P_D A_1} P_D^K A_1}_{\text{binding to } A_1} - \underbrace{d_{P_D} P_D^K}_{\text{degradation}} , \quad (3.3.41)$$

$$\frac{dQ_A^{T_8}}{dt} = \underbrace{\lambda_{P_D A_1} P_D^{T_8} A_1}_{\text{formation of } Q_A^{T_8}} - \underbrace{\lambda_{Q_A} Q_A^{T_8}}_{\text{dissociation of } Q_A^{T_8}} - \underbrace{d_{Q_A} Q_A^{T_8}}_{\text{internalisation}} , \quad (3.3.42)$$

$$\frac{dQ_A^{T_1}}{dt} = \underbrace{\lambda_{P_D A_1} P_D^{T_1} A_1}_{\text{formation of } Q_A^{T_1}} - \underbrace{\lambda_{Q_A} Q_A^{T_1}}_{\text{dissociation of } Q_A^{T_1}} - \underbrace{d_{Q_A} Q_A^{T_1}}_{\text{internalisation}} , \quad (3.3.43)$$

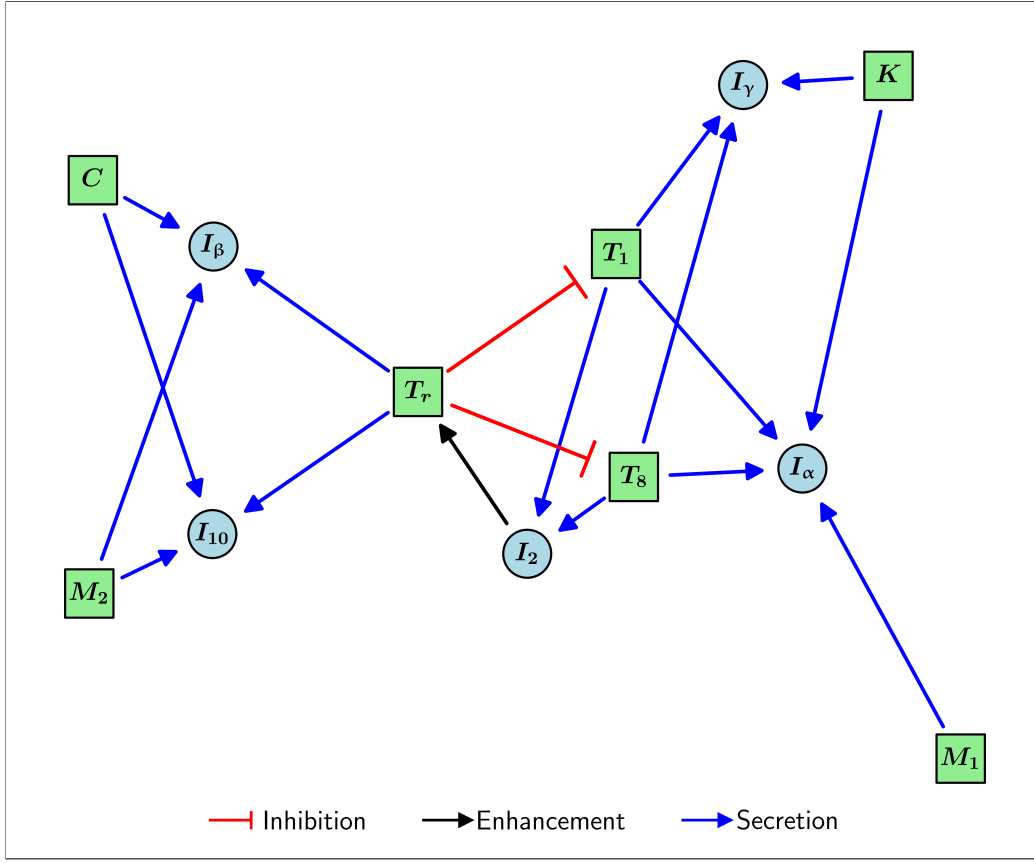


Figure 4: Schematic diagram of the interactions of cytokines in the full model.

$$\frac{dQ_A^K}{dt} = \underbrace{\lambda_{P_D A_1} P_D^K A_1}_{\text{formation of } Q_A^K} - \underbrace{\lambda_{Q_A} Q_A^K}_{\text{dissociation of } Q_A^K} - \underbrace{d_{Q_A} Q_A^K}_{\text{internalisation}}, \quad (3.3.44)$$

$$\frac{dA_1}{dt} = \underbrace{\sum_{j=1}^n \xi_j f_{\text{pembro}} \delta(t - t_j)}_{\text{infusion}} + \underbrace{\lambda_{Q_A} (Q_A^{T_8} + Q_A^{T_1} + Q_A^K)}_{\text{dissociation of } Q_A^{T_8}, Q_A^{T_1}, \text{ and } Q_A^K} - \underbrace{\lambda_{P_D A_1} (P_D^{T_8} + P_D^{T_1} + P_D^K) A_1}_{\text{formation of } Q_A^{T_8}, Q_A^{T_1}, \text{ and } Q_A^K} - \underbrace{d_{A_1} A_1}_{\text{elimination}}, \quad (3.3.45)$$

$$\frac{dP_L}{dt} = \underbrace{\sum_{X \in \mathcal{X}} \lambda_{P_L X} X}_{\text{synthesis}} - \underbrace{d_{P_L} P_L}_{\text{degradation}}, \quad (3.3.46)$$

where $\mathcal{X} := \{C, D, T_8, T_1, T_r, M_2\}$.

$$Q^{T_8} = \frac{\lambda_{P_D P_L}}{\lambda_Q} P_D^{T_8} P_L, \quad (3.3.47)$$

$$Q^{T_1} = \frac{\lambda_{P_D P_L}}{\lambda_Q} P_D^{T_1} P_L, \quad (3.3.48)$$

$$Q^K = \frac{\lambda_{P_D P_L}}{\lambda_Q} P_D^K P_L. \quad (3.3.49)$$

A diagram encompassing the interactions of components is shown in [Figure 5](#).

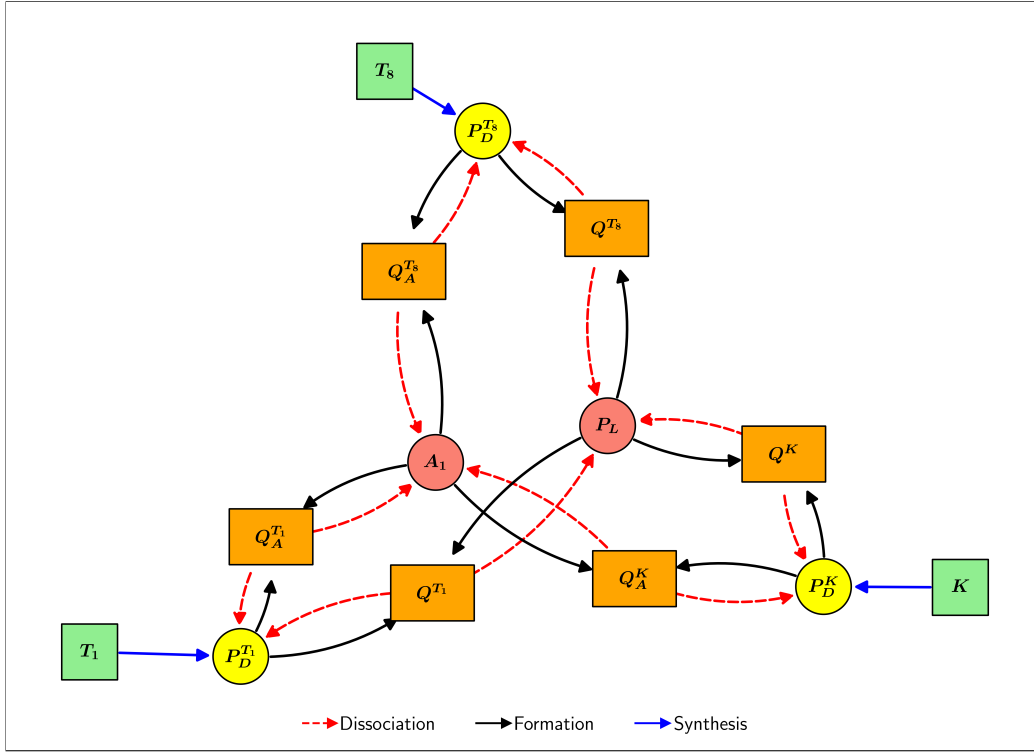


Figure 5: Schematic diagram of the interactions of immune checkpoint-associated components in the TS in the full model.

3.3.2.6 Equations for Immune Checkpoint-Associated Components in the TDLN

$$\frac{dP_D^{8LN}}{dt} = \underbrace{\lambda_{P_D^{8LN}} T_A^8}_{\text{synthesis}} + \underbrace{\lambda_{Q_A} Q_A^{8LN}}_{\text{dissociation of } Q_A^{8LN}} - \underbrace{\lambda_{P_D A_1} P_D^{8LN} A_1^{LN}}_{\text{binding to } A_1^{LN}} - \underbrace{d_{P_D} P_D^{8LN}}_{\text{degradation}}, \quad (3.3.50)$$

$$\frac{dP_D^{1LN}}{dt} = \underbrace{\lambda_{P_D^{1LN}} T_A^1}_{\text{synthesis}} + \underbrace{\lambda_{Q_A} Q_A^{1LN}}_{\text{dissociation of } Q_A^{1LN}} - \underbrace{\lambda_{P_D A_1} P_D^{1LN} A_1^{LN}}_{\text{binding to } A_1^{LN}} - \underbrace{d_{P_D} P_D^{1LN}}_{\text{degradation}}, \quad (3.3.51)$$

$$\frac{dQ_A^{8LN}}{dt} = \underbrace{\lambda_{P_D A_1} P_D^{8LN} A_1^{LN}}_{\text{formation of } Q_A^{8LN}} - \underbrace{\lambda_{Q_A} Q_A^{8LN}}_{\text{dissociation of } Q_A^{8LN}} - \underbrace{d_{Q_A} Q_A^{8LN}}_{\text{internalisation}}, \quad (3.3.52)$$

$$\frac{dQ_A^{1LN}}{dt} = \underbrace{\lambda_{P_D A_1} P_D^{1LN} A_1^{LN}}_{\text{formation of } Q_A^{1LN}} - \underbrace{\lambda_{Q_A} Q_A^{1LN}}_{\text{dissociation of } Q_A^{1LN}} - \underbrace{d_{Q_A} Q_A^{1LN}}_{\text{internalisation}}, \quad (3.3.53)$$

$$\frac{dA_1^{LN}}{dt} = \underbrace{\sum_{j=1}^n \xi_j f_{\text{pembro}} \delta(t - t_j)}_{\text{infusion}} + \underbrace{\lambda_{Q_A} (Q_A^{8LN} + Q_A^{1LN})}_{\text{dissociation of } Q_A^{8LN} \text{ and } Q_A^{1LN}} - \underbrace{\lambda_{P_D A_1} (P_D^{8LN} + P_D^{1LN}) A_1^{LN}}_{\text{formation of } Q_A^{8LN} \text{ and } Q_A^{1LN}} - \underbrace{d_{A_1} A_1^{LN}}_{\text{elimination}}, \quad (3.3.54)$$

$$\frac{dP_L^{LN}}{dt} = \underbrace{\sum_{Y \in \mathcal{Y}} \lambda_{P_L^{LN} Y} Y}_{\text{synthesis}} - \underbrace{d_{P_L} P_L^{LN}}_{\text{degradation}}, \quad (3.3.55)$$

where $\mathcal{Y} := \{D^{\text{LN}}, T_A^8, T_A^1, T_A^r\}$.

$$Q^{\text{8LN}} = \frac{\lambda_{P_D P_L}}{\lambda_Q} P_D^{\text{8LN}} P_L^{\text{LN}}, \quad (3.3.56)$$

$$Q^{\text{1LN}} = \frac{\lambda_{P_D P_L}}{\lambda_Q} P_D^{\text{1LN}} P_L^{\text{LN}}. \quad (3.3.57)$$

A diagram encompassing the interactions of these components is shown in Figure 6.

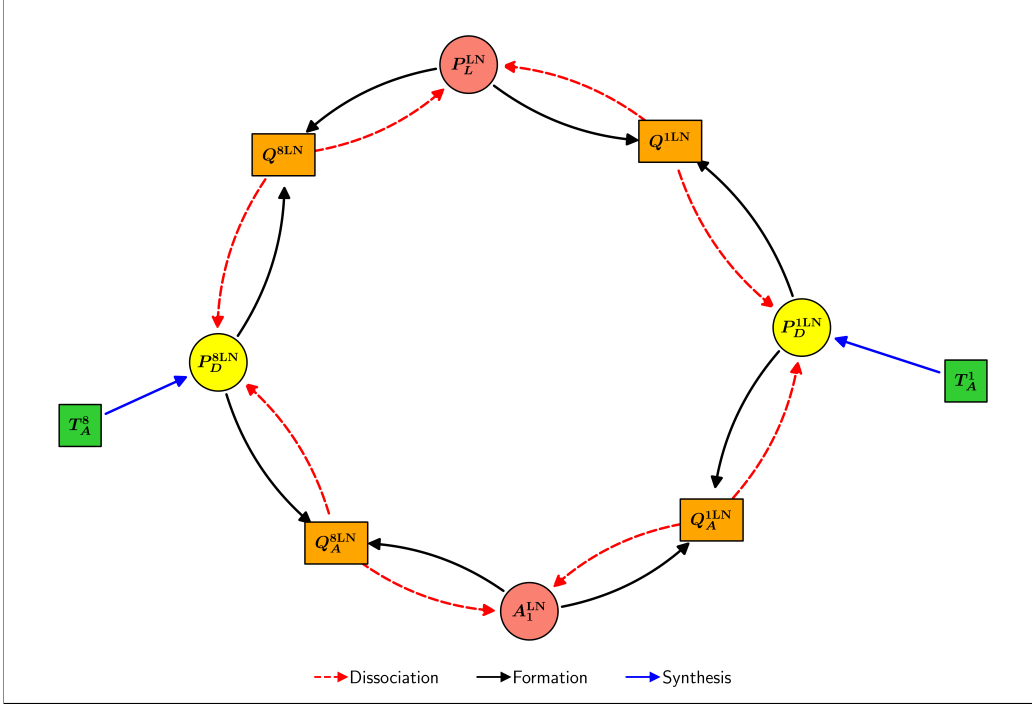


Figure 6: Schematic diagram of the interactions of immune checkpoint-associated components in the TDLN in the full model.

3.3.3 Steady States and Initial Conditions

All steady states and initial conditions are as in [38], but are repeated here for completeness.

3.3.3.1 Steady States and Initial Conditions for Cells in the TS

Table 2: TS steady-state cell densities for the full model. All values are in cell/cm³.

C	N_c	D_0	D	T_8	T_{ex}	T_1
7.02×10^7	3.69×10^6	9.55×10^5	1.91×10^6	1.77×10^5	1.24×10^5	1.06×10^5
T_r	M_0	M_1	M_2	K_0	K	
2.78×10^5	7.93×10^5	3.27×10^5	1.30×10^6	3.88×10^6	1.94×10^5	

Table 3: TS initial condition cell densities for the full model. All values are in cell/cm³.

C	N_c	D_0	D	T_8	T_{ex}	T_1
3.90×10^7	2.05×10^6	1.04×10^6	1.04×10^6	1.61×10^5	1.93×10^5	1.01×10^5
T_r	M_0	M_1	M_2	K_0	K	
2.02×10^5	2.50×10^5	2.09×10^5	1.29×10^6	4.47×10^6	4.47×10^5	

3.3.3.2 Steady States and Initial Conditions for Cells in the TDLN

Table 4: TDLN steady-state cell densities for the full model. All values are in cell/cm³.

D^{LN}	T_0^8	T_A^8	T_0^4	T_A^1	T_0^r	T_A^r
3.28×10^7	1.16×10^7	8.31×10^5	6.73×10^6	6.66×10^6	3.23×10^5	1.47×10^6

Table 5: TDLN initial condition cell densities for the full model. All values are in cell/cm³.

D^{LN}	T_0^8	T_A^8	T_0^4	T_A^1	T_0^r	T_A^r
1.78×10^7	1.20×10^7	8.60×10^5	4.31×10^6	7.76×10^6	1.72×10^5	7.81×10^5

3.3.3.3 Steady States and Initial Conditions for DAMPs

Table 6: DAMP steady states and initial conditions for the full model. All values are in units of g/cm³.

DAMP	Steady State	Initial Condition
H	1.94×10^{-8}	1.33×10^{-8}
S	4.50×10^{-8}	3.25×10^{-8}

3.3.3.4 Steady States and Initial Conditions for Cytokines

Table 7: Cytokine steady states and initial conditions for the full model. All values are in units of g/cm³.

Cytokine	Steady State	Initial Condition
I_2	2.00×10^{-12}	1.87×10^{-12}
I_γ	4.93×10^{-11}	1.10×10^{-10}
I_α	9.00×10^{-11}	1.25×10^{-10}
I_β	1.51×10^{-6}	9.20×10^{-7}
I_{10}	1.84×10^{-10}	1.15×10^{-10}

3.3.3.5 Steady States and Initial Conditions for Immune Checkpoint-Associated Components in the TS

Table 8: TS immune checkpoint-associated component steady states and initial conditions for the full model. All values are in units of molec/cm³.

Protein	Steady State	Initial Condition
$P_D^{T_8}$	4.87×10^8	4.44×10^8
$P_D^{T_1}$	2.17×10^8	2.07×10^8
P_D^K	1.07×10^8	2.46×10^8
P_L	1.30×10^{13}	7.40×10^{12}
Q^{T_8}	1.35×10^6	6.99×10^5
Q^{T_1}	6.01×10^5	3.26×10^5
Q^K	2.96×10^5	3.88×10^5

3.3.3.6 Steady States and Initial Conditions for Immune Checkpoint-Associated Components in the TDLN

Table 9: TDLN immune checkpoint-associated component steady states and initial conditions for the full model. All values are in units of molec/cm³.

Protein	Steady State	Initial Condition
P_D^{8LN}	2.29×10^9	2.37×10^9
P_D^{1LN}	1.37×10^{10}	1.59×10^{10}
P_L^{LN}	5.99×10^{11}	3.34×10^{11}
Q^{8LN}	2.92×10^5	1.69×10^5
Q^{1LN}	1.74×10^6	1.13×10^6

3.3.3.7 Steady States and Initial Conditions for Pembrolizumab-Associated Components in the TS

Table 10: Steady states and initial conditions for pembrolizumab-associated components in the TS in the full model. All values are in units of molec/cm³.

Protein	Steady State	Initial Condition
$Q_A^{T_8}$	0	0
$Q_A^{T_1}$	0	0
Q_A^K	0	0
A_1	0	0

3.3.3.8 Steady States and Initial Conditions for Pembrolizumab-Associated Components in the TDLN

Table 11: Steady states and initial conditions for pembrolizumab-associated components in the TDLN in the full model. All values are in units of molec/cm³.

Protein	Steady State	Initial Condition
Q_A^{8LN}	0	0
Q_A^{1LN}	0	0
A_1^{LN}	0	0

3.3.4 Sensitivity Analysis

We now perform a sensitivity analysis on the full model in order to assess the significance of its parameters of its parameters and identify avenues for model reduction. We simulated the standard regimen using the initial conditions in [Section 3.3.3](#) for 180.9 days—the duration of time needed for the cancer concentrations to reach their steady-state value without treatment as explained in [\[38\]](#). However, whilst we have gone into detail about variance-based sensitivity analysis methods for a function with single-valued output in [Section 2](#), the full model is multidimensional and time-dependent in its output. As such, we perform a sensitivity analysis on the constant vector defined by the root mean squared relative error (RMSRE) between the trajectories of the full model using parameters from [Table 1](#), and those generated from a given set of parameter inputs, at 180.9 days. To define the RMSRE, we first denote the trajectory of a state variable, X , using parameters from [Table 1](#) as $X(t)$, and the trajectory using a given set of parameters, \mathbf{p} , as $X_{\mathbf{p}}(t)$. The RMSRE at time t is then defined by

$$\text{RMSRE}_{\mathbf{p}}(t) := \sqrt{\frac{1}{t} \int_0^t \left(\frac{X_{\mathbf{p}}(s) - X(s)}{X(s)} \right)^2 ds}. \quad (3.3.58)$$

In particular, the RMSRE represents the overall accuracy of the reduction for a given variable by aggregating relative errors across the entire period of integration and penalising large deviations more heavily. We used the FAST method to compute the first-order sensitivity indices and the EFAST method for the total-order indices, with the model simulations carried out using the dde23 integrator. We then aggregated the output via [\(3.3.58\)](#) for each state variable, and a separate sensitivity analysis was performed for each state variable to obtain the corresponding indices.

One question that needs to be answered is regarding the number of parameters sampled. Denoting N as the number of samples per parameter, and noting that the full model contains 157 independent parameters, this corresponds to $157N$ combinations of parameters to be evaluated as part of the sensitivity analysis. Whilst in an ideal world one could have an arbitrarily large sample size, limits on the memory available to computers, as well as the time available for the computation to execute, restrict N . As such, we chose $N = 10,000$, corresponding to 1,570,000 parameter combinations in total, observing that the sensitivity indices showed convergence as the sample size approached this value, as indicated by minimal deviations in the indices. Similarly, choosing the value of M is a compromise between accuracy and computational expense. We choose $M = 4$ as this is the value that is usually used and is less susceptible to numerical error in the characteristic amplitudes, which tend to be larger for higher values of M [\[53\]](#). Additionally, we considered parameter ranges corresponding to a $\pm 50\%$ deviation for each parameter, noting that n_{\max}^8 , n_{\max}^1 , and n_{\max}^r are integers and were therefore rounded to the nearest integer.

The SALib Python library [54] was used to perform FAST and EFAST analysis on the full model with the aforementioned configuration, leading to the indices in Table F.1.

3.4 Reduced Model

We now aim to use the sensitivity analysis results of the full model found in Table F.1 to remove as many parameters as possible while still replicating the original trajectories and dynamics for each state variable. Each parameter in the model corresponds to a biochemical process, however, some processes are more influential on the model than others. In particular, by considering parameters with low maximal first-order and total-order sensitivity indices, we can assess whether the corresponding process has a sufficiently low impact. If so, we can simplify the model by eliminating the process—in most cases by setting the associated parameter to zero [21]. Indeed, we performed this for all insensitive parameters, with the exception of insensitive half-saturation and inhibition constants, which were treated separately. Before we proceeded, we made two key observations.

- 1) Regardless of the set of parameters eliminated, the degradation terms must remain. This is obvious from a biological standpoint and is well-supported by Table F.1. This makes sense from a mathematical standpoint as well—since we expect the state variables to be bounded.
- 2) These degradation terms cannot be the only terms present for any differential equation. If this were the case for a particular state variable, then the system would decouple, with that state variable exponentially decaying over time, and approaching 0 as $t \rightarrow \infty$. However, we expect the system to be persistent, with none of the biological state variables $\rightarrow 0$, as $t \rightarrow \infty$, implying that each differential equation must have both a positive and negative contribution — that is, at least 2 terms.

As a result, the following variables were set to 0: λ_{CI_γ} , λ_{DS} , $\lambda_{T_8 I_2}$, $\lambda_{T_1 I_2}$, λ_{MI_γ} , λ_{MI_α} , λ_{MI_β} , λ_{KD_0} , $\lambda_{I_\gamma T_8}$, $\lambda_{I_\gamma T_1}$, $\lambda_{I_{10} T_r}$, $\lambda_{I_{10} I_2}$, $\lambda_{P_L D}$, $\lambda_{P_L T_8}$, $\lambda_{P_L T_1}$, $\lambda_{P_L T_r}$, $\lambda_{P_L^{LN} T_A^8}$, $\lambda_{P_L^{LN} T_A^r}$, $K_{I_\gamma T_r}$, τ_8^{act} , τ_a , τ_l , τ_4^{act} , and τ_r^{act} . In particular, this also results in the elimination of K_{CI_γ} , K_{DS} , $K_{T_8 I_2}$, $K_{T_1 I_2}$, K_{MI_γ} , K_{MI_α} , K_{MI_β} , K_{KD_0} , $K_{I_{10} I_2}$, $K_{T_8 T_r}$. Additionally, we eliminate the inhibition constant, $K_{I_\gamma T_r}$ by removing the entire $\frac{1}{1+T_r/K_{I_\gamma T_r}}$ term from (3.3.33).

The elimination of τ_l and the T cell activation times requires special care, as the associated integrals will degenerate, and the corresponding half-saturation and inhibition constants must be redefined. As such, we replace all affected integrals with point estimate values evaluated at the lower bound of integration. As such, the following replacements are made:

$$\begin{aligned}
\int_{t-\tau_l}^t C(s) ds &\mapsto C(t) \text{ in (3.3.13) and (3.3.14),} \\
\int_{t-\tau_8^{\text{act}}}^t T_A^r(s) ds &\mapsto T_A^r(t) \text{ in (3.3.10),} \\
\int_{t-\tau_8^{\text{act}}}^t Q^{8\text{LN}}(s) ds &\mapsto Q^{8\text{LN}}(t) \text{ in (3.3.10),} \\
\int_{t-\tau_4^{\text{act}}}^t T_A^r(s) ds &\mapsto T_A^r(t) \text{ in (3.3.16),} \\
\int_{t-\tau_4^{\text{act}}}^t Q^{1\text{LN}}(s) ds &\mapsto Q^{1\text{LN}}(t) \text{ in (3.3.16).}
\end{aligned}$$

We also perform a similar simplification for the T cell proliferation integrals, such that

$$\begin{aligned} \int_{t-\tau_{T_A^8}}^t T_A^r(s) ds &\mapsto T_A^r(t - \tau_{T_A^8}) \text{ in (3.3.11),} \\ \int_{t-\tau_{T_A^8}}^t Q^{8\text{LN}}(s) ds &\mapsto Q^{8\text{LN}}(t - \tau_{T_A^8}) \text{ in (3.3.11),} \\ \int_{t-\tau_{T_A^1}}^t T_A^r(s) ds &\mapsto T_A^r(t - \tau_{T_A^1}) \text{ in (3.3.17),} \\ \int_{t-\tau_{T_A^1}}^t Q^{1\text{LN}}(s) ds &\mapsto Q^{1\text{LN}}(t - \tau_{T_A^1}) \text{ in (3.3.17).} \end{aligned}$$

It is worth noting that, by performing the model reduction in this manner, the biological interpretation of the individual parameters is preserved, as the approach does not rely on any transformations.

3.4.1 Model Equations

The model variables for the reduced models are the same as those in [Table 1](#).

$$\begin{aligned} \frac{dC}{dt} = & \underbrace{\lambda_C C \left(1 - \frac{C}{C_0}\right)}_{\text{growth}} - \underbrace{\lambda_{CT_8} T_8 \frac{1}{1 + I_\beta / K_{CI_\beta}} \frac{1}{1 + Q^{T_8} / K_{CQ^{T_8}}} C}_{\substack{\text{elimination by } T_8 \\ \text{inhibited by } I_\beta \text{ and } Q^{T_8}}} - \underbrace{\lambda_{CK} K \frac{1}{1 + I_\beta / K_{CI_\beta}} \frac{1}{1 + Q^K / K_{CQ^K}} C}_{\substack{\text{elimination by } K \\ \text{inhibited by } I_\beta \text{ and } Q^K}} \\ & - \underbrace{\lambda_{CI_\alpha} \frac{I_\alpha}{K_{CI_\alpha} + I_\alpha} C}_{\text{elimination by } I_\alpha}, \end{aligned} \tag{3.4.1}$$

$$\frac{dN_c}{dt} = \underbrace{\lambda_{CI_\alpha} \frac{I_\alpha}{K_{CI_\alpha} + I_\alpha} C}_{\text{Elimination by } I_\alpha} - \underbrace{d_{N_c} N_c}_{\text{Removal}}, \tag{3.4.2}$$

$$\begin{aligned} \frac{dV_{\text{TS}}}{dt} = & \frac{1}{f_C + f_{N_c}} \left[\lambda_C f_C V_{\text{TS}} \left(1 - \frac{f_C V_{\text{TS}}}{C_0}\right) - \lambda_{CT_8} T_8 \frac{1}{1 + I_\beta / K_{CI_\beta}} \frac{1}{1 + Q^{T_8} / K_{CQ^{T_8}}} f_C V_{\text{TS}} \right. \\ & \left. - \lambda_{CK} K \frac{1}{1 + I_\beta / K_{CI_\beta}} \frac{1}{1 + Q^K / K_{CQ^K}} f_C V_{\text{TS}} - d_{N_c} f_{N_c} V_{\text{TS}} \right], \end{aligned} \tag{3.4.3}$$

where $C(t) = f_C V_{\text{TS}}(t)$ and $N_c(t) = f_{N_c} V_{\text{TS}}(t)$.

$$\frac{dH}{dt} = \underbrace{\lambda_{HN_c} N_c}_{\text{production by } N_c} - \underbrace{d_H H}_{\text{degradation}}, \tag{3.4.4}$$

$$\frac{dS}{dt} = \underbrace{\lambda_{SN_c} N_c}_{\text{production by } N_c} - \underbrace{d_S S}_{\text{degradation}}, \tag{3.4.5}$$

$$\frac{dD_0}{dt} = \underbrace{\mathcal{A}_{D_0}}_{\text{source}} - \underbrace{\lambda_{DH}D_0 \frac{H}{K_{DH} + H}}_{D_0 \rightarrow D \text{ by } H} - \underbrace{\lambda_{D_0K}D_0K \frac{1}{1 + I_\beta/K_{D_0I_\beta}}}_{\text{elimination by } K \text{ inhibited by } I_\beta} - \underbrace{d_{D_0}D_0}_{\text{death}}, \quad (3.4.6)$$

$$\frac{dD}{dt} = \underbrace{\lambda_{DH}D_0 \frac{H}{K_{DH} + H}}_{D_0 \rightarrow D \text{ by } H} - \underbrace{\lambda_{DD^{\text{LN}}}D}_{D \text{ migration to TDLN}} - \underbrace{d_D D}_{\text{death}}, \quad (3.4.7)$$

$$\frac{dD^{\text{LN}}}{dt} = \frac{V_{\text{TS}}}{V_{\text{LN}}} \underbrace{\lambda_{DD^{\text{LN}}}e^{-d_D\tau_m}D(t - \tau_m)}_{D \text{ migration to TDLN}} - \underbrace{d_D D^{\text{LN}}}_{\text{death}}, \quad (3.4.8)$$

$$\frac{dT_0^8}{dt} = \underbrace{\mathcal{A}_{T_0^8}}_{\text{source}} - \underbrace{R^8(t)}_{\text{CD8+ T cell activation}} - \underbrace{d_{T_0^8}T_0^8}_{\text{death}}, \quad (3.4.9)$$

where $R^8(t)$ is defined as

$$R^8(t) := \frac{\lambda_{T_0^8 T_A^8} D^{\text{LN}}(t) T_0^8(t)}{\underbrace{\left(1 + T_A^r(t)/K_{T_0^8 T_A^r}\right) \left(1 + Q^{\text{8LN}}(t)/K_{T_0^8 Q^{\text{8LN}}}\right)}_{\text{CD8+ T cell activation inhibited by } T_A^r \text{ and } Q^{\text{8LN}}}}. \quad (3.4.10)$$

$$\frac{dT_A^8}{dt} = \frac{2^{n_{\text{max}}^8} e^{-d_{T_0^8} \tau_{T_A^8}} R^8(t - \tau_{T_A^8})}{\underbrace{\left(1 + T_A^r(t - \tau_{T_A^8}) ds/K_{T_A^8 T_A^r}\right) \left(1 + Q^{\text{8LN}}(t - \tau_{T_A^8})/K_{T_A^8 Q^{\text{8LN}}}\right)}_{\text{CD8+ T cell proliferation inhibited by } T_A^r \text{ and } Q^{\text{8LN}}}} - \underbrace{\lambda_{T_A^8 T_8} T_A^8}_{T_A^8 \text{ migration to the TS}} - \underbrace{d_{T_8} T_A^8}_{\text{death}}, \quad (3.4.11)$$

where $\tau_{T_A^8}$ is defined as

$$\tau_{T_A^8} := \Delta_8^0 + (n_{\text{max}}^8 - 1)\Delta_8. \quad (3.4.12)$$

$$\frac{dT_8}{dt} = \frac{V_{\text{LN}}}{V_{\text{TS}}} \underbrace{\lambda_{T_A^8 T_8} T_A^8}_{T_A^8 \text{ migration to the TS}} - \underbrace{\lambda_{T_8 C} \frac{T_8 C}{K_{T_8 C} + C}}_{T_8 \rightarrow T_{\text{ex}} \text{ from } C \text{ exposure}} + \underbrace{\lambda_{T_{\text{ex}} A_1} \frac{T_{\text{ex}} A_1}{K_{T_{\text{ex}} A_1} + A_1}}_{T_{\text{ex}} \rightarrow T_8 \text{ by } A_1} - \underbrace{\frac{d_{T_8} T_8}{1 + I_{10}/K_{T_8 I_{10}}}}_{\text{death inhibited by } I_{10}}, \quad (3.4.13)$$

$$\frac{dT_{\text{ex}}}{dt} = \underbrace{\lambda_{T_8 C} \frac{T_8 C}{K_{T_8 C} + C}}_{T_8 \rightarrow T_{\text{ex}} \text{ from } C \text{ exposure}} - \underbrace{\lambda_{T_{\text{ex}} A_1} \frac{T_{\text{ex}} A_1}{K_{T_{\text{ex}} A_1} + A_1}}_{T_{\text{ex}} \rightarrow T_8 \text{ by } A_1} - \underbrace{\frac{d_{T_{\text{ex}}} T_{\text{ex}}}{1 + I_{10}/K_{T_{\text{ex}} I_{10}}}}_{\text{death inhibited by } I_{10}}, \quad (3.4.14)$$

$$\frac{dT_0^4}{dt} = \underbrace{\mathcal{A}_{T_0^4}}_{\text{source}} - \underbrace{R^1(t)}_{\text{Th1 cell activation}} - \underbrace{d_{T_0^4} T_0^4}_{\text{death}}, \quad (3.4.15)$$

where $R^1(t)$ is defined as

$$R^1(t) := \frac{\lambda_{T_0^4 T_A^1} D^{\text{LN}}(t) T_0^4(t)}{\underbrace{\left(1 + T_A^r(t)/K_{T_0^4 T_A^r}\right) \left(1 + Q^{\text{1LN}}(t)/K_{T_0^4 Q^{\text{1LN}}}\right)}_{\text{Th1 cell activation inhibited by } T_A^r \text{ and } Q^{\text{1LN}}}}. \quad (3.4.16)$$

$$\frac{dT_A^1}{dt} = \underbrace{\frac{2^{n_{\max}^1} e^{-d_{T_0^1} \tau_{T_A^1}} R^1(t - \tau_{T_A^1})}{\left(1 + Q^{\text{ILN}}(t - \tau_{T_A^1})/K_{T_A^1 Q^{\text{ILN}}}\right) \left(1 + T_A^r(t - \tau_{T_A^1})/K_{T_A^1 T_A^r}\right)}}_{\text{Th1 cell proliferation inhibited by } T_A^r \text{ and } Q^{\text{ILN}}} - \underbrace{\lambda_{T_A^1 T_1} T_A^1}_{T_A^1 \text{ migration to the TS}} - \underbrace{d_{T_1} T_A^1}_{\text{death}}, \quad (3.4.17)$$

where $\tau_{T_A^1}$ is defined as

$$\tau_{T_A^1} := \Delta_1^0 + (n_{\max}^1 - 1)\Delta_1. \quad (3.4.18)$$

$$\frac{dT_1}{dt} = \frac{V_{\text{LN}}}{V_{\text{TS}}} \underbrace{\lambda_{T_A^1 T_1} T_A^1}_{T_A^1 \text{ migration to the TS}} - \underbrace{\lambda_{T_1 T_r} T_1 \frac{Q^{T_1}}{K_{T_1 T_r} + Q^{T_1}}}_{T_1 \rightarrow T_r \text{ by } Q^{T_1}} - \underbrace{d_{T_1} T_1}_{\text{death}}, \quad (3.4.19)$$

$$\frac{dT_0^r}{dt} = \underbrace{\mathcal{A}_{T_0^r}}_{\text{source}} - \underbrace{R^r(t)}_{\text{Treg activation}} - \underbrace{d_{T_0^r} T_0^r}_{\text{death}}, \quad (3.4.20)$$

where $R^r(t)$ is defined as

$$R^r(t) := \underbrace{\lambda_{T_0^r T_A^r} D^{\text{LN}}(t) T_0^r(t)}_{\text{Treg activation}}. \quad (3.4.21)$$

$$\frac{dT_A^r}{dt} = \underbrace{2^{n_{\max}^r} e^{-d_{T_0^r} \tau_{T_A^r}} R^r(t - \tau_{T_A^r})}_{\text{Treg proliferation}} - \underbrace{\lambda_{T_A^r T_r} T_A^r}_{T_A^r \text{ migration to the TS}} - \underbrace{d_{T_r} T_A^r}_{\text{death}}, \quad (3.4.22)$$

where $\tau_{T_A^r}$ is defined as

$$\tau_{T_A^r} := \Delta_r^0 + (n_{\max}^r - 1)\Delta_r. \quad (3.4.23)$$

$$\frac{dT_r}{dt} = \frac{V_{\text{LN}}}{V_{\text{TS}}} \underbrace{\lambda_{T_A^r T_r} T_A^r}_{T_A^r \text{ migration to the TS}} + \underbrace{\lambda_{T_1 T_r} T_1 \frac{Q^{T_1}}{K_{T_1 T_r} + Q^{T_1}}}_{T_1 \rightarrow T_r \text{ by } Q^{T_1}} - \underbrace{d_{T_r} T_r}_{\text{death}}, \quad (3.4.24)$$

$$\begin{aligned} \frac{dM_0}{dt} = & \underbrace{\mathcal{A}_{M_0}}_{\text{source}} - \underbrace{\lambda_{M_1 I_\alpha} M_0 \frac{I_\alpha}{K_{M_1 I_\alpha} + I_\alpha}}_{M_0 \rightarrow M_1 \text{ by } I_\alpha} - \underbrace{\lambda_{M_1 I_\gamma} M_0 \frac{I_\gamma}{K_{M_1 I_\gamma} + I_\gamma}}_{M_0 \rightarrow M_1 \text{ by } I_\gamma} - \underbrace{\lambda_{M_2 I_{10}} M_0 \frac{I_{10}}{K_{M_2 I_{10}} + I_{10}}}_{M_0 \rightarrow M_2 \text{ by } I_{10}} \\ & - \underbrace{\lambda_{M_2 I_\beta} M_0 \frac{I_\beta}{K_{M_2 I_\beta} + I_\beta}}_{M_0 \rightarrow M_2 \text{ by } I_\beta} - \underbrace{d_{M_0} M_0}_{\text{degradation}}, \end{aligned} \quad (3.4.25)$$

$$\frac{dM_1}{dt} = \underbrace{\lambda_{M_1 I_\alpha} M_0 \frac{I_\alpha}{K_{M_1 I_\alpha} + I_\alpha}}_{M_0 \rightarrow M_1 \text{ by } I_\alpha} + \underbrace{\lambda_{M_1 I_\gamma} M_0 \frac{I_\gamma}{K_{M_1 I_\gamma} + I_\gamma}}_{M_0 \rightarrow M_1 \text{ by } I_\gamma} - \underbrace{d_{M_1} M_1}_{\text{degradation}}, \quad (3.4.26)$$

$$\frac{dM_2}{dt} = \underbrace{\lambda_{M_2 I_{10}} M_0 \frac{I_{10}}{K_{M_2 I_{10}} + I_{10}}}_{M_0 \rightarrow M_2 \text{ by } I_{10}} + \underbrace{\lambda_{M_2 I_\beta} M_0 \frac{I_\beta}{K_{M_2 I_\beta} + I_\beta}}_{M_0 \rightarrow M_2 \text{ by } I_\beta} - \underbrace{d_{M_2} M_2}_{\text{degradation}}, \quad (3.4.27)$$

$$\frac{dK_0}{dt} = \underbrace{\mathcal{A}_{K_0}}_{\text{source}} - \left(\underbrace{\lambda_{KI_2} K_0 \frac{I_2}{K_{KI_2} + I_2}}_{K_0 \rightarrow K \text{ by } I_2} + \underbrace{\lambda_{KD} K_0 \frac{D}{K_{KD} + D}}_{K_0 \rightarrow K \text{ by } D} \right) \underbrace{\frac{1}{1 + I_\beta / K_{KI_\beta}}}_{\substack{\text{activation} \\ \text{inhibited by } I_\beta}} - \underbrace{d_{K_0} K_0}_{\text{degradation}}, \quad (3.4.28)$$

$$\frac{dK}{dt} = \left(\underbrace{\lambda_{KI_2} K_0 \frac{I_2}{K_{KI_2} + I_2}}_{K_0 \rightarrow K \text{ by } I_2} + \underbrace{\lambda_{KD} K_0 \frac{D}{K_{KD} + D}}_{K_0 \rightarrow K \text{ by } D} \right) \underbrace{\frac{1}{1 + I_\beta / K_{KI_\beta}}}_{\substack{\text{activation} \\ \text{inhibited by } I_\beta}} - \underbrace{d_K K}_{\text{degradation}}, \quad (3.4.29)$$

$$\frac{dI_2}{dt} = \underbrace{\lambda_{I_2 T_8} T_8}_{\text{production by } T_8} + \underbrace{\lambda_{I_2 T_1} T_1}_{\text{production by } T_1} - \underbrace{d_{I_2} I_2}_{\text{degradation}}. \quad (3.4.30)$$

After applying a QSSA, this becomes

$$I_2 = \frac{1}{d_{I_2}} (\lambda_{I_2 T_8} T_8 + \lambda_{I_2 T_1} T_1). \quad (3.4.31)$$

$$\frac{dI_\gamma}{dt} = \underbrace{\lambda_{I_\gamma K} K}_{\text{production by } K} - \underbrace{d_{I_\gamma} I_\gamma}_{\text{degradation}}. \quad (3.4.32)$$

After applying a QSSA, this becomes

$$I_\gamma = \frac{\lambda_{I_\gamma K}}{d_{I_\gamma}} K. \quad (3.4.33)$$

$$\frac{dI_\alpha}{dt} = \underbrace{\lambda_{I_\alpha T_8} T_8}_{\text{production by } T_8} + \underbrace{\lambda_{I_\alpha T_1} T_1}_{\text{production by } T_1} + \underbrace{\lambda_{I_\alpha M_1} M_1}_{\text{production by } M_1} + \underbrace{\lambda_{I_\alpha K} K}_{\text{production by } K} - \underbrace{d_{I_\alpha} I_\alpha}_{\text{degradation}}. \quad (3.4.34)$$

After applying a QSSA, this becomes

$$I_\alpha = \frac{1}{d_{I_\alpha}} (\lambda_{I_\alpha T_8} T_8 + \lambda_{I_\alpha T_1} T_1 + \lambda_{I_\alpha M_1} M_1 + \lambda_{I_\alpha K} K). \quad (3.4.35)$$

$$\frac{dI_\beta}{dt} = \underbrace{\lambda_{I_\beta C} C}_{\text{production by } C} + \underbrace{\lambda_{I_\beta T_r} T_r}_{\text{production by } T_r} + \underbrace{\lambda_{I_\beta M_2} M_2}_{\text{production by } M_2} - \underbrace{d_{I_\beta} I_\beta}_{\text{degradation}}. \quad (3.4.36)$$

After applying a QSSA, this becomes

$$I_\beta = \frac{1}{d_{I_\beta}} (\lambda_{I_\beta C} C + \lambda_{I_\beta T_r} T_r + \lambda_{I_\beta M_2} M_2). \quad (3.4.37)$$

$$\frac{dI_{10}}{dt} = \underbrace{\lambda_{I_{10} C} C}_{\text{production by } C} + \underbrace{\lambda_{I_{10} M_2} M_2}_{\text{production by } M_2} - \underbrace{d_{I_{10}} I_{10}}_{\text{degradation}}, \quad (3.4.38)$$

$$\frac{dP_D^{T_8}}{dt} = \underbrace{\lambda_{P_D^{T_8}} T_8}_{\text{synthesis}} + \underbrace{\lambda_{Q_A} Q_A^{T_8}}_{\substack{\text{dissociation} \\ \text{of } Q_A^{T_8}}} - \underbrace{\lambda_{P_D A_1} P_D^{T_8} A_1}_{\text{binding to } A_1} - \underbrace{d_{P_D} P_D^{T_8}}_{\text{degradation}}, \quad (3.4.39)$$

$$\frac{dP_D^{T_1}}{dt} = \underbrace{\lambda_{P_D^{T_1}} T_1}_{\text{synthesis}} + \underbrace{\lambda_{Q_A} Q_A^{T_1}}_{\text{dissociation of } Q_A^{T_1}} - \underbrace{\lambda_{P_D A_1} P_D^{T_1} A_1}_{\text{binding to } A_1} - \underbrace{d_{P_D} P_D^{T_1}}_{\text{degradation}}, \quad (3.4.40)$$

$$\frac{dP_D^K}{dt} = \underbrace{\lambda_{P_D^K} K}_{\text{synthesis}} + \underbrace{\lambda_{Q_A} Q_A^K}_{\text{dissociation of } Q_A^K} - \underbrace{\lambda_{P_D A_1} P_D^K A_1}_{\text{binding to } A_1} - \underbrace{d_{P_D} P_D^K}_{\text{degradation}}, \quad (3.4.41)$$

$$\frac{dQ_A^{T_8}}{dt} = \underbrace{\lambda_{P_D A_1} P_D^{T_8} A_1}_{\text{formation of } Q_A^{T_8}} - \underbrace{\lambda_{Q_A} Q_A^{T_8}}_{\text{dissociation of } Q_A^{T_8}} - \underbrace{d_{Q_A} Q_A^{T_8}}_{\text{internalisation}}, \quad (3.4.42)$$

$$\frac{dQ_A^{T_1}}{dt} = \underbrace{\lambda_{P_D A_1} P_D^{T_1} A_1}_{\text{formation of } Q_A^{T_1}} - \underbrace{\lambda_{Q_A} Q_A^{T_1}}_{\text{dissociation of } Q_A^{T_1}} - \underbrace{d_{Q_A} Q_A^{T_1}}_{\text{internalisation}}, \quad (3.4.43)$$

$$\frac{dQ_A^K}{dt} = \underbrace{\lambda_{P_D A_1} P_D^K A_1}_{\text{formation of } Q_A^K} - \underbrace{\lambda_{Q_A} Q_A^K}_{\text{dissociation of } Q_A^K} - \underbrace{d_{Q_A} Q_A^K}_{\text{internalisation}}, \quad (3.4.44)$$

$$\frac{dA_1}{dt} = \underbrace{\sum_{j=1}^n \xi_j f_{\text{pembro}} \delta(t - t_j)}_{\text{infusion}} + \underbrace{\lambda_{Q_A} (Q_A^{T_8} + Q_A^{T_1} + Q_A^K)}_{\text{dissociation of } Q_A^{T_8}, Q_A^{T_1}, \text{ and } Q_A^K} - \underbrace{\lambda_{P_D A_1} (P_D^{T_8} + P_D^{T_1} + P_D^K) A_1}_{\text{formation of } Q_A^{T_8}, Q_A^{T_1}, \text{ and } Q_A^K} - \underbrace{d_{A_1} A_1}_{\text{elimination}}, \quad (3.4.45)$$

$$\frac{dP_L}{dt} = \underbrace{\lambda_{P_L C} C + \lambda_{P_L M_2} M_2}_{\text{synthesis}} - \underbrace{d_{P_L} P_L}_{\text{degradation}}, \quad (3.4.46)$$

$$Q^{T_8} = \frac{\lambda_{P_D P_L} P_D^{T_8} P_L}{\lambda_Q}, \quad (3.4.47)$$

$$Q^{T_1} = \frac{\lambda_{P_D P_L} P_D^{T_1} P_L}{\lambda_Q}, \quad (3.4.48)$$

$$Q^K = \frac{\lambda_{P_D P_L} P_D^K P_L}{\lambda_Q}, \quad (3.4.49)$$

$$\frac{dP_D^{8LN}}{dt} = \underbrace{\lambda_{P_D^{8LN}} T_A^8}_{\text{synthesis}} + \underbrace{\lambda_{Q_A} Q_A^{8LN}}_{\text{dissociation of } Q_A^{8LN}} - \underbrace{\lambda_{P_D A_1} P_D^{8LN} A_1^{LN}}_{\text{binding to } A_1^{LN}} - \underbrace{d_{P_D} P_D^{8LN}}_{\text{degradation}}, \quad (3.4.50)$$

$$\frac{dP_D^{1LN}}{dt} = \underbrace{\lambda_{P_D^{1LN}} T_A^1}_{\text{synthesis}} + \underbrace{\lambda_{Q_A} Q_A^{1LN}}_{\text{dissociation of } Q_A^{1LN}} - \underbrace{\lambda_{P_D A_1} P_D^{1LN} A_1^{LN}}_{\text{binding to } A_1^{LN}} - \underbrace{d_{P_D} P_D^{1LN}}_{\text{degradation}}, \quad (3.4.51)$$

$$\frac{dQ_A^{8LN}}{dt} = \underbrace{\lambda_{P_D A_1} P_D^{8LN} A_1^{LN}}_{\text{formation of } Q_A^{8LN}} - \underbrace{\lambda_{Q_A} Q_A^{8LN}}_{\text{dissociation of } Q_A^{8LN}} - \underbrace{d_{Q_A} Q_A^{8LN}}_{\text{internalisation}}, \quad (3.4.52)$$

$$\frac{dQ_A^{1LN}}{dt} = \underbrace{\lambda_{P_D A_1} P_D^{1LN} A_1^{LN}}_{\text{formation of } Q_A^{1LN}} - \underbrace{\lambda_{Q_A} Q_A^{1LN}}_{\text{dissociation of } Q_A^{1LN}} - \underbrace{d_{Q_A} Q_A^{1LN}}_{\text{internalisation}}, \quad (3.4.53)$$

$$\frac{dA_1^{\text{LN}}}{dt} = \underbrace{\sum_{j=1}^n \xi_j f_{\text{pembro}} \delta(t - t_j)}_{\text{infusion}} + \underbrace{\lambda_{Q_A} (Q_A^{8\text{LN}} + Q_A^{1\text{LN}})}_{\text{dissociation of } Q_A^{8\text{LN}} \text{ and } Q_A^{1\text{LN}}} - \underbrace{\lambda_{P_D A_1} (P_D^{8\text{LN}} + P_D^{1\text{LN}}) A_1^{\text{LN}}}_{\text{formation of } Q_A^{8\text{LN}} \text{ and } Q_A^{1\text{LN}}} - \underbrace{d_{A_1} A_1^{\text{LN}}}_{\text{elimination}}, \quad (3.4.54)$$

$$\frac{dP_L^{\text{LN}}}{dt} = \underbrace{\lambda_{P_L^{\text{LN}} D^{\text{LN}}} D^{\text{LN}} + \lambda_{P_L^{\text{LN}} T_A^1} T_A^1}_{\text{synthesis}} - \underbrace{d_{P_L} P_L^{\text{LN}}}_{\text{degradation}}, \quad (3.4.55)$$

$$Q^{8\text{LN}} = \frac{\lambda_{P_D P_L}}{\lambda_Q} P_D^{8\text{LN}} P_L^{\text{LN}}, \quad (3.4.56)$$

$$Q^{1\text{LN}} = \frac{\lambda_{P_D P_L}}{\lambda_Q} P_D^{1\text{LN}} P_L^{\text{LN}}. \quad (3.4.57)$$

The model parameter values are estimated in [Appendix B](#) and are listed in [Table C.1](#).

3.4.2 Steady States and Initial Conditions

All steady states and initial conditions are the same as those in [Section 3.3.3](#), except for cytokines and the TS and TDLN immune checkpoint protein steady states and initial conditions, which are provided in [Table 12](#), [Table 13](#), and [Table 14](#), respectively. Justification for the choice of these values is done in [Appendix B.3](#), [Appendix B.7](#), and [Appendix B.8](#), respectively.

Table 12: Cytokine steady states and initial conditions for the reduced model. All values are in units of g/cm³.

Cytokine	Steady State	Initial Condition
I_2	2.00×10^{-12}	1.87×10^{-12}
I_γ	4.93×10^{-11}	1.14×10^{-10}
I_α	9.00×10^{-11}	1.25×10^{-10}
I_β	1.51×10^{-6}	9.20×10^{-7}
I_{10}	1.84×10^{-10}	1.15×10^{-10}

Table 13: TS immune checkpoint-associated component steady states and initial conditions for the reduced model. All values are in units of molec/cm³.

Protein	Steady State	Initial Condition
$P_D^{T_8}$	4.87×10^8	4.44×10^8
$P_D^{T_1}$	2.17×10^8	2.07×10^8
P_D^K	1.07×10^8	2.46×10^8
P_L	1.30×10^{13}	7.36×10^{12}
Q^{T_8}	1.35×10^6	6.96×10^5
Q^{T_1}	5.99×10^5	3.24×10^5
Q^K	2.95×10^5	3.86×10^5

Table 14: TDLN immune checkpoint-associated component steady states and initial conditions for the reduced model. All values are in units of molec/cm³.

Protein	Steady State	Initial Condition
P_D^{8LN}	2.29×10^9	2.37×10^9
P_D^{1LN}	1.37×10^{10}	1.59×10^{10}
P_L^{LN}	5.94×10^{11}	3.31×10^{11}
Q^{8LN}	2.90×10^5	1.67×10^5
Q^{1LN}	1.73×10^6	1.12×10^6

3.4.3 Sensitivity Analysis

We now perform a sensitivity analysis on the reduced model, following the same procedure as for the full model. We simulated the standard regimen for 180.9 days using the initial conditions from [Section 3.4.2](#), using the dde23 integrator and applying the FAST and EFAST methods to compute the first-order and total-order sensitivity indices, respectively. We sampled 10,000 samples for each parameter, as this was sufficient to reach convergence in the indices, setting $M = 4$, and considered parameter ranges corresponding to a $\pm 50\%$ deviation for each parameter, noting that n_{\max}^8 , n_{\max}^1 , and n_{\max}^r are integers, and were therefore rounded to the nearest integer.

The SALib Python library [\[54\]](#) was used to perform FAST and EFAST analysis on the reduced model with the aforementioned configuration, leading to the indices in [Table G.1](#).

3.5 Minimal Model

We now aim to use the sensitivity analysis results of the reduced model, presented in [Table G.1](#), to remove as many parameters and state variables as possible while still retaining the original trajectories and dynamics of the remaining state variables. Performing a similar analysis to that for the reduced model led us to eliminate the following state variables: S , T_A^1 , T_1 , M_0 , M_1 , M_2 , I_γ , $P_D^{T_1}$, $Q_A^{T_1}$, Q^{T_1} , P_D^{1LN} , Q_A^{1LN} , and Q^{1LN} . This was done simply by setting them to zero, resulting in the elimination of parameters associated with these variables as well. We also eliminated T_0^4 and K_0 by assuming that they are equal to positive constants, with their values absorbed into the corresponding kinetic constants. That is, we implicitly apply the transformations $\lambda_{T_0^8 T_A^8} \bar{T}_0^8 \mapsto \lambda_{T_0^8 T_A^8}$, $\lambda_{K I_2} \bar{K}_0 \mapsto \lambda_{K I_2}$, and $\lambda_{K D} \bar{K}_0 \mapsto \lambda_{K D}$, where \bar{T}_0^8 and \bar{K}_0 are as in both the full and reduced models.

We can further simplify the model by performing a QSSA on H , by considering the solution to $\frac{dH}{dt}$, or equivalently

$$H = \frac{\lambda_{H N_c}}{d_H} N_c. \quad (3.5.1)$$

We can eliminate H from the model by substituting (3.5.1) into (3.4.6) and (3.4.7) to get that

$$\begin{aligned} \frac{dD_0}{dt} &= \underbrace{\mathcal{A}_{D_0}}_{\text{source}} - \underbrace{\lambda_{D N_c} D_0 \frac{N_c}{K_{D N_c} + N_c}}_{D_0 \rightarrow D \text{ by } N_c} - \underbrace{\lambda_{D_0 K} D_0 K \frac{1}{1 + I_\beta / K_{D_0 I_\beta}}}_{\text{elimination by } K \text{ inhibited by } I_\beta} - \underbrace{d_{D_0} D_0}_{\text{death}}, \\ \frac{dD}{dt} &= \underbrace{\lambda_{D N_c} D_0 \frac{N_c}{K_{D N_c} + N_c}}_{D_0 \rightarrow D \text{ by } N_c} - \underbrace{\lambda_{D D^{LN}} D}_{D \text{ migration to TDLN}} - \underbrace{d_D D}_{\text{death}}, \end{aligned}$$

where $\lambda_{DN_c} = \lambda_{DH}$, and $K_{DN_c} = d_H K_{DH} / \lambda_{HN_c} = \overline{N_c}$.

Similarly, we can perform a QSSA on I_2 and I_{10} , leading to

$$I_2 = \frac{\lambda_{I_2 T_8}}{d_{I_2}} T_8, \quad (3.5.2)$$

$$I_{10} = \frac{\lambda_{I_{10} C}}{d_{I_{10}}} C, \quad (3.5.3)$$

respectively. We can thus similarly eliminate I_2 from the model by substituting (3.5.2) into (3.4.29), so that

$$\frac{dK}{dt} = \left(\underbrace{\lambda_{KT_8} \frac{T_8}{K_{KT_8} + T_8}}_{K_0 \rightarrow K \text{ by } T_8} + \underbrace{\lambda_{KD} \frac{D}{K_{KD} + D}}_{K_0 \rightarrow K \text{ by } D} \right) \underbrace{\frac{1}{1 + I_\beta / K_{KI_\beta}}}_{\substack{\text{activation} \\ \text{inhibited by } I_\beta}} - \underbrace{d_K K}_{\text{degradation}},$$

where $\lambda_{KT_8} = \lambda_{KI_2}$, and $K_{KT_8} = d_{I_2} K_{KI_2} / \lambda_{I_2 T_8} = \overline{T_8}$. Repeating this process to eliminate I_{10} , by substituting (3.5.3) into (3.5.13) and (3.5.14), leads to

$$\begin{aligned} \frac{dT_8}{dt} &= \frac{V_{LN}}{V_{TS}} \underbrace{\lambda_{T_A^8 T_8} T_A^8}_{\substack{T_A^8 \text{ migration} \\ \text{to the TS}}} - \underbrace{\lambda_{T_8 C} \frac{T_8 C}{K_{T_8 T_{ex}} + C}}_{T_8 \rightarrow T_{ex} \text{ from } C \text{ exposure}} + \underbrace{\lambda_{T_{ex} A_1} \frac{T_{ex} A_1}{K_{T_{ex} A_1} + A_1}}_{T_{ex} \rightarrow T_8 \text{ by } A_1} - \underbrace{\frac{d_{T_8} T_8}{1 + C / K_{T_8 C}}}_{\substack{\text{death} \\ \text{inhibited by } C}}, \\ \frac{dT_{ex}}{dt} &= \underbrace{\lambda_{T_8 C} \frac{T_8 C}{K_{T_8 T_{ex}} + C}}_{T_8 \rightarrow T_{ex} \text{ from } C \text{ exposure}} - \underbrace{\lambda_{T_{ex} A_1} \frac{T_{ex} A_1}{K_{T_{ex} A_1} + A_1}}_{T_{ex} \rightarrow T_8 \text{ by } A_1} - \underbrace{\frac{d_{T_{ex}} T_{ex}}{1 + C / K_{T_{ex} C}}}_{\substack{\text{death} \\ \text{inhibited by } C}}, \end{aligned}$$

where $K_{T_8 C} = d_{I_{10}} K_{T_8 I_{10}} / \lambda_{I_{10} C} = \overline{C}$ and $K_{T_{ex} C} = d_{I_{10}} K_{T_{ex} I_{10}} / \lambda_{I_{10} C} = \overline{C}$. We note that we have relabelled the half-saturation constant for CD8+ T cell exhaustion due to prolonged cancer antigen exposure as $K_{T_8 T_{ex}}$ to avoid confusion with the inhibition constant associated with CD8+ T cell death mediated by IL-10.

3.5.1 Model Variables

The variables and their units in the minimal model are shown in Table 15.

Table 15: Variables used in the minimal model. Quantities in the top box are in units of cell/cm³, quantities in the second box are in units of g/cm³, and all other quantities are in units of molec/cm³. All quantities pertain to the tumour site unless otherwise specified. TDLN denotes the tumour-draining lymph node, whilst TS denotes the tumour site.

Var	Description	Var	Description
V_{TS}	Primary tumour volume		
C	Viable cancer cell density	N_c	Necrotic cell density
D_0	Immature DC density	D	Mature DC density in the TS
D^{LN}	Mature DC density at TDLN	T_A^8	Effector CD8+ T cell density in the TDLN
T_8	Effector CD8+ T cell density in the TS	T_{ex}	Exhausted CD8+ T cell density in the TS
T_0^r	Naive Treg density in the TDLN	T_A^r	Effector Treg density in the TDLN
T_r	Effector Treg density in the TS	K	Activated NK cell density
I_α	TNF concentration	I_β	TGF- β concentration
$P_D^{T_8}$	Unbound PD-1 receptor concentration on effector CD8+ T cells in the TS	P_D^K	Unbound PD-1 receptor concentration on activated NK cells
$Q_A^{T_8}$	PD-1/pembrolizumab complex concentration on effector CD8+ T cells in the TS	Q_A^K	PD-1/pembrolizumab complex concentration on activated NK cells
P_L	Unbound PD-L1 concentration in the TS	Q^{T_8}	PD-1/PD-L1 complex concentration on effector CD8+ T cells in the TS
Q^K	PD-1/PD-L1 complex concentration on activated NK cells	A_1	Concentration of pembrolizumab in the TS
P_D^{8LN}	Unbound PD-1 receptor concentration on effector CD8+ T cells in the TDLN	Q_A^{8LN}	PD-1/pembrolizumab complex concentration on effector CD8+ T cells in the TDLN
P_L^{LN}	Unbound PD-L1 concentration in the TDLN	Q^{8LN}	PD-1/PD-L1 complex concentration on effector CD8+ T cells in the TDLN
A_1^{LN}	Concentration of pembrolizumab in the TDLN		

3.5.2 Model Equations

$$\begin{aligned}
\frac{dC}{dt} = & \underbrace{\lambda_C C \left(1 - \frac{C}{C_0}\right)}_{\text{growth}} - \underbrace{\lambda_{CT_8} T_8 \frac{1}{1 + I_\beta / K_{CI_\beta}} \frac{1}{1 + Q^{T_8} / K_{CQ^{T_8}}} C}_{\substack{\text{elimination by } T_8 \\ \text{inhibited by } I_\beta \text{ and } Q^{T_8}}} - \underbrace{\lambda_{CK} K \frac{1}{1 + I_\beta / K_{CI_\beta}} \frac{1}{1 + Q^K / K_{CQ^K}} C}_{\substack{\text{elimination by } K \\ \text{inhibited by } I_\beta \text{ and } Q^K}} \\
& - \underbrace{\lambda_{CI_\alpha} \frac{I_\alpha}{K_{CI_\alpha} + I_\alpha} C}_{\text{elimination by } I_\alpha},
\end{aligned} \tag{3.5.4}$$

$$\frac{dN_c}{dt} = \underbrace{\lambda_{CI_\alpha} \frac{I_\alpha}{K_{CI_\alpha} + I_\alpha} C}_{\text{Elimination by } I_\alpha} - \underbrace{d_{N_c} N_c}_{\text{Removal}}, \tag{3.5.5}$$

$$\begin{aligned}
\frac{dV_{TS}}{dt} = & \frac{1}{f_C + f_{N_c}} \left[\lambda_C f_C V_{TS} \left(1 - \frac{f_C V_{TS}}{C_0}\right) - \lambda_{CT_8} T_8 \frac{1}{1 + I_\beta / K_{CI_\beta}} \frac{1}{1 + Q^{T_8} / K_{CQ^{T_8}}} f_C V_{TS} \right. \\
& \left. - \lambda_{CK} K \frac{1}{1 + I_\beta / K_{CI_\beta}} \frac{1}{1 + Q^K / K_{CQ^K}} f_C V_{TS} - d_{N_c} f_{N_c} V_{TS} \right],
\end{aligned} \tag{3.5.6}$$

where $C(t) = f_C V_{TS}(t)$ and $N_c(t) = f_{N_c} V_{TS}(t)$.

$$\frac{dD_0}{dt} = \underbrace{\mathcal{A}_{D_0}}_{\text{source}} - \underbrace{\lambda_{DN_c} D_0 \frac{N_c}{K_{DN_c} + N_c}}_{D_0 \rightarrow D \text{ by DAMPs}} - \underbrace{\lambda_{D_0 K} D_0 K \frac{1}{1 + I_\beta / K_{D_0 I_\beta}}}_{\text{elimination by } K \text{ inhibited by } I_\beta} - \underbrace{d_{D_0} D_0}_{\text{death}}, \quad (3.5.7)$$

$$\frac{dD}{dt} = \underbrace{\lambda_{DN_c} D_0 \frac{N_c}{K_{DN_c} + N_c}}_{D_0 \rightarrow D \text{ by DAMPs}} - \underbrace{\lambda_{DD^{LN}} D}_{D \text{ migration to TDLN}} - \underbrace{d_D D}_{\text{death}}, \quad (3.5.8)$$

$$\frac{dD^{LN}}{dt} = \frac{V_{TS}}{V_{LN}} \underbrace{\lambda_{DD^{LN}} e^{-d_D \tau_m} D(t - \tau_m)}_{D \text{ migration to TDLN}} - \underbrace{d_D D^{LN}}_{\text{death}}, \quad (3.5.9)$$

$$\frac{dT_A^8}{dt} = \frac{2^{n_{\max}^8} e^{-d_{T_0^8} \tau_{T_A^8}} R^8(t - \tau_{T_A^8})}{\underbrace{\left(1 + T_A^r(t - \tau_{T_A^8}) \frac{ds}{K_{T_A^8 T_A^r}}\right) \left(1 + Q^{8LN}(t - \tau_{T_A^8}) / K_{T_A^8 Q^{8LN}}\right)}_{\text{CD8+ T cell proliferation inhibited by } T_A^r \text{ and } Q^{8LN}}} - \underbrace{\lambda_{T_A^8 T_8} T_A^8}_{T_A^8 \text{ migration to the TS}} - \underbrace{d_{T_8} T_A^8}_{\text{death}}, \quad (3.5.10)$$

where $\tau_{T_A^8}$ is defined as

$$\tau_{T_A^8} := \Delta_8^0 + (n_{\max}^8 - 1) \Delta_8, \quad (3.5.11)$$

and where $R^8(t)$ is defined as

$$R^8(t) := \frac{\lambda_{T_0^8 T_A^8} D^{LN}(t)}{\underbrace{\left(1 + T_A^r(t) / K_{T_0^8 T_A^r}\right) \left(1 + Q^{8LN}(t) / K_{T_0^8 Q^{8LN}}\right)}_{\text{CD8+ T cell activation inhibited by } T_A^r \text{ and } Q^{8LN}}}. \quad (3.5.12)$$

$$\frac{dT_8}{dt} = \frac{V_{LN}}{V_{TS}} \underbrace{\lambda_{T_A^8 T_8} T_A^8}_{T_A^8 \text{ migration to the TS}} - \underbrace{\lambda_{T_8 C} \frac{T_8 C}{K_{T_8 T_{\text{ex}}} + C}}_{T_8 \rightarrow T_{\text{ex}} \text{ from } C \text{ exposure}} + \underbrace{\lambda_{T_{\text{ex}} A_1} \frac{T_{\text{ex}} A_1}{K_{T_{\text{ex}} A_1} + A_1}}_{T_{\text{ex}} \rightarrow T_8 \text{ by } A_1} - \underbrace{\frac{d_{T_8} T_8}{1 + C / K_{T_8 C}}}_{\text{death inhibited by IL-10}}, \quad (3.5.13)$$

$$\frac{dT_{\text{ex}}}{dt} = \underbrace{\lambda_{T_8 C} \frac{T_8 C}{K_{T_8 T_{\text{ex}}} + C}}_{T_8 \rightarrow T_{\text{ex}} \text{ from } C \text{ exposure}} - \underbrace{\lambda_{T_{\text{ex}} A_1} \frac{T_{\text{ex}} A_1}{K_{T_{\text{ex}} A_1} + A_1}}_{T_{\text{ex}} \rightarrow T_8 \text{ by } A_1} - \underbrace{\frac{d_{T_{\text{ex}}} T_{\text{ex}}}{1 + C / K_{T_{\text{ex}} C}}}_{\text{death inhibited by IL-10}}, \quad (3.5.14)$$

$$\frac{dT_0^r}{dt} = \underbrace{\mathcal{A}_{T_0^r}}_{\text{source}} - \underbrace{R^r(t)}_{\text{Treg activation}} - \underbrace{d_{T_0^r} T_0^r}_{\text{death}}, \quad (3.5.15)$$

where $R^r(t)$ is defined as

$$R^r(t) := \underbrace{\lambda_{T_0^r T_A^r} D^{LN}(t) T_0^r(t)}_{\text{Treg activation}}. \quad (3.5.16)$$

$$\frac{dT_A^r}{dt} = \underbrace{2^{n_{\max}^r} e^{-d_{T_0^r} \tau_{T_A^r}} R^r(t - \tau_{T_A^r})}_{\text{Treg proliferation}} - \underbrace{\lambda_{T_A^r T_r} T_A^r}_{T_A^r \text{ migration to the TS}} - \underbrace{d_{T_r} T_A^r}_{\text{death}}, \quad (3.5.17)$$

where $\tau_{T_A^r}$ is defined as

$$\tau_{T_A^r} := \Delta_r^0 + (n_{\max}^r - 1) \Delta_r. \quad (3.5.18)$$

$$\frac{dT_r}{dt} = \frac{V_{LN}}{V_{TS}} \underbrace{\lambda_{T_A^r T_r} T_A^r}_{T_A^r \text{ migration to the TS}} - \underbrace{d_{T_r} T_r}_{\text{death}}, \quad (3.5.19)$$

$$\frac{dK}{dt} = \left(\underbrace{\lambda_{KT_8} \frac{T_8}{K_{KT_8} + T_8}}_{K_0 \rightarrow K \text{ by IL-2}} + \underbrace{\lambda_{KD} \frac{D}{K_{KD} + D}}_{K_0 \rightarrow K \text{ by } D} \right) \underbrace{\frac{1}{1 + I_\beta / K_{KI_\beta}}}_{\text{activation inhibited by } I_\beta} - \underbrace{d_K K}_{\text{degradation}}, \quad (3.5.20)$$

$$\frac{dI_\alpha}{dt} = \underbrace{\lambda_{I_\alpha T_8} T_8}_{\text{production by } T_8} + \underbrace{\lambda_{I_\alpha K} K}_{\text{production by } K} - \underbrace{d_{I_\alpha} I_\alpha}_{\text{degradation}}. \quad (3.5.21)$$

After applying a QSSA, this becomes

$$I_\alpha = \frac{1}{d_{I_\alpha}} (\lambda_{I_\alpha T_8} T_8 + \lambda_{I_\alpha K} K). \quad (3.5.22)$$

$$\frac{dI_\beta}{dt} = \underbrace{\lambda_{I_\beta C} C}_{\text{production by } C} + \underbrace{\lambda_{I_\beta T_r} T_r}_{\text{production by } T_r} - \underbrace{d_{I_\beta} I_\beta}_{\text{degradation}}. \quad (3.5.23)$$

After applying a QSSA, this becomes

$$I_\beta = \frac{1}{d_{I_\beta}} (\lambda_{I_\beta C} C + \lambda_{I_\beta T_r} T_r). \quad (3.5.24)$$

$$\frac{dP_D^{T_8}}{dt} = \underbrace{\lambda_{P_D^{T_8}} T_8}_{\text{synthesis}} + \underbrace{\lambda_{Q_A} Q_A^{T_8}}_{\text{dissociation of } Q_A^{T_8}} - \underbrace{\lambda_{P_D A_1} P_D^{T_8} A_1}_{\text{binding to } A_1} - \underbrace{d_{P_D} P_D^{T_8}}_{\text{degradation}}, \quad (3.5.25)$$

$$\frac{dP_D^K}{dt} = \underbrace{\lambda_{P_D^K} K}_{\text{synthesis}} + \underbrace{\lambda_{Q_A} Q_A^K}_{\text{dissociation of } Q_A^K} - \underbrace{\lambda_{P_D A_1} P_D^K A_1}_{\text{binding to } A_1} - \underbrace{d_{P_D} P_D^K}_{\text{degradation}}, \quad (3.5.26)$$

$$\frac{dQ_A^{T_8}}{dt} = \underbrace{\lambda_{P_D A_1} P_D^{T_8} A_1}_{\text{formation of } Q_A^{T_8}} - \underbrace{\lambda_{Q_A} Q_A^{T_8}}_{\text{dissociation of } Q_A^{T_8}} - \underbrace{d_{Q_A} Q_A^{T_8}}_{\text{internalisation}}, \quad (3.5.27)$$

$$\frac{dQ_A^K}{dt} = \underbrace{\lambda_{P_D A_1} P_D^K A_1}_{\text{formation of } Q_A^K} - \underbrace{\lambda_{Q_A} Q_A^K}_{\text{dissociation of } Q_A^K} - \underbrace{d_{Q_A} Q_A^K}_{\text{internalisation}}, \quad (3.5.28)$$

$$\frac{dA_1}{dt} = \underbrace{\sum_{j=1}^n \xi_j f_{\text{pembro}} \delta(t - t_j)}_{\text{infusion}} + \underbrace{\lambda_{Q_A} (Q_A^{T_8} + Q_A^K)}_{\text{dissociation of } Q_A^{T_8} \text{ and } Q_A^K} - \underbrace{\lambda_{P_D A_1} (P_D^{T_8} + P_D^K) A_1}_{\text{formation of } Q_A^{T_8} \text{ and } Q_A^K} - \underbrace{d_{A_1} A_1}_{\text{elimination}}, \quad (3.5.29)$$

$$\frac{dP_L}{dt} = \underbrace{\lambda_{P_L C} C}_{\text{synthesis}} - \underbrace{d_{P_L} P_L}_{\text{degradation}}, \quad (3.5.30)$$

$$Q^{T_8} = \frac{\lambda_{P_D P_L} P_D^{T_8} P_L}{\lambda_Q}, \quad (3.5.31)$$

$$Q^K = \frac{\lambda_{P_D P_L} P_D^K P_L}{\lambda_Q}, \quad (3.5.32)$$

$$\frac{dP_D^{8LN}}{dt} = \underbrace{\lambda_{P_D^{8LN}} T_A^8}_{\text{synthesis}} + \underbrace{\lambda_{Q_A} Q_A^{8LN}}_{\text{dissociation of } Q_A^{8LN}} - \underbrace{\lambda_{P_D A_1} P_D^{8LN} A_1^{LN}}_{\text{binding to } A_1^{LN}} - \underbrace{d_{P_D} P_D^{8LN}}_{\text{degradation}}, \quad (3.5.33)$$

$$\frac{dQ_A^{8LN}}{dt} = \underbrace{\lambda_{P_D A_1} P_D^{8LN} A_1^{LN}}_{\text{formation of } Q_A^{8LN}} - \underbrace{\lambda_{Q_A} Q_A^{8LN}}_{\text{dissociation of } Q_A^{8LN}} - \underbrace{d_{Q_A} Q_A^{8LN}}_{\text{internalisation}}, \quad (3.5.34)$$

$$\frac{dA_1^{LN}}{dt} = \underbrace{\sum_{j=1}^n \xi_j f_{\text{pembro}} \delta(t - t_j)}_{\text{infusion}} + \underbrace{\lambda_{Q_A} Q_A^{8LN}}_{\text{dissociation of } Q_A^{8LN}} - \underbrace{\lambda_{P_D A_1} P_D^{8LN} A_1^{LN}}_{\text{formation of } Q_A^{8LN}} - \underbrace{d_{A_1} A_1^{LN}}_{\text{elimination}}, \quad (3.5.35)$$

$$\frac{dP_L^{LN}}{dt} = \underbrace{\lambda_{P_L^{LN} D^{LN}} D^{LN}}_{\text{synthesis}} - \underbrace{d_{P_L} P_L^{LN}}_{\text{degradation}}, \quad (3.5.36)$$

$$Q^{8LN} = \frac{\lambda_{P_D P_L}}{\lambda_Q} P_D^{8LN} P_L^{LN}. \quad (3.5.37)$$

The model parameter values are estimated in [Appendix D](#) and are listed in [Table E.1](#).

3.5.3 Steady States and Initial Conditions

All steady states and initial conditions are the same as those in [Section 3.3.3](#), except for cytokines and the TS and TDLN immune checkpoint protein steady states and initial conditions, which are provided in [Table 16](#), [Table 17](#), and [Table 18](#), respectively. Justification for the choice of these values is done in [Appendix D.3](#), [Appendix D.6](#), and [Appendix D.7](#), respectively.

Table 16: Cytokine steady states and initial conditions for the minimal model. All values are in units of g/cm³.

Cytokine	Steady State	Initial Condition
I_α	9.00×10^{-11}	1.64×10^{-10}
I_β	1.51×10^{-6}	8.45×10^{-7}

Table 17: TS immune checkpoint-associated component steady states and initial conditions for the minimal model. All values are in units of molec/cm³.

Protein	Steady State	Initial Condition
$P_D^{T_8}$	4.87×10^8	4.44×10^8
P_D^K	1.07×10^8	2.46×10^8
P_L	1.26×10^{13}	7.02×10^{12}
Q^{T_8}	1.31×10^6	6.63×10^5
Q^K	2.87×10^5	3.68×10^5

Table 18: TDLN immune checkpoint-associated component steady states and initial conditions for the minimal model. All values are in units of molec/cm³.

Protein	Steady State	Initial Condition
P_D^{SLN}	2.29×10^9	2.37×10^9
P_L^{LN}	5.81×10^{11}	3.15×10^{11}
Q^{SLN}	2.83×10^5	1.59×10^5

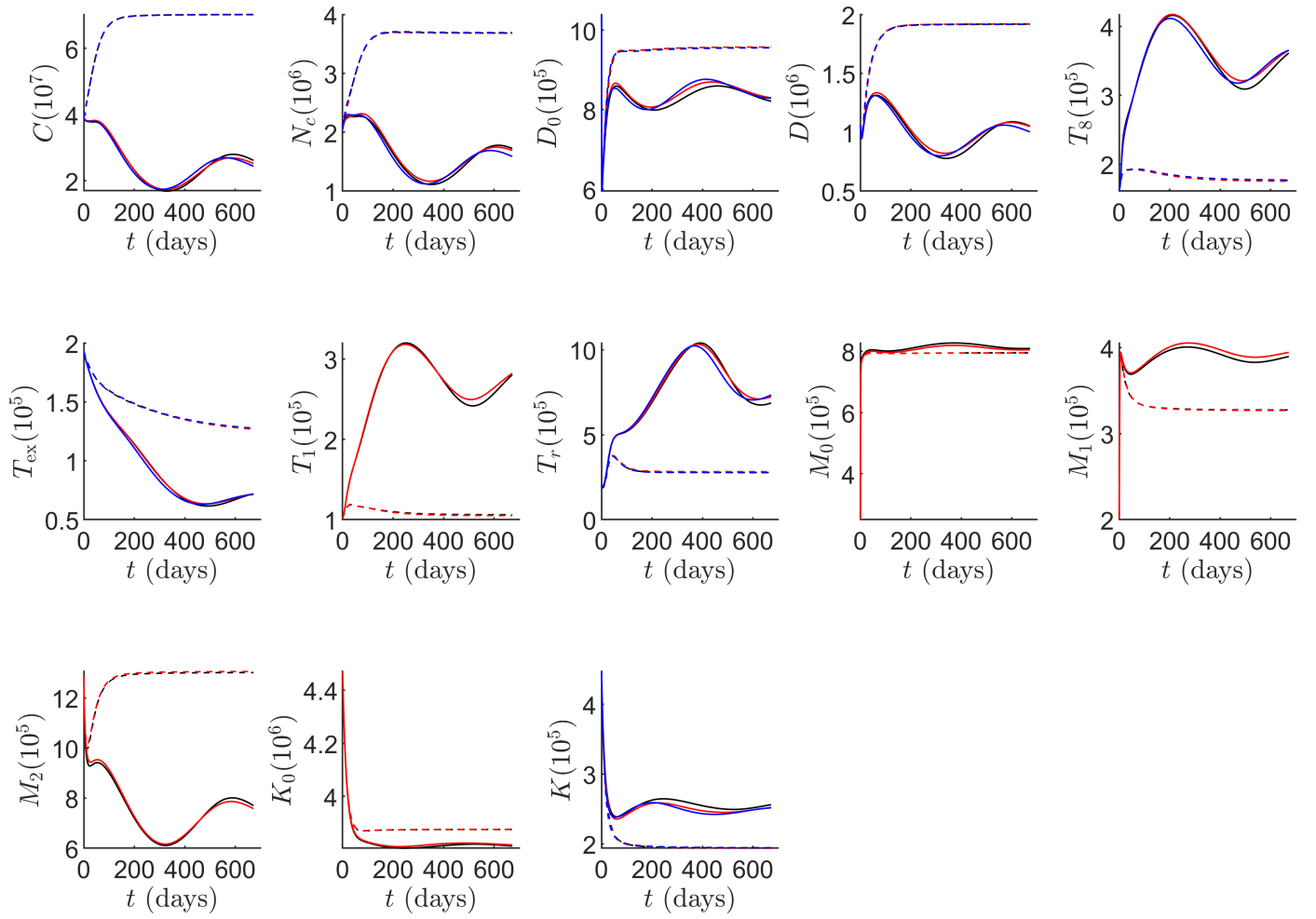
3.5.4 Sensitivity Analysis

We now perform a sensitivity analysis on the minimal model, following the same procedure as for the full and reduced models. We simulated the standard regimen for 180.9 days using the initial conditions from [Section 3.5.3](#), using the dde23 integrator and applying the FAST and EFAST methods to compute the first-order and total-order sensitivity indices, respectively. We sampled 10,000 samples for each parameter, as this was sufficient to reach convergence in the indices, setting $M = 4$, and considered parameter ranges corresponding to a $\pm 50\%$ deviation for each parameter, noting that n_{\max}^8 and n_{\max}^r are integers, and were therefore rounded to the nearest integer.

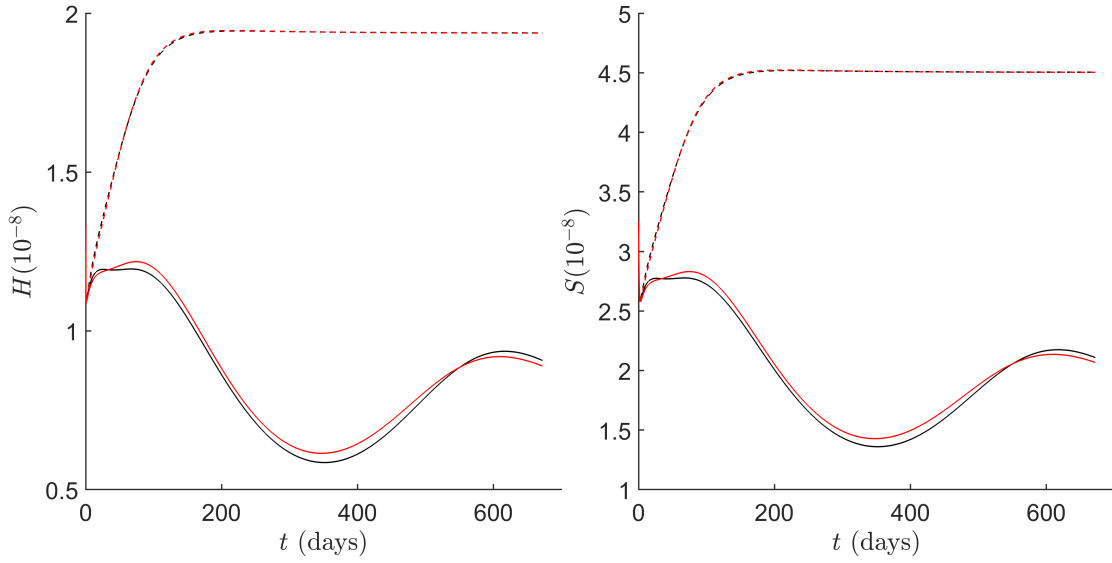
The SALib Python library [\[54\]](#) was used to perform FAST and EFAST analysis on the reduced model with the aforementioned configuration, leading to the indices in [Table H.1](#).

4 Results

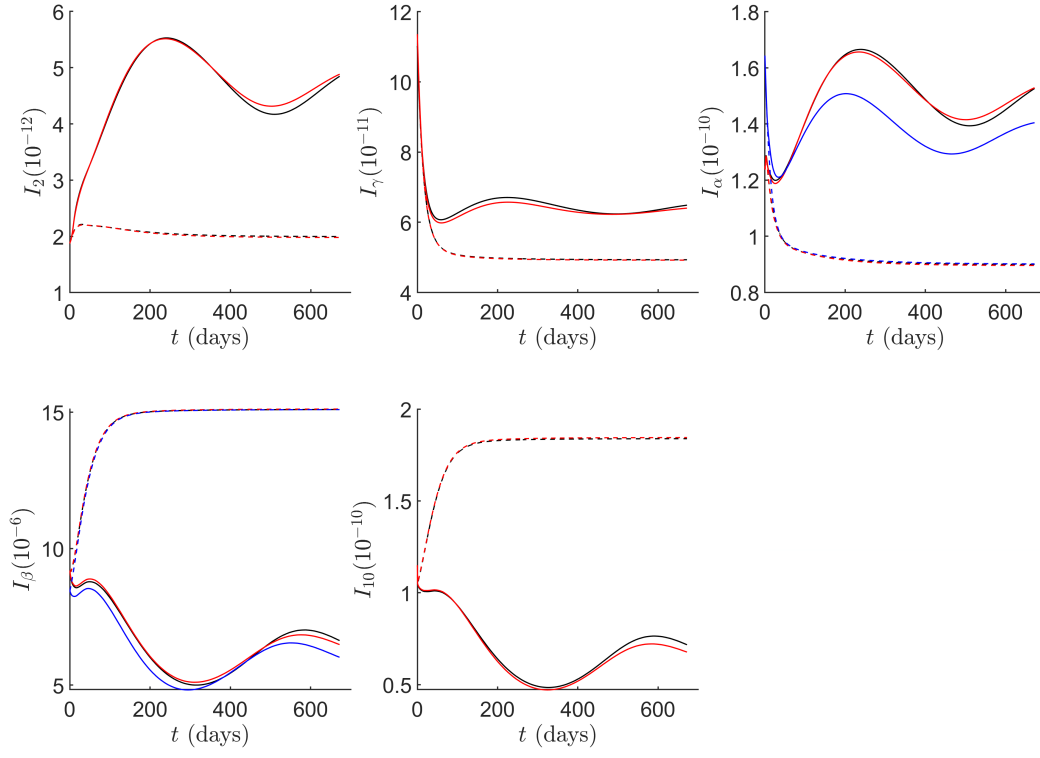
We compare the trajectories of the full, reduced, and minimal models by examining the time traces of model variables in the cases of no treatment and the standard regimen, as shown in [Figure 7](#). Furthermore, time traces for the primary tumour volume, V_{TS} , from the full, reduced, and minimal models in the cases of no treatment and the standard regimen are shown in [Figure 8](#).



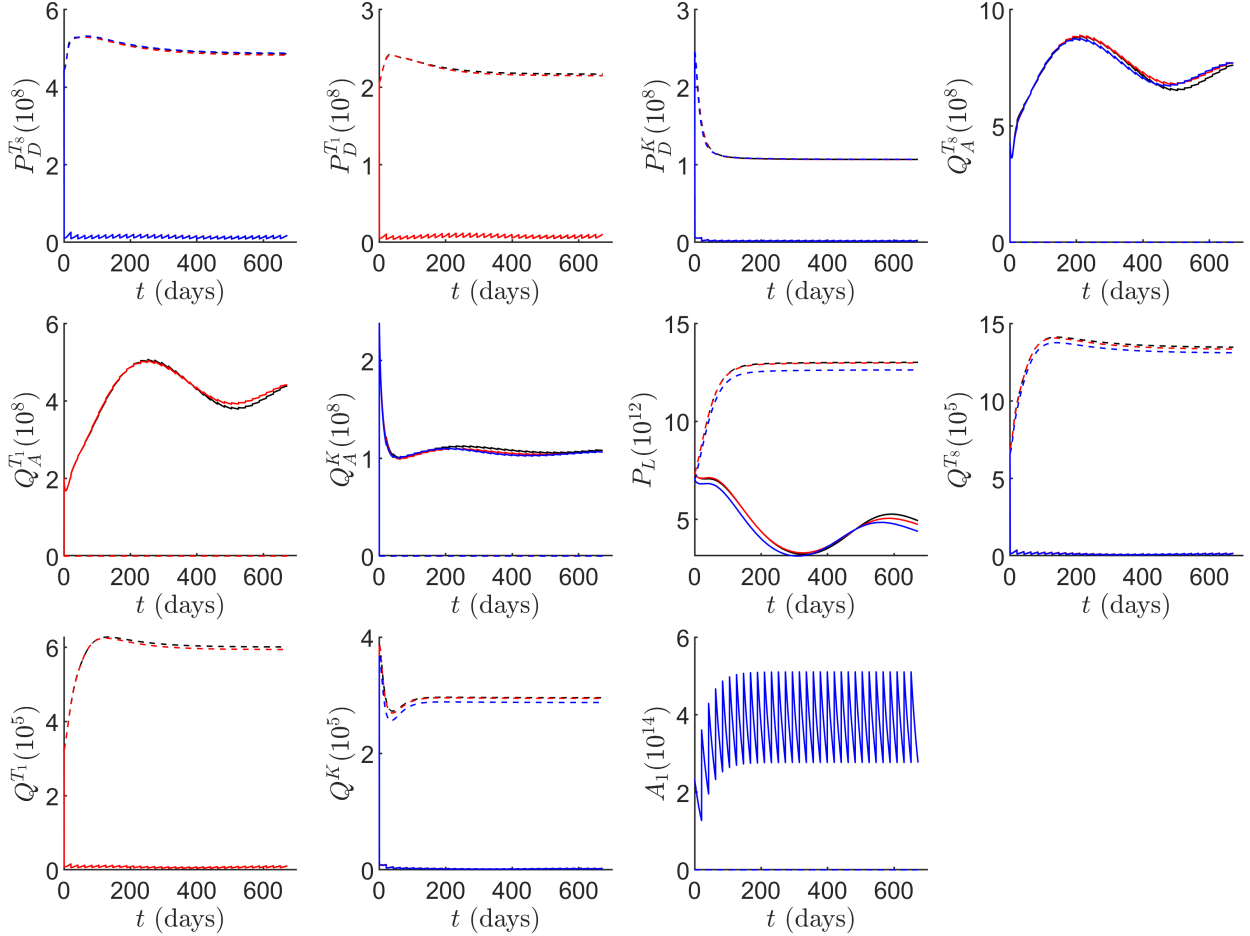
(a) Time traces of cell densities in the TS.



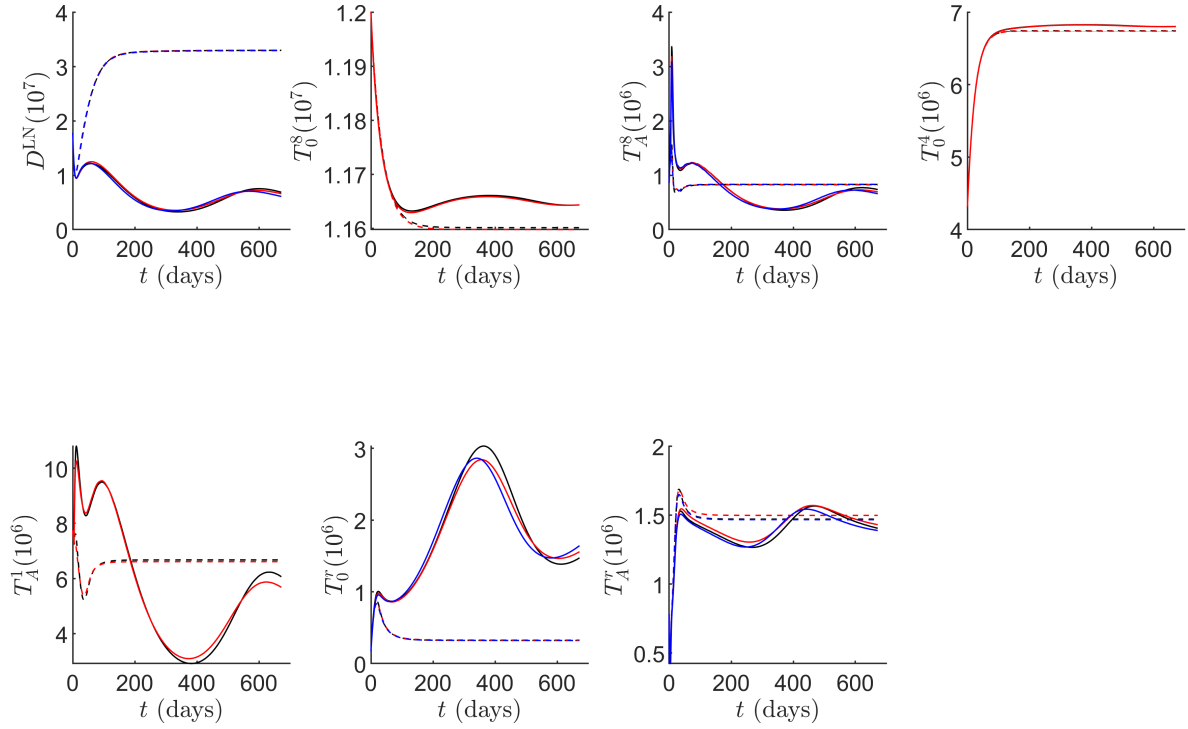
(b) Time traces of DAMP concentrations in the TS.



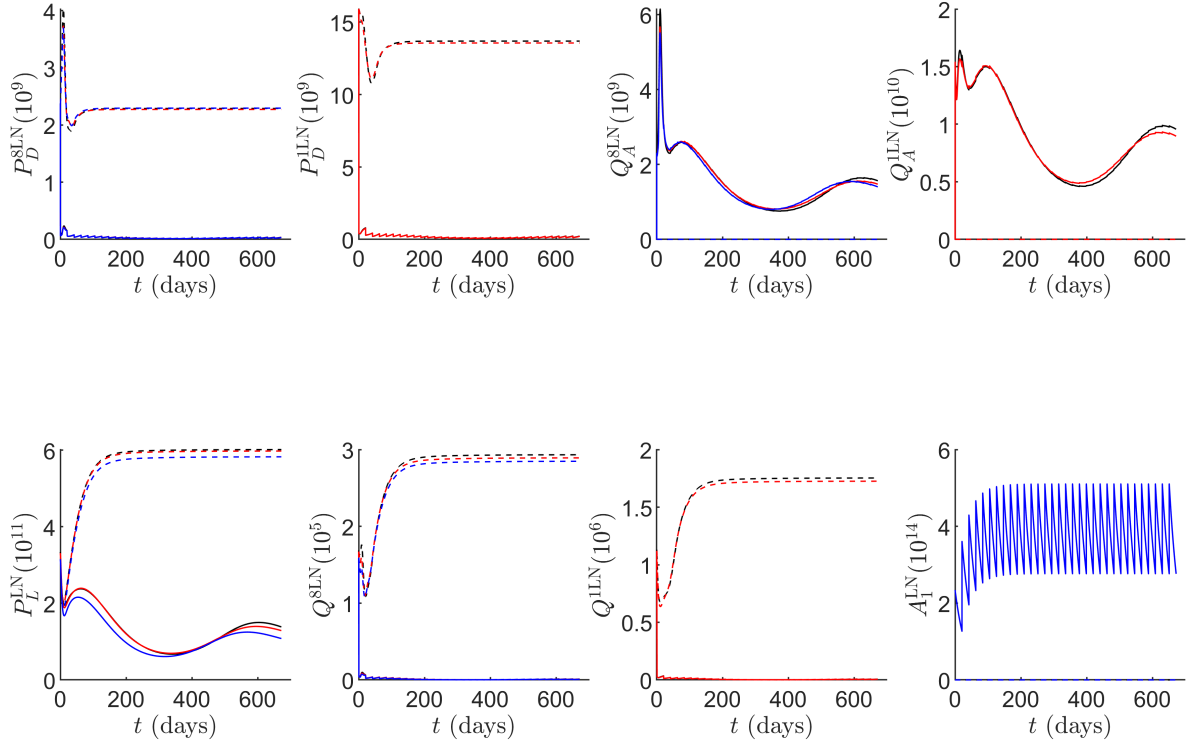
(c) Time traces of cytokine concentrations in the TS.



(d) Time traces of pembrolizumab and immune checkpoint-associated concentrations in the TS.



(e) Time traces of cell densities in the TDLN.



(f) Time traces of pembrolizumab and immune checkpoint-associated concentrations in the TDLN.

Figure 7: Time traces of variables up to 672 days in the minimal, reduced, and full models, with the units of the variables as in Table 1. Time traces from the full model are shown in black, from the reduced model in red, and from the minimal model in blue, with dashed lines indicating no treatment and solid lines indicating the standard regimen.

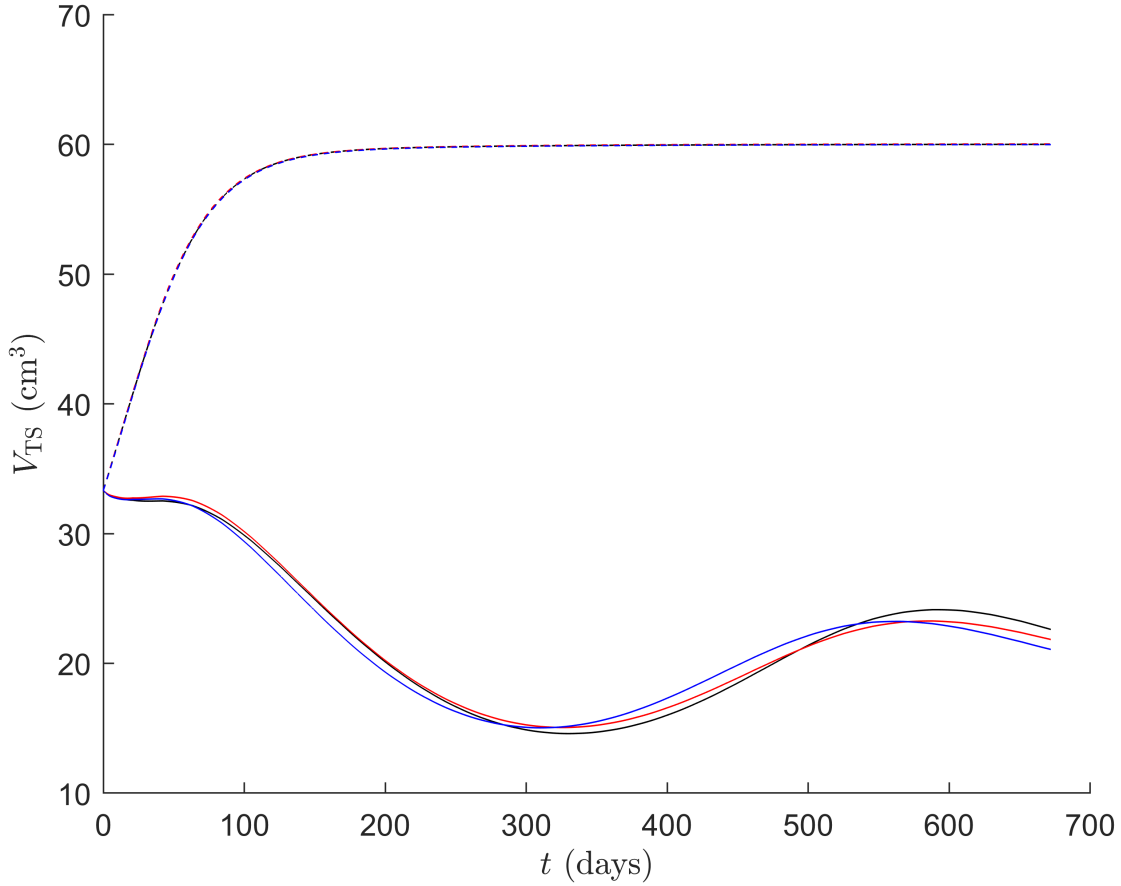


Figure 8: Time traces of V_{TS} up to 672 days from commencement from the minimal, reduced, and full models. Time traces from the full model are shown in black, from the reduced model in red, and from the minimal model in blue, with dashed lines indicating no treatment and solid lines indicating the standard regimen.

To quantitatively evaluate how well the reduced and minimal models replicate the trajectories of the full model, we consider two statistical measures: the maximum relative error (MRE) and the RMSRE. These measures are particularly well-suited for comparing models with dimensioned data and variables that span multiple orders of magnitude.

To define these measures, we first denote X_{approx} as the variable in the reduced and minimal models corresponding to the variable X_{full} in the full model. The MRE at time t is then defined as

$$\text{MRE}(t) := \max_{s \in [0, t]} \left| \frac{X_{\text{approx}}(s) - X_{\text{full}}(s)}{X_{\text{full}}(s)} \right|, \quad (4.1)$$

whilst the RMSRE at time t is defined as

$$\text{RMSRE}(t) := \sqrt{\frac{1}{t} \int_0^t \left(\frac{X_{\text{approx}}(s) - X_{\text{full}}(s)}{X_{\text{full}}(s)} \right)^2 ds}, \quad (4.2)$$

in identical fashion to (3.3.58). In particular, the MRE represents the maximum deviation in a variable's trajectory between the full and simplified models. The MRE and RMSRE at 180.9 days and 672 days, both without treatment and under the standard regimen, are shown in Table 19 and Table 20

for variables in the reduced and minimal models, respectively.

Table 19: MRE and RMSRE between the reduced model and the full model at 180.9 days and 672 days, in the cases of no treatment and the standard regimen.

Variable	No Treatment				Standard Regimen			
	MRE at 180.9 days	RMSRE at 180.9 days	MRE at 672 days	RMSRE at 672 days	MRE at 180.9 days	RMSRE at 180.9 days	MRE at 672 days	RMSRE at 672 days
V_{TS}	0.0023734	0.0011311	0.0023734	0.0008632	0.0121151	0.0082577	0.0393465	0.0238138
C	0.0028276	0.0014299	0.0028276	0.0010730	0.0119563	0.0077838	0.0406321	0.0237730
N_c	0.0116307	0.0070559	0.0116307	0.0050830	0.0239736	0.0193486	0.0532521	0.0306637
D_0	0.0111911	0.0060997	0.0111911	0.0044845	0.0130414	0.0069654	0.0199002	0.0116856
D	0.0050825	0.0024155	0.0050825	0.0017696	0.0212771	0.0162837	0.0583087	0.0323700
D^{LN}	0.0074041	0.0032461	0.0074041	0.0024157	0.0292734	0.0239427	0.0976282	0.0530018
T_0^8	0.0003015	0.0001725	0.0003036	0.0002443	0.0002914	0.0002265	0.0002914	0.0001807
T_A^8	0.1176080	0.0554367	0.1176080	0.0402138	0.3381936	0.0426412	0.3381936	0.0490073
T_8	0.0118881	0.0046049	0.0118881	0.0056179	0.0215579	0.0073560	0.0418209	0.0209546
T_{ex}	0.0041987	0.0023023	0.0041987	0.0023141	0.0023742	0.0007896	0.0315004	0.0150487
T_0^4	0.0006140	0.0003765	0.0006197	0.0005077	0.0006537	0.0005110	0.0006537	0.0003966
T_A^1	0.0509770	0.0246850	0.0509770	0.0189467	0.0752486	0.0134399	0.0772959	0.0403713
T_1	0.0058466	0.0025310	0.0095796	0.0066107	0.0074193	0.0048965	0.0349808	0.0163249
T_0^r	0.0579932	0.0337331	0.0579932	0.0262837	0.0564815	0.0158846	0.0729100	0.0417866
T_A^r	0.3607671	0.0932472	0.3607671	0.0682983	0.3575233	0.0428688	0.3575233	0.0288222
T_r	0.0426825	0.0245072	0.0426825	0.0208654	0.0396430	0.0129175	0.0542403	0.0223937
M_0	0.0090110	0.0054764	0.0090110	0.0039405	0.0092214	0.0062718	0.0096419	0.0077581
M_1	0.0175630	0.0050505	0.0175630	0.0037992	0.0175664	0.0057575	0.0175664	0.0118202
M_2	0.0234309	0.0143249	0.0234309	0.0105519	0.0252418	0.0137304	0.0252418	0.0118795
K_0	0.0008137	0.0004406	0.0008137	0.0003211	0.0010401	0.0008128	0.0020765	0.0013507
K	0.0128971	0.0066352	0.0128971	0.0048838	0.0158519	0.0124569	0.0305380	0.0200647
H	0.0116299	0.0070071	0.0116299	0.0050480	0.0239736	0.0193350	0.0532520	0.0306621
S	0.0116177	0.0068527	0.0116177	0.0049372	0.0239730	0.0192928	0.0532508	0.0306566
I_2	0.0071315	0.0031239	0.0086286	0.0061209	0.0102981	0.0054271	0.0369606	0.0175178
I_γ	0.0305339	0.0138417	0.0305339	0.0101214	0.0305339	0.0183497	0.0305339	0.0143329
I_α	0.0069435	0.0034038	0.0069435	0.0037210	0.0095717	0.0035390	0.0178490	0.0087006
I_β	0.0050327	0.0034577	0.0050327	0.0025952	0.0116172	0.0085044	0.0277417	0.0165819
I_{10}	0.0043210	0.0033474	0.0043210	0.0032899	0.0182637	0.0080897	0.0589050	0.0322900
P_D^{Ts}	0.0106262	0.0038416	0.0106262	0.0053039	0.0203469	0.0073149	0.0418084	0.0209389
$P_D^{T_1}$	0.0056780	0.0022927	0.0095794	0.0065533	0.0074107	0.0048876	0.0349697	0.0163154
P_D^K	0.0127414	0.0060668	0.0127414	0.0044844	0.0158096	0.0123657	0.0305355	0.0200480
Q_A^{Ts}	0.0000000	0.0000000	0.0000000	0.0000000	0.0203293	0.0073279	0.0418054	0.0209380
$Q_A^{T_1}$	0.0000000	0.0000000	0.0000000	0.0000000	0.0074095	0.0048879	0.0349663	0.0163140
Q_A^K	0.0000000	0.0000000	0.0000000	0.0000000	0.0158079	0.0123532	0.0305338	0.0200462
P_L	0.0054054	0.0018101	0.0054054	0.0020073	0.0083754	0.0048989	0.0437430	0.0224439
Q^{Ts}	0.0106080	0.0043049	0.0106080	0.0067769	0.0178932	0.0086467	0.0449959	0.0240326
Q^{T_1}	0.0082186	0.0031159	0.0116895	0.0081573	0.0134638	0.0085448	0.0330700	0.0185309
Q^K	0.0125800	0.0066470	0.0125800	0.0054160	0.0155286	0.0091175	0.0560795	0.0265618
A_1	0.0000000	0.0000000	0.0000000	0.0000000	0.3901297	0.0041671	0.3901297	0.0031769
P_D^{8LN}	0.0970748	0.0451112	0.0970748	0.0328601	0.2211528	0.0317253	0.2211528	0.0466997
P_D^{1LN}	0.0445350	0.0206293	0.0445350	0.0162430	0.0458369	0.0125530	0.0772799	0.0401409
Q_A^{8LN}	0.0000000	0.0000000	0.0000000	0.0000000	0.2054100	0.0314589	0.2054100	0.0466267
Q_A^{1LN}	0.0000000	0.0000000	0.0000000	0.0000000	0.0457394	0.0125347	0.0772585	0.0401058
P_L^{LN}	0.0232450	0.0130925	0.0232450	0.0104517	0.0373812	0.0092167	0.0738867	0.0346097
Q^{8LN}	0.1165856	0.0540520	0.1165856	0.0400645	0.2362887	0.0372978	0.2362887	0.0757193
Q^{1LN}	0.0639956	0.0315627	0.0639956	0.0252690	0.0776799	0.0212030	0.1309049	0.0698038
A_1^{LN}	0.0000000	0.0000000	0.0000000	0.0000000	0.3905869	0.0041715	0.3905869	0.0031790

Table 20: MRE and RMSRE between the minimal model and the full model at 180.9 days and at 672 days, in the cases of no treatment and the standard regimen.

Variable	No Treatment				Standard Regimen			
	MRE at 180.9 days	RMSRE at 180.9 days	MRE at 672 days	RMSRE at 672 days	MRE at 180.9 days	RMSRE at 180.9 days	MRE at 672 days	RMSRE at 672 days
V_{TS}	0.0024068	0.0015786	0.0024068	0.0011702	0.0393053	0.0218701	0.0836609	0.0454335
C	0.0034820	0.0022233	0.0034820	0.0016458	0.0390739	0.0221238	0.0856075	0.0461282
N_c	0.0180043	0.0110073	0.0180043	0.0081071	0.0425986	0.0202978	0.0785886	0.0386240
D_0	0.0173109	0.0091230	0.0173109	0.0066168	0.0151593	0.0093197	0.0324771	0.0165763
D	0.0240020	0.0117156	0.0240020	0.0084664	0.0322543	0.0198373	0.0627882	0.0340109
D^{LN}	0.0212806	0.0087804	0.0212806	0.0064094	0.0698406	0.0393707	0.1515504	0.0796794
T_A^8	0.1205968	0.0600061	0.1205968	0.0432066	0.3483231	0.0577471	0.3483231	0.0823991
T_8	0.0123520	0.0056882	0.0123520	0.0046167	0.0293080	0.0088689	0.0491172	0.0247417
T_{ex}	0.0037352	0.0017204	0.0037427	0.0025960	0.0251028	0.0112476	0.0458564	0.0273572
T_0^r	0.0663734	0.0423494	0.0663734	0.0304796	0.0647645	0.0384575	0.1339163	0.0715741
T_A^r	0.3475644	0.0869672	0.3475644	0.0625942	0.3443561	0.0384203	0.3443561	0.0271378
T_r	0.0372989	0.0203915	0.0372989	0.0149035	0.0409380	0.0210639	0.0687808	0.0368607
K	0.0394841	0.0222479	0.0394841	0.0161036	0.0349595	0.0118913	0.0472535	0.0276112
I_α	0.3160494	0.1203937	0.3160494	0.0866372	0.3160355	0.0712895	0.3160355	0.0875083
I_β	0.0815496	0.0346187	0.0815496	0.0249066	0.0815496	0.0544669	0.0930705	0.0545702
$P_D^{T_8}$	0.0109792	0.0049939	0.0109792	0.0041829	0.0279134	0.0088848	0.0490822	0.0247239
P_D^K	0.0386324	0.0194238	0.0386324	0.0140869	0.0343874	0.0117107	0.0472614	0.0275892
$Q_A^{T_8}$	0.0000000	0.0000000	0.0000000	0.0000000	0.0278835	0.0089090	0.0490940	0.0247264
Q_A^K	0.0000000	0.0000000	0.0000000	0.0000000	0.0343683	0.0117090	0.0472444	0.0275741
P_L	0.0513514	0.0380499	0.0513514	0.0343658	0.0840797	0.0593228	0.1107315	0.0614505
Q^{T_8}	0.0513514	0.0385474	0.0513514	0.0334537	0.0881127	0.0597162	0.0995980	0.0584293
Q^K	0.0729991	0.0525336	0.0729991	0.0423383	0.0909687	0.0627461	0.1257442	0.0743049
A_1	0.0000000	0.0000000	0.0000000	0.0000000	0.4868756	0.0048969	0.4868756	0.0036682
P_D^{SLN}	0.0963670	0.0494992	0.0963670	0.0356555	0.2311865	0.0501352	0.2311865	0.0809391
Q_A^{SLN}	0.0000000	0.0000000	0.0000000	0.0000000	0.2156159	0.0496510	0.2156159	0.0808541
P_L^{LN}	0.0990899	0.0632076	0.0990899	0.0505471	0.1931496	0.1386761	0.2195455	0.1367663
Q^{SLN}	0.1798825	0.0966435	0.1798825	0.0724442	0.3020117	0.1689593	0.3020117	0.1771299
A_1^{LN}	0.0000000	0.0000000	0.0000000	0.0000000	0.4882693	0.0049396	0.4882693	0.0036959

5 Discussion

We first discuss the results in Table F.1, which pertain to SA of the full model. We observe that the most significant parameters underpinning tumour growth over time, and by extension the viable and necrotic cancer cell density over time, are f_C , λ_C , λ_{CT_8} , λ_{CK} , C_0 , K_{CI_β} . These processes correspond to the logistic growth of cancer cells and their lysis by effector CD8+ T cells and NK cells, which is inhibited by TGF- β . We must also note that cancer cell necrosis via TNF is also significant, however only appears in the equations for C and N_c , and does not appear in the equation for V_{TS} . We note that the parameters $\lambda_{CQ^{T_8}}$ and λ_{CQ^K} are also important; however, their exact values are less critical, as the concentration of the PD-1/PD-L1 complex on effector CD8+ T cells and NK cells will be orders of magnitude less with treatment compared to without. Consequently, a $\pm 50\%$ deviation in these parameters does not lead to major deviations in model trajectories, which is consistent with their low first-order and total-order sensitivity indices for V_{TS} .

As mentioned in Section 3.4, SA revealed that approximately one quarter of parameters/processes in the full model could be appropriately removed without significantly affecting the model trajectories. Specifically, these parameters are λ_{CI_γ} , λ_{DS} , $\lambda_{T_8I_2}$, $\lambda_{T_1I_2}$, λ_{MI_γ} , λ_{MI_α} , λ_{MI_β} , λ_{KD_0} , $\lambda_{I_\gamma T_8}$, $\lambda_{I_\gamma T_1}$, $\lambda_{I_{10}T_r}$, $\lambda_{I_{10}I_2}$, λ_{P_LD} , $\lambda_{P_LT_8}$, $\lambda_{P_LT_1}$, $\lambda_{P_LT_r}$, $\lambda_{P_L^{LN}T_A^{T_8}}$, $\lambda_{P_L^{LN}T_A^r}$, $K_{I_\gamma T_r}$, τ_8^{act} , τ_a , τ_l , τ_4^{act} , and τ_r^{act} , K_{CI_γ} , K_{DS} , $K_{T_8I_2}$,

$K_{T_1I_2}$, K_{MI_γ} , K_{MI_α} , K_{MI_β} , K_{KD_0} , $K_{I_{10}I_2}$, $K_{T_8T_r}$, and $K_{I_\gamma T_r}$. It is worth noting that while many parameters have low first-order sensitivity indices, they may still exhibit significant higher-order interactions, as indicated by their large total-order indices. This highlights the nonlinear nature of the model—a phenomenon that cannot be captured by more commonly used local SA methods.

We observe that the reduced model, obtained by appropriately removing the aforementioned variables, faithfully replicates the trajectories of the full model under both treatment and no-treatment conditions. In both cases, the vast majority of MREs are below 5%, with the exception of those corresponding to T cell concentrations in the TDLN and certain immune checkpoint and pembrolizumab-associated components. In particular, these exceptions primarily arise from very brief, transient dynamics immediately following the administration of the first pembrolizumab dose. However, these values represent only the maximum deviation over the entire timespan of integration and do not reflect the overall deviation, which is better captured by the RMSRE. The RMSRE more clearly demonstrates the validity of the reduction, with most values below 1% regardless of whether treatment is applied. The largest RMSRE occurs for T_A^r without treatment, reaching less than 10% at 180.9 days. Furthermore, as shown in Figure 7, the differences in trajectories across all state variables are minimal, confirming that the reduction performs as intended. This also demonstrates the robustness of the reduction, as the trajectories remain accurate over timespans significantly longer than those used for the sensitivity analysis, which was performed over 180.9 days.

As a result, replacing the integrals in the full model with point estimates is justified, suggesting that delay integro-differential equations may be unnecessarily complex for modelling the immunobiology of MSI-H/dMMR CRC, and that delay differential equations may be sufficient. We also note that the equations governing the concentrations of unbound PD-1 receptors, PD-1/PD-L1 complexes, and PD-1/pembrolizumab complexes on effector CD8+ T cells, CD4+ T cells, and NK cells cannot be simplified or reduced without significantly affecting model trajectories. This suggests that the current mass-action structure of these equations is already as minimal as possible while still preserving accuracy.

We next examine the SA results of the reduced model, which are summarised in Table G.1. To identify which variables could be eliminated, we sought the smallest subset of variables such that all parameters with large sensitivity indices are associated only with variables within this subset. TCombin with the application of quasi-steady-state approximations (QSSA) to HMGB1, IL-2, and IL-10 concentrations, this analysis led to the removal of variables representing the concentration of: DAMPs, CD4+ T cells and associated variables, macrophages, naive NK and CD8+ T cells, IL-2, IFN- γ , and IL-10, along with their corresponding parameters. The resulting minimal model achieves over a 50% reduction in system dimensionality, along with more than 50% and 33% reductions in the number of parameters compared to the full and reduced models, respectively—representing a significant simplification of the original model.

In a similar fashion to before, we verify the validity of the reduction for the minimal model by considering the MRE and RMSRE with and without treatment. As before, we observe that, in both cases, the vast majority of MREs remain below 10%, with the exception of variables related to the concentration of the cytokines TNF and TGF- β , T cell concentrations in the TDLN and immune checkpoint and pembrolizumab-associated components. Notably, the RMSREs for most variables are very low under both treatment conditions, with the exceptions being the concentrations of TNF, TGF- β , and immune checkpoint-associated components. These deviations are expected due to the nature and application of QSSA, which results in different initial conditions for these variables compared to

the full and reduced models. Additionally, minor differences in the steady states and initial conditions of certain immune checkpoint-associated components contribute to these deviations. However, since most of these components only influence the system through half-saturation or inhibition constants, their absolute concentrations are less critical, and their variation has minimal impact on the trajectories of other variables. Considering [Figure 7](#), we see that the minimal model successfully replicates the trajectories of its state variables well, in cases with and without treatment, even over timespans significantly longer than those used in the original sensitivity analysis, similar to the reduced model.

We can verify that the minimal model cannot be simplified any further without losing substantial accuracy by considering the indices for its SA presented in [Table G.1](#). Indeed, every parameter exhibits either a high first-order or total-order sensitivity index for at least one state variable, confirming that each retained process and parameter significantly influences the model’s dynamics. In contrast to the full and reduced models, which possess greater dimensionality and display additional complexity, each component of the minimal model is functionally important, contributing meaningfully to the system’s behaviour. This, in turn, not only enhances the model’s interpretability but also increases the identifiability of individual parameters, positioning it well for future research.

In this work, we have used global variance-based SA to guide model reduction of our model of dnmMCRC to construct reduced and minimal models that faithfully replicate the original model’s trajectories. Moreover, the minimal model is fully self-contained and is highly extensible, offering a robust foundation for future experimentation and theoretical exploration. Importantly, the reduced model remains valuable as a simplified model for modelling and analysing the interactions and dynamics of many immune cell and cytokine types in MSI-H/dMMR CRC. Thus, one may use the reduced model as a guide for the sequential incorporation of additional variables, enabling targeted investigation of specific aspects of the tumour–immune response in MSI-H/dMMR CRC, as well as in other cancer types. This approach avoids introducing unnecessary complexity while enhancing the adaptability of the model through facilitating the straightforward integration of additional immune cell types, cytokines, or spatial compartments as needed.

6 CRediT authorship contribution statement

Georgio Hawi: conceptualisation, data curation, formal analysis, funding acquisition, investigation, methodology, project administration, resources, software, validation, visualisation, writing — original draft, writing — review & editing.

Peter S. Kim: conceptualisation, formal analysis, funding acquisition, investigation, methodology, project administration, resources, supervision, validation, visualisation, writing — original draft, writing — review & editing.

Peter P. Lee: conceptualisation, formal analysis, investigation, methodology, project administration, resources, supervision, validation, visualisation, writing — original draft, writing — review & editing.

7 Declaration of Competing Interests

The authors declare that they have no known competing financial interests or personal relationships that could have appeared to influence the work reported in this paper.

8 Data availability

All data and procedures are available within the manuscript and its Supporting Information file.

9 Acknowledgements

This work was supported by an Australian Government Research Training Program Scholarship. PSK gratefully acknowledges support from the Australian Research Council Discovery Project (DP230100485).

10 Supporting information

References

- [1] Biller LH, Schrag D. Diagnosis and Treatment of Metastatic Colorectal Cancer: A Review. JAMA. 2021 Feb;325(7):669. Available from: <https://doi.org/10.1001/jama.2021.0106>.
- [2] Sifaki-Pistolla D, Poimenaki V, Fotopoulou I, Saloustros E, Mavroudis D, Vamvakas L, et al. Significant Rise of Colorectal Cancer Incidence in Younger Adults and Strong Determinants: 30 Years Longitudinal Differences between under and over 50s. Cancers. 2022 Sep;14(19):4799. Available from: <https://doi.org/10.3390/cancers14194799>.
- [3] Siegel RL, Wagle NS, Cercek A, Smith RA, Jemal A. Colorectal cancer statistics, 2023. CA: A Cancer Journal for Clinicians. 2023 Mar;73(3):233–254. Available from: <https://doi.org/10.3322/caac.21772>.
- [4] Siegel RL, Giaquinto AN, Jemal A. Cancer statistics, 2024. CA: A Cancer Journal for Clinicians. 2024 Jan;74(1):12–49. Available from: <https://doi.org/10.3322/caac.21820>.
- [5] Rawla P, Sunkara T, Barsouk A. Epidemiology of colorectal cancer: incidence, mortality, survival, and risk factors. Gastroenterology Review. 2019;14(2):89–103. Available from: <https://doi.org/10.5114/pg.2018.81072>.
- [6] Cook AD, Single R, McCahill LE. Surgical Resection of Primary Tumors in Patients Who Present With Stage IV Colorectal Cancer: An Analysis of Surveillance, Epidemiology, and End Results Data, 1988 to 2000. Annals of Surgical Oncology. 2005 Jun;12(8):637–645. Available from: <https://doi.org/10.1245/ASO.2005.06.012>.
- [7] Shulman K, Barnett-Griness O, Friedman V, Greenson JK, Gruber SB, Lejbkowitz F, et al. Outcomes of Chemotherapy for Microsatellite Instable–High Metastatic Colorectal Cancers. JCO Precision Oncology. 2018 Nov;(2):1–10. Available from: <https://doi.org/10.1200/P0.17.00253>.
- [8] Topalian SL, Hodi FS, Brahmer JR, Gettinger SN, Smith DC, McDermott DF, et al. Safety, Activity, and Immune Correlates of Anti–PD-1 Antibody in Cancer. New England Journal of Medicine. 2012 Jun;366(26):2443–2454. Available from: <https://doi.org/10.1056/NEJMoa1200690>.
- [9] Sarshekeh AM, Overman MJ, Kopetz S. Nivolumab in the Treatment of Microsatellite Instability High Metastatic Colorectal Cancer. Future Oncology. 2018 Feb;14(18):1869–1874. Available from: <https://doi.org/10.2217/fon-2017-0696>.

- [10] Yaghoubi N, Soltani A, Ghazvini K, Hassanian SM, Hashemy SI. PD-1/ PD-L1 blockade as a novel treatment for colorectal cancer. *Biomedicine & Pharmacotherapy*. 2019 Feb;110:312–318. Available from: <https://doi.org/10.1016/j.biopha.2018.11.105>.
- [11] Lin X, Kang K, Chen P, Zeng Z, Li G, Xiong W, et al. Regulatory mechanisms of PD-1/PD-L1 in cancers. *Molecular Cancer*. 2024 May;23(1). Available from: <https://doi.org/10.1186/s12943-024-02023-w>.
- [12] Han Y, Liu D, Li L. PD-1/PD-L1 pathway: current researches in cancer. *American journal of cancer research*. 2020;10(3):727. Available from: <https://pmc.ncbi.nlm.nih.gov/articles/PMC7136921/>.
- [13] Oliveira AF, Bretes L, Furtado I. Review of PD-1/PD-L1 Inhibitors in Metastatic dMMR/MSI-H Colorectal Cancer. *Frontiers in Oncology*. 2019 May;9. Available from: <https://doi.org/10.3389/fonc.2019.00396>.
- [14] Lee J, Ahn E, Kissick HT, Ahmed R. Reinvigorating Exhausted T Cells by Blockade of the PD-1 Pathway. *Forum on Immunopathological Diseases and Therapeutics*. 2015;6(1–2):7–17. Available from: <https://doi.org/10.1615/ForumImmunDisTher.2015014188>.
- [15] Zhang Y, Zhang Z. The history and advances in cancer immunotherapy: understanding the characteristics of tumor-infiltrating immune cells and their therapeutic implications. *Cellular & Molecular Immunology*. 2020 Jul;17(8):807–821. Available from: <https://doi.org/10.1038/s41423-020-0488-6>.
- [16] Merck. KEYTRUDA (pembrolizumab) injection Label; 2021. Available from: https://www.accessdata.fda.gov/drugsatfda_docs/label/2021/125514s0961b1.pdf.
- [17] Zhang XY, Trame M, Lesko L, Schmidt S. Sobol Sensitivity Analysis: A Tool to Guide the Development and Evaluation of Systems Pharmacology Models. *CPT: Pharmacometrics & Systems Pharmacology*. 2015 Feb;4(2):69–79. Available from: <https://doi.org/10.1002/psp4.6>.
- [18] Morris MD. Factorial Sampling Plans for Preliminary Computational Experiments. *Technometrics*. 1991 May;33(2):161–74. Available from: <https://doi.org/10.1080/00401706.1991.10484804>.
- [19] Bertram R, Rubin JE. Multi-timescale Systems and Fast-Slow Analysis. *Mathematical Biosciences*. 2017 May;287:105–21. Available from: <https://doi.org/10.1016/j.mbs.2016.07.003>.
- [20] Padoan A, Forni F, Sepulchre R. Balanced Truncation for Model Reduction of Biological Oscillators. *Biol Cybern*. 2021;115(4):383–95. Available from: <https://doi.org/10.1007/s00422-021-00888-4>.
- [21] Snowden TJ, van der Graaf PH, Tindall MJ. Methods of Model Reduction for Large-Scale Biological Systems: A Survey of Current Methods and Trends. *Bulletin of Mathematical Biology*. 2017 Jun;79(7):1449–86. Available from: <https://doi.org/10.1007/s11538-017-0277-2>.
- [22] Marzban C. Variance-Based Sensitivity Analysis: An Illustration on the Lorenz'63 Model. *Monthly Weather Review*. 2013 Oct;141(11):4069–79. Available from: <https://doi.org/10.1175/mwr-d-13-00032.1>.

- [23] Qian G, Mahdi A. Sensitivity Analysis Methods in the Biomedical Sciences. *Mathematical Biosciences*. 2020 May;323:108306. Available from: <https://doi.org/10.1016/j.mbs.2020.108306>.
- [24] Marino S, Hogue IB, Ray CJ, Kirschner DE. A methodology for performing global uncertainty and sensitivity analysis in systems biology. *Journal of Theoretical Biology*. 2008 Sep;254(1):178–196. Available from: <https://doi.org/10.1016/j.jtbi.2008.04.011>.
- [25] Lai X, Friedman A. Combination therapy of cancer with cancer vaccine and immune checkpoint inhibitors: A mathematical model. *PLOS ONE*. 2017 May;12(5):e0178479. Available from: <https://doi.org/10.1371/journal.pone.0178479>.
- [26] Lai X, Friedman A. How to schedule VEGF and PD-1 inhibitors in combination cancer therapy? *BMC Systems Biology*. 2019 Mar;13(1). Available from: <https://doi.org/10.1186/s12918-019-0706-y>.
- [27] Liao KL, Bai XF, Friedman A. IL-27 in combination with anti-PD-1 can be anti-cancer or pro-cancer. *Journal of Theoretical Biology*. 2024 Feb;579:111704. Available from: <https://doi.org/10.1016/j.jtbi.2023.111704>.
- [28] Siewe N, Friedman A. TGF- β inhibition can overcome cancer primary resistance to PD-1 blockade: A mathematical model. *PLOS ONE*. 2021 Jun;16(6):e0252620. Available from: <https://doi.org/10.1371/journal.pone.0252620>.
- [29] Kirshtein A, Akbarinejad S, Hao W, Le T, Su S, Aronow RA, et al. Data Driven Mathematical Model of Colon Cancer Progression. *Journal of Clinical Medicine*. 2020 Dec;9(12):3947. Available from: <https://doi.org/10.3390/jcm9123947>.
- [30] Budithi A, Su S, Kirshtein A, Shahriyari L. Data Driven Mathematical Model of FOLFIRI Treatment for Colon Cancer. *Cancers*. 2021 May;13(11):2632. Available from: <https://doi.org/10.3390/cancers13112632>.
- [31] Reed PM, Hadjimichael A, Malek K, Karimi T, Vernon CR, Srikrishnan V, et al.. Addressing Uncertainty in Multisector Dynamics Research. *Zenodo*; 2022. Available from: <https://zenodo.org/record/6110623>.
- [32] Campolongo F, Cariboni J, Saltelli A. An Effective Screening Design for Sensitivity Analysis of Large Models. *Environ Model Softw*. 2007;22(10):1509-18. Available from: <https://doi.org/10.1016/j.envsoft.2006.10.004>.
- [33] Li G, Rosenthal C, Rabitz H. High Dimensional Model Representations. *The Journal of Physical Chemistry A*. 2001 Jul;105(33):7765–7777. Available from: <https://doi.org/10.1021/jp010450t>.
- [34] Gratiet LL, Marelli S, Sudret B. Metamodel-Based Sensitivity Analysis: Polynomial Chaos Expansions and Gaussian Processes. In: *Handbook of Uncertainty Quantification*. Springer International Publishing; 2015. p. 1-37. Available from: https://doi.org/10.1007/978-3-319-11259-6_38-1.
- [35] Jayachandran D, Rundell AE, Hannemann RE, Vik TA, Ramkrishna D. Optimal Chemotherapy for Leukemia: A Model-Based Strategy for Individualized Treatment. *PLoS ONE*. 2014 Oct;9(10):e109623. Available from: <https://doi.org/10.1371/journal.pone.0109623>.

- [36] Dela A, Shtylla B, de Pillis L. Multi-method global sensitivity analysis of mathematical models. *Journal of Theoretical Biology*. 2022 Aug;546:111159. Available from: <https://doi.org/10.1016/j.jtbi.2022.111159>.
- [37] Vazquez-Cruz MA, Guzman-Cruz R, Lopez-Cruz IL, Cornejo-Perez O, Torres-Pacheco I, Guevara-Gonzalez RG. Global sensitivity analysis by means of EFAST and Sobol' methods and calibration of reduced state-variable TOMGRO model using genetic algorithms. *Computers and Electronics in Agriculture*. 2014 Jan;100:1–12. Available from: <https://doi.org/10.1016/j.compag.2013.10.006>.
- [38] Hawi G, Kim PS, Lee PP. Optimisation of pembrolizumab therapy for de novo metastatic MSI-H/dMMR colorectal cancer using data-driven delay integro-differential equations. *bioRxiv*. 2025. Available from: <https://www.biorxiv.org/content/early/2025/05/24/2025.05.23.655752>.
- [39] Hawi G, Kim PS, Lee PP. Optimisation of neoadjuvant pembrolizumab therapy for locally advanced MSI-H/dMMR colorectal cancer using data-driven delay integro-differential equations; 2025. arXiv:2411.12123 [q-bio.CB]. Available from: <https://doi.org/10.48550/arXiv.2411.12123>.
- [40] Cannavó F. Sensitivity Analysis for Volcanic Source Modeling Quality Assessment And Model Selection. *Comput Geosci*. 2012;44:52-9. Available from: <https://doi.org/10.1016/j.cageo.2012.03.008>.
- [41] Sobol' IM. Sensitivity Analysis for Non-Linear Mathematical Models. *Math Modeling Comput Exp*. 1993;1:407-14.
- [42] Hoeffding W. A Class of Statistics with Asymptotically Normal Distribution. *The Annals of Mathematical Statistics*. 1948 Sep;19(3):293-325. Available from: <https://doi.org/10.1214/aoms/1177730196>.
- [43] Borgonovo E. A New Uncertainty Importance Measure. *Reliability Engineering & System Safety*. 2007 Jun;92(6):771-84. Available from: <https://doi.org/10.1016/j.res.2006.04.015>.
- [44] Homma T, Saltelli A. Importance Measures in Global Sensitivity Analysis of Nonlinear Models. *Reliability Engineering & System Safety*. 1996 Apr;52(1):1-17. Available from: [https://doi.org/10.1016/0951-8320\(96\)00002-6](https://doi.org/10.1016/0951-8320(96)00002-6).
- [45] Cukier RI, Fortuin CM, Shuler KE, Petschek AG, Schaibly JH. Study of the sensitivity of coupled reaction systems to uncertainties in rate coefficients. I Theory. *The Journal of Chemical Physics*. 1973 Oct;59(8):3873-8. Available from: <https://doi.org/10.1063/1.1680571>.
- [46] Saltelli A, Bolado R. An Alternative Way to Compute Fourier Amplitude Sensitivity Test (FAST). *Computational Statistics & Data Analysis*. 1998 Feb;26(4):445-60. Available from: [https://doi.org/10.1016/S0167-9473\(97\)00043-1](https://doi.org/10.1016/S0167-9473(97)00043-1).
- [47] Saltelli A, Tarantola S, Chan KPS. A Quantitative Model-Independent Method for Global Sensitivity Analysis of Model Output. *Technometrics*. 1999 Feb;41(1):39–56. Available from: <https://doi.org/10.1080/00401706.1999.10485594>.
- [48] Weyl H. Mean Motion. *American Journal of Mathematics*. 1938 Oct;60(4):889. Available from: <https://doi.org/10.2307/2371267>.

- [49] McRae GJ, Tilden JW, Seinfeld JH. Global sensitivity analysis—a computational implementation of the Fourier Amplitude Sensitivity Test (FAST). *Computers & Chemical Engineering*. 1982 Jan;6(1):15-25. Available from: [https://doi.org/10.1016/0098-1354\(82\)80003-3](https://doi.org/10.1016/0098-1354(82)80003-3).
- [50] Schaibly JH, Shuler KE. Study of the Sensitivity of Coupled Reaction Systems to Uncertainties in Rate Coefficients. II Applications. *The Journal of Chemical Physics*. 1973 Oct;59(8):3879-88. Available from: <https://doi.org/10.1063/1.1680572>.
- [51] Koda M, Mcrae GJ, Seinfeld JH. Automatic Sensitivity Analysis of Kinetic Mechanisms. *International Journal of Chemical Kinetics*. 1979 Apr;11(4):427-44. Available from: <https://doi.org/10.1002/kin.550110408>.
- [52] Wang Y, Zhu T, Shi Q, Zhu G, Zhu S, Hou F. Tumor-draining lymph nodes: opportunities, challenges, and future directions in colorectal cancer immunotherapy. *Journal for ImmunoTherapy of Cancer*. 2024 Jan;12(1):e008026. Available from: <https://doi.org/10.1136/jitc-2023-008026>.
- [53] Xu C, Gertner GZ. A General First-Order Global Sensitivity Analysis Method. *Reliab Eng Syst Saf*. 2008;93(7):1060-71. Available from: <https://doi.org/10.1016/j.ress.2007.04.001>.
- [54] Iwanaga T, Usher W, Herman J. Toward SALib 2.0: Advancing the Accessibility and Interpretability of Global Sensitivity Analyses. *Socio-Environmental Systems Modelling*. 2022 May;4:18155. Available from: <https://doi.org/10.18174/sesmo.18155>.

Supporting Information: Sensitivity analysis–guided model reduction of a mathematical model of pembrolizumab therapy for de novo metastatic MSI-H/dMMR colorectal cancer

Georgio Hawi^{1, *}, Peter S. Kim^{1, †}, and Peter P. Lee^{2, †}

¹School of Mathematics and Statistics, University of Sydney, Sydney, Australia

²Department of Immuno-Oncology, Beckman Research Institute, City of Hope, Duarte, California, USA

*Corresponding author: georgio.hawi@sydney.edu.au

†These authors contributed comparably to this work

A Model Parameters for the Full Model

The model parameter values are estimated in [1] and are listed in Table A.1.

Table A.1: Parameter values for the full model. TDLN denotes the tumour-draining lymph node, whilst TS denotes the tumour site. est. denotes estimated parameters.

Parameter	Description	Value	Unit	References
f_{pembro}	A_1/A_1^{LN} dose scaling factor	1.17×10^{12}	(molec/cm ³)/mg	est.
f_C	C to V_{TS} scaling factor	1.17×10^6	cell/(cm ³) ²	est.
f_{N_c}	N_c to V_{TS} scaling factor	6.16×10^4	cell/(cm ³) ²	est.
\mathcal{A}_{D_0}	Source of D_0	1.18×10^6	(cell/cm ³) day ⁻¹	est.
$\mathcal{A}_{T_0^8}$	Source of T_0^8	3.76×10^5	(cell/cm ³) day ⁻¹	est.
$\mathcal{A}_{T_0^4}$	Source of T_0^4	2.76×10^5	(cell/cm ³) day ⁻¹	est.
$\mathcal{A}_{T_0^r}$	Source of T_0^r	1.15×10^5	(cell/cm ³) day ⁻¹	est.
\mathcal{A}_{M_0}	Source of M_0	1.08×10^6	(cell/cm ³) day ⁻¹	est.
\mathcal{A}_{K_0}	Source of K_0	2.82×10^5	(cell/cm ³) day ⁻¹	est.
λ_C	Growth rate of C	5.25×10^{-2}	day ⁻¹	fitted
λ_{CT_8}	Elimination rate of C by T_8	8.01×10^{-8}	(cell/cm ³) ⁻¹ day ⁻¹	fitted
λ_{CK}	Elimination rate of C by K	8.01×10^{-8}	(cell/cm ³) ⁻¹ day ⁻¹	est.
λ_{CI_α}	Necrosis rate of C by I_α	6.02×10^{-3}	day ⁻¹	est.
λ_{CI_γ}	Necrosis rate of C by I_γ	1.20×10^{-3}	day ⁻¹	est.
λ_{HN_c}	Production rate of H by N_c	2.92×10^{-14}	(g/cell) day ⁻¹	est.
λ_{SN_c}	Production rate of S by N_c	1.70×10^{-14}	(g/cell) day ⁻¹	est.

λ_{DH}	Maturation rate of D_0 by H	1.21	day ⁻¹	est.
λ_{DS}	Maturation rate of D_0 by S	1.21×10^{-1}	day ⁻¹	est.
λ_{D_0K}	Killing rate of D_0 by K	5.49×10^{-6}	(cell/cm ³) ⁻¹ day ⁻¹	est.
$\lambda_{DD^{LN}}$	Migration rate of D to TDLN	1.68×10^{-2}	day ⁻¹	est.
$\lambda_{T_0^8 T_A^8}$	Kinetic rate constant for T_0^8 activation	2.73×10^{-11}	(cell/cm ³) ⁻¹ day ⁻¹	est.
$\lambda_{T_A^8 T_8}$	Kinetic rate constant for T_A^8 migration to the TS	6.32×10^{-1}	day ⁻¹	est.
$\lambda_{T_8 I_2}$	Growth rate of T_8 by I_2	1.53×10^{-3}	day ⁻¹	est.
$\lambda_{T_8 C}$	Exhaustion rate of T_8 due to C exposure	6.31×10^{-3}	day ⁻¹	est.
$\lambda_{T_{ex} A_1}$	Reinvigoration rate of T_{ex} by A_1	2.25×10^{-3}	day ⁻¹	est.
$\lambda_{T_0^4 T_A^1}$	Kinetic rate constant for T_0^4 activation into T_A^1	8.26×10^{-11}	(cell/cm ³) ⁻¹ day ⁻¹	est.
$\lambda_{T_A^1 T_1}$	Kinetic rate constant for T_A^1 migration to the TS	6.17×10^{-2}	day ⁻¹	est.
$\lambda_{T_1 I_2}$	Growth rate of T_1 by I_2	2.00×10^{-3}	day ⁻¹	est.
$\lambda_{T_1 T_r}$	Conversion rate of T_1 to T_r by Q^{T_1}	4.00×10^{-3}	day ⁻¹	est.
$\lambda_{T_0^r T_A^r}$	Kinetic rate constant for T_0^r activation into T_A^r	1.08×10^{-8}	(cell/cm ³) ⁻¹ day ⁻¹	est.
$\lambda_{T_A^r T_r}$	Kinetic rate constant for T_A^r migration to the TS	4.88	day ⁻¹	est.
$\lambda_{M_1 I_\alpha}$	Polarisation rate of M_0 to M_1 by I_α	3.59×10^{-1}	day ⁻¹	est.
$\lambda_{M_1 I_\gamma}$	Polarisation rate of M_0 to M_1 by I_γ	4.18×10^{-1}	day ⁻¹	est.
$\lambda_{M_2 I_{10}}$	Polarisation rate of M_0 to M_2 by I_{10}	2.27×10^{-1}	day ⁻¹	est.
$\lambda_{M_2 I_\beta}$	Polarisation rate of M_0 to M_2 by I_β	2.54×10^{-1}	day ⁻¹	est.
$\lambda_{M I_\gamma}$	Polarisation rate of M_2 to M_1 by I_γ	1.39×10^{-2}	day ⁻¹	est.
$\lambda_{M I_\alpha}$	Polarisation rate of M_2 to M_1 by I_α	1.15×10^{-2}	day ⁻¹	est.
$\lambda_{M I_\beta}$	Polarisation rate of M_1 to M_2 by I_β	6.39×10^{-3}	day ⁻¹	est.
$\lambda_{K I_2}$	Maturation rate of K_0 by I_2	4.62×10^{-3}	day ⁻¹	est.
$\lambda_{K D_0}$	Maturation rate of K_0 by D_0	1.54×10^{-3}	day ⁻¹	est.
$\lambda_{K D}$	Maturation rate of K_0 by D	7.70×10^{-3}	day ⁻¹	est.
$\lambda_{I_2 T_8}$	Production rate of I_2 by T_8	5.95×10^{-16}	(g/cell) day ⁻¹	est.
$\lambda_{I_2 T_1}$	Production rate of I_2 by T_1	1.74×10^{-15}	(g/cell) day ⁻¹	est.
$\lambda_{I_\gamma T_8}$	Production rate of I_γ by T_8	8.62×10^{-16}	(g/cell) day ⁻¹	est.
$\lambda_{I_\gamma T_1}$	Production rate of I_γ by T_1	3.02×10^{-16}	(g/cell) day ⁻¹	est.
$\lambda_{I_\gamma K}$	Production rate of I_γ by K	7.99×10^{-15}	(g/cell) day ⁻¹	est.
$\lambda_{I_\alpha T_8}$	Production rate of I_α by T_8	5.55×10^{-15}	(g/cell) day ⁻¹	est.
$\lambda_{I_\alpha T_1}$	Production rate of I_α by T_1	9.17×10^{-15}	(g/cell) day ⁻¹	est.

$\lambda_{I_\alpha M_1}$	Production rate of I_α by M_1	3.36×10^{-15}	(g/cell) day ⁻¹	est.
$\lambda_{I_\alpha K}$	Production rate of I_α by K	9.68×10^{-15}	(g/cell) day ⁻¹	est.
$\lambda_{I_\beta C}$	Production rate of I_β by C	7.42×10^{-12}	(g/cell) day ⁻¹	est.
$\lambda_{I_\beta T_r}$	Production rate of I_β by T_r	4.30×10^{-11}	(g/cell) day ⁻¹	est.
$\lambda_{I_\beta M_2}$	Production rate of I_β by M_2	5.34×10^{-11}	(g/cell) day ⁻¹	est.
$\lambda_{I_{10} C}$	Production rate of I_{10} by C	1.55×10^{-17}	(g/cell) day ⁻¹	est.
$\lambda_{I_{10} M_2}$	Production rate of I_{10} by M_2	3.10×10^{-17}	(g/cell) day ⁻¹	est.
$\lambda_{I_{10} T_r}$	Production rate of I_{10} by T_r	5.86×10^{-18}	(g/cell) day ⁻¹	est.
$\lambda_{I_{10} I_2}$	Production ratio of I_{10} by I_2	3	dimensionless	[2] est.
$\lambda_{P_D^{T_8}}$	Synthesis rate of $P_D^{T_8}$	9.25×10^2	(molec/cell) day ⁻¹	est.
λ_{Q_A}	Dissociation rate of the PD-1/pembrolizumab complex	2.6	day ⁻¹	[3]
λ_Q	Dissociation rate of the PD-1/PD-L1 complex	1.24×10^5	day ⁻¹	[4]
$\lambda_{P_D A_1}$	Formation rate of the PD-1/pembrolizumab complex	4.63×10^{-13}	(molec/cm ³) ⁻¹ day ⁻¹	fitted
$\lambda_{P_D P_L}$	Formation rate of the PD-1/PD-L1 complex	2.64×10^{-11}	(molec/cm ³) ⁻¹ day ⁻¹	[4]
$\lambda_{P_D^{T_1}}$	Synthesis rate of $P_D^{T_1}$	6.87×10^2	(molec/cell) day ⁻¹	est.
$\lambda_{P_D^K}$	Synthesis rate of P_D^K	1.85×10^2	(molec/cell) day ⁻¹	est.
$\lambda_{P_L C}$	Synthesis rate of P_L by C	2.50×10^5	(molec/cell) day ⁻¹	est.
$\lambda_{P_L D}$	Synthesis rate of P_L by D	2.46×10^4	(molec/cell) day ⁻¹	est.
$\lambda_{P_L T_8}$	Synthesis rate of P_L by T_8	2.07×10^3	(molec/cell) day ⁻¹	est.
$\lambda_{P_L T_1}$	Synthesis rate of P_L by T_1	2.89×10^3	(molec/cell) day ⁻¹	est.
$\lambda_{P_L T_r}$	Synthesis rate of P_L by T_r	2.89×10^3	(molec/cell) day ⁻¹	est.
$\lambda_{P_L M_2}$	Synthesis rate of P_L by M_2	3.71×10^5	(molec/cell) day ⁻¹	est.
$\lambda_{P_D^{8LN}}$	Synthesis rate of P_D^{8LN}	9.27×10^2	(molec/cell) day ⁻¹	est.
$\lambda_{P_D^{1LN}}$	Synthesis rate of P_D^{1LN}	6.89×10^2	(molec/cell) day ⁻¹	est.
$\lambda_{P_L^{LN} D^{LN}}$	Synthesis rate of P_L^{LN} by D^{LN}	2.46×10^4	(molec/cell) day ⁻¹	est.
$\lambda_{P_L^{LN} T_A^8}$	Synthesis rate of P_L^{LN} by T_A^8	2.07×10^3	(molec/cell) day ⁻¹	est.
$\lambda_{P_L^{LN} T_A^1}$	Synthesis rate of P_L^{LN} by T_A^1	2.89×10^3	(molec/cell) day ⁻¹	est.
$\lambda_{P_L^{LN} T_A^r}$	Synthesis rate of P_L^{LN} by T_A^r	2.89×10^3	(molec/cell) day ⁻¹	est.
K_{CI_α}	Half-saturation constant of I_α for C	9.00×10^{-11}	g/cm ³	est.
K_{CI_γ}	Half-saturation constant of I_γ for C	4.93×10^{-11}	g/cm ³	est.
K_{DH}	Half-saturation constant of H for D	1.94×10^{-8}	g/cm ³	est.
K_{DS}	Half-saturation constant of S for D	4.50×10^{-8}	g/cm ³	est.
$K_{T_8 I_2}$	Half-saturation constant of I_2 for T_8	2.00×10^{-12}	g/cm ³	est.
$K_{T_8 C}$	Half-saturation constant T_8 exhaustion due to C exposure	7.02×10^8	(cell/cm ³) day	est.
$K_{T_{ex} A_1}$	Half-saturation constant of T_{ex} reinvigoration by A_1	2.05×10^{14}	molec/cm ³	est.

$K_{T_1 I_2}$	Half-saturation constant of I_2 for T_1	2.00×10^{-12}	g/cm ³	est.
$K_{T_1 T_r}$	Half-saturation constant of T_1 conversion to T_r by Q^{T_1}	6.01×10^5	molec/cm ³	est.
$K_{M_1 I_\alpha}$	Half-saturation constant of I_α for M_1	9.00×10^{-11}	g/cm ³	est.
$K_{M_1 I_\gamma}$	Half-saturation constant of I_γ for M_1	4.93×10^{-11}	g/cm ³	est.
$K_{M_2 I_{10}}$	Half-saturation constant of I_{10} for M_2	1.84×10^{-10}	g/cm ³	est.
$K_{M_2 I_\beta}$	Half-saturation constant of I_β for M_2	1.51×10^{-6}	g/cm ³	est.
$K_{M I_\gamma}$	Half-saturation constant of I_γ for M_1/M_2	4.93×10^{-11}	g/cm ³	est.
$K_{M I_\alpha}$	Half-saturation constant of I_α for M_1/M_2	9.00×10^{-11}	g/cm ³	est.
$K_{M I_\beta}$	Half-saturation constant of I_β for M_1/M_2	1.51×10^{-6}	g/cm ³	est.
$K_{K I_2}$	Half-saturation constant of I_2 for K	2.00×10^{-12}	g/cm ³	est.
$K_{K D_0}$	Half-saturation constant of D_0 for K	9.55×10^5	cell/cm ³	est.
$K_{K D}$	Half-saturation constant of D for K	1.91×10^6	cell/cm ³	est.
$K_{I_{10} I_2}$	Half-saturation constant of I_2 for I_{10}	2.00×10^{-12}	g/cm ³	est.
C_0	Carrying capacity of C	8.89×10^7	cell/cm ³	fitted
$K_{C I_\beta}$	Inhibition constant of T_8 and K elimination of C by I_β	1.51×10^{-6}	g/cm ³	est.
$K_{C Q^{T_8}}$	Inhibition constant of T_8 elimination of C by Q^{T_8}	1.35×10^6	molec/cm ³	est.
$K_{C Q^K}$	Inhibition constant of K elimination of C by Q^K	2.96×10^5	molec/cm ³	est.
$K_{D_0 I_\beta}$	Inhibition constant of K elimination of D_0 by I_β	1.51×10^{-6}	g/cm ³	est.
V_{LN}	Volume of the TDLN	1.47×10^{-1}	cm ³	[5] est.
$K_{T_0^8 T_A^r}$	Inhibition constant of T_0^8 activation by T_A^r	2.94×10^6	(cell/cm ³) day	est.
$K_{T_0^8 Q^{8LN}}$	Inhibition constant of T_0^8 activation by Q^{8LN}	5.84×10^5	(molec/cm ³) day	est.
$K_{T_A^8 T_A^r}$	Inhibition constant of T_A^8 activation by T_A^r	7.16×10^6	(cell/cm ³) day	est.
$K_{T_A^8 Q^{8LN}}$	Inhibition constant of T_A^8 proliferation by Q^{8LN}	1.42×10^6	(molec/cm ³) day	est.
$K_{T_8 T_r}$	Inhibition constant of I_2 -mediated growth of T_8 by T_r	2.78×10^5	cell/cm ³	est.
$K_{T_8 I_{10}}$	Inhibition constant of T_8 death by I_{10}	1.84×10^{-10}	g/cm ³	est.

$K_{T_{\text{ex}}I_{10}}$	Inhibition constant of T_{ex} death by I_{10}	1.84×10^{-10}	g/cm^3	est.
$K_{T_0^4 T_A^r}$	Inhibition constant of T_0^4 activation by T_A^r	2.21×10^6	$(\text{cell}/\text{cm}^3) \text{ day}$	est.
$K_{T_0^4 Q^{1\text{LN}}}$	Inhibition constant of T_0^4 activation by $Q^{1\text{LN}}$	2.61×10^6	$(\text{molec}/\text{cm}^3) \text{ day}$	est.
$K_{T_A^1 T_A^r}$	Inhibition constant of T_A^1 proliferation by T_A^r	6.07×10^6	$(\text{cell}/\text{cm}^3) \text{ day}$	est.
$K_{T_A^1 Q^{1\text{LN}}}$	Inhibition constant of T_A^1 proliferation by $Q^{1\text{LN}}$	7.19×10^6	$(\text{molec}/\text{cm}^3) \text{ day}$	est.
$K_{T_1 T_r}$	Inhibition constant of I_2 -mediated growth of T_1 by T_r	2.78×10^5	cell/cm^3	est.
$K_{K I_\beta}$	Inhibition constant of NK cell activation by I_β	1.51×10^{-6}	g/cm^3	est.
$K_{I_\gamma T_r}$	Inhibition constant of T cell production of I_γ by T_r	2.78×10^5	cell/cm^3	est.
d_{N_c}	Removal rate of N_c	6.88×10^{-2}	day^{-1}	est.
d_H	Degradation rate of H	5.55	day^{-1}	[6] est.
d_S	Degradation rate of S	1.39	day^{-1}	[7, 8] est.
d_{D_0}	Death rate of D_0	3.57×10^{-2}	day^{-1}	[9] est.
d_D	Death rate of D	3.15×10^{-1}	day^{-1}	[10] est.
$d_{T_0^8}$	Death rate of T_0^8	3.22×10^{-2}	day^{-1}	[11] est.
d_{T_8}	Death rate of T_8	9×10^{-3}	day^{-1}	[12]
$d_{T_{\text{ex}}}$	Death rate of T_{ex}	9×10^{-3}	day^{-1}	[12]
$d_{T_0^4}$	Death rate of T_0^4	4.03×10^{-2}	day^{-1}	[11] est.
d_{T_1}	Death rate of T_1	8×10^{-3}	day^{-1}	[12]
$d_{T_0^r}$	Death rate of T_0^r	2.2×10^{-3}	day^{-1}	[13]
d_{T_r}	Death rate of T_r	6.30×10^{-2}	day^{-1}	[14] est.
d_{M_0}	Death rate of M_0	0.73	day^{-1}	[15]
d_{M_1}	Death rate of M_1	0.99	day^{-1}	[15]
d_{M_2}	Death rate of M_2	1.35×10^{-1}	day^{-1}	[15]
d_{K_0}	Death rate of K_0	6.93×10^{-2}	day^{-1}	[16–18] est.
d_K	Death rate of K	6.93×10^{-2}	day^{-1}	[16–18] est.
d_{I_2}	Degradation rate of I_2	1.45×10^2	day^{-1}	[19] est.
d_{I_γ}	Degradation rate of I_γ	3.33×10^1	day^{-1}	[20] est.
d_{I_α}	Degradation rate of I_α	5.48×10^1	day^{-1}	[21, 22] est.
d_{I_β}	Degradation rate of I_β	3.99×10^2	day^{-1}	[23] est.
$d_{I_{10}}$	Degradation rate of I_{10}	6.16	day^{-1}	[24] est.
d_{P_D}	Degradation rate of unbound PD-1 receptors	3.36×10^{-1}	day^{-1}	[25]
d_{Q_A}	Internalisation rate of the PD-1/pembrolizumab complex	0.43	day^{-1}	[3]
d_{A_1}	Elimination rate of A_1/A_1^{LN}	2.92×10^{-2}	day^{-1}	[26–28] est.
d_{P_L}	Degradation rate of unbound PD-L1	1.39	day^{-1}	[29]
τ_m	DC migration time from TDLN to the TS	0.75	day	[30] est.

τ_8^{act}	CD8+ T cell activation time	2	day	[31]
Δ_8^0	Time taken for first CTL division	1.63	day	[32]
n_{max}^8	Maximal number of CTL divisions in the TDLN	10	dimensionless	[33, 34] est.
Δ_8	Time taken for successive CTL divisions	0.36	day	[33]
$\tau_{T_A^8}$	Time taken for CTL division program	4.87	day	est.
τ_a	T cell migration time between the TDLN to the TS	0.27	day	est.
τ_l	Time for CTL to become exhausted in TS	10	day	[35, 36] est.
τ_4^{act}	CD4+ T cell activation time	1.5	day	[37] est.
Δ_1^0	Time taken for first Th1 cell division	0.77	day	[38] est.
n_{max}^1	Maximal number of Th1 cell divisions in the TDLN	9	dimensionless	[39] est.
Δ_1	Time taken for successive Th1 cell divisions	0.42	day	[38] est.
$\tau_{T_A^1}$	Time taken for Th1 cell division program	4.13	day	est.
τ_r^{act}	Treg activation time	1.5	day	[37] est.
Δ_r^0	Time taken for first Treg division	0.77	day	[38] est.
n_{max}^r	Maximal number of Treg divisions in the TDLN	6	dimensionless	[40] est.
Δ_r	Time taken for successive Treg divisions	0.42	day	[38] est.
$\tau_{T_A^r}$	Time taken for Treg division program	2.87	day	est.

B Reduced Model Parameter Estimation

We estimate all parameters, where possible, under the assumption that no pembrolizumab has/will be administered. The exception to this is the parameters directly related to pembrolizumab treatment, for which the assumptions are explicitly stated during estimation. Many of the assumptions and techniques in this section are adopted from [1] and [41].

For the sake of brevity, we present parameter estimation only for those parameters that differ between the full and the reduced model. The absence of a parameter in this section implies that its value and derivation are identical to those provided in [1] and Table A.1.

B.1 Half-Saturation Constants

We recall that for some species X , K_X is denoted the half-saturation constant of X in a term of the form

$$\frac{X}{K_X + X}.$$

For simplicity, we assume that if \bar{X} denotes the steady state value of X , then

$$\frac{\bar{X}}{K_X + \bar{X}} = \frac{1}{2} \implies K_X = \bar{X}. \quad (\text{B.1})$$

Using (B.1), we have that

$$\begin{aligned} K_{T_8C} &= \bar{C} = 7.02 \times 10^7 \text{ cell/cm}^3, \\ K_{T_1T_r} &= \bar{Q^{T_1}} = 6.01 \times 10^5 \text{ molec/cm}^3. \end{aligned}$$

B.2 Inhibition Constants

We recall that for some species X , K_X is denoted as the inhibition constant of X in a term of the form

$$\frac{1}{1 + X/K_X}.$$

For simplicity, we assume that if \bar{X} denotes the steady state value of X , then

$$\frac{1}{1 + \bar{X}/K_X} = \frac{1}{2} \implies K_X = \bar{X}. \quad (\text{B.2})$$

Using (B.2), we have that

$$\begin{aligned} K_{CQ^{T_8}} &= \bar{Q^{T_8}} = 1.35 \times 10^6 \text{ molec/cm}^3, \\ K_{CQ^K} &= \bar{Q^K} = 2.95 \times 10^6 \text{ molec/cm}^3, \\ K_{T_0^8T_A^r} &= K_{T_A^8T_A^r} = K_{T_0^4T_A^r} = K_{T_A^1T_A^r} = \bar{T_A^r} = 1.47 \times 10^6 \text{ cell/cm}^3, \\ K_{T_0^8Q^{8LN}} &= K_{T_A^8Q^{8LN}} = \bar{Q^{8LN}} = 2.90 \times 10^5 \text{ molec/cm}^3, \\ K_{T_0^4Q^{1LN}} &= K_{T_A^1Q^{1LN}} = \bar{Q^{1LN}} = 1.73 \times 10^6 \text{ molec/cm}^3. \end{aligned}$$

B.3 Cytokine Production Parameters

B.3.1 Estimates for I_γ

Considering (3.4.32) at steady state, or equivalently considering (3.4.33), leads to

$$\lambda_{I_\gamma K} \bar{K} - d_{I_\gamma} \bar{I}_\gamma = 0.$$

Solving this leads to

$$\lambda_{I_\gamma K} = 8.46 \times 10^{-15} \text{ (g/cell) day}^{-1}.$$

Consequently, considering (3.4.33), we have that

$$I_\gamma(0) = \frac{\lambda_{I_\gamma K}}{d_{I_\gamma}} K(0) = 1.14 \times 10^{-10} \text{ g/cm}^3.$$

B.3.2 Estimates for I_{10}

Amongst 48 different cell lines tested, it was found in [42] that cancer IL-10 production was maximised in cell lines derived from colon carcinomas. As such, we assume that at steady state, cancer production of IL-10 is equal to half of that by M_2 macrophages. This, in conjunction with considering (3.4.38) at steady state, leads to the equations

$$\frac{\lambda_{I_{10}C}}{1} = \frac{\lambda_{I_{10}M_2}}{2},$$

and

$$\lambda_{I_{10}C} \bar{C} + \lambda_{I_{10}M_2} \bar{M}_2 - d_{I_{10}} \bar{I}_{10} = 0.$$

Solving these simultaneously leads to

$$\begin{aligned} \lambda_{I_{10}C} &= 1.56 \times 10^{-17} \text{ (g/cell) day}^{-1}, \\ \lambda_{I_{10}M_2} &= 3.11 \times 10^{-17} \text{ (g/cell) day}^{-1}. \end{aligned}$$

B.4 Parameters for DCs, Macrophages, and NK Cells

B.4.1 Estimates for D_0 and D

Adding (3.4.6) and (3.4.7) at steady state, leads to

$$\mathcal{A}_{D_0} - \frac{\lambda_{D_0 K} \bar{D}_0 \bar{K}}{2} - d_{D_0} \bar{D}_0 - \lambda_{DD^{\text{LN}}} \bar{D} - d_D \bar{D} = 0.$$

In [43], it was also shown that the percentage of immature DCs that were lysed as a result of NK cells is roughly linear in the ratio of NK cells to immature DCs. When a 1:1 ratio of activated NK cells to immature DCs is present, after 24 hours, roughly 35.5% of immature DCs are lysed, whereas if a 5:1 ratio is present, 85.5% of immature DCs are lysed. At steady state, the ratio of NK cells to immature DCs is $\approx 2.39 : 1$, corresponding to an approximate 52.85% being lysed. However, if we consider only immature DC loss due to degradation, after 24 hours, only $1 - e^{-d_{D_0}} \approx 3.54\%$ are lost to it. Thus, we

assume at steady state that

$$\frac{\lambda_{D_0K} \overline{D_0K}}{2 \times 0.5285} = \frac{d_{D_0} \overline{D_0}}{0.0354} \implies \lambda_{D_0K} = 5.49 \times 10^{-6} \text{ (cell/cm}^3\text{)}^{-1} \text{ day}^{-1}.$$

Considering (3.4.7) at steady state leads to

$$\frac{\lambda_{DH} \overline{D_0}}{2} - \lambda_{DD^{\text{LN}}} \overline{D} - d_D \overline{D} = 0.$$

Finally, it was found in [44] that only a limited number of DCs migrate up to the TDLN, with at most 4% of DCs reaching the TDLN in melanoma patients when DCs were injected intradermally. We assume at steady state that this holds, too, for MSI-H/dMMR CRC. Taking into account that only $e^{-d_D \tau_m}$ of mature DCs that leave the TS survive their migration to the TDLN, we have that

$$\frac{\lambda_{DD^{\text{LN}}}}{0.04e^{d_D \tau_m}} = \frac{d_D}{1 - 0.04e^{d_D \tau_m}}.$$

This leads to

$$\begin{aligned} \mathcal{A}_{D_0} &= 1.18 \times 10^6 \text{ (cell/cm}^3\text{)} \text{ day}^{-1}, \\ \lambda_{DH} &= 1.33 \text{ day}^{-1}, \\ \lambda_{DD^{\text{LN}}} &= 1.68 \times 10^{-2} \text{ day}^{-1}. \end{aligned}$$

B.4.2 Estimates for M_0 , M_1 , and M_2

To estimate the macrophage production constants, we consider (3.4.25), (3.4.26), (3.4.27) at steady state, and use the data from [45]. We assume that the magnitude of response to a specific cytokine is proportional to its corresponding macrophage polarisation rate, where the response is defined as the Euclidean distance between the centroid vectors of cytokine-treated macrophages and phosphate-buffered saline (PBS)-treated macrophages.

Adding (3.4.25), (3.4.26), and (3.4.27) at steady state, leads to

$$\mathcal{A}_{M_0} - d_{M_0} \overline{M_0} - d_{M_1} \overline{M_1} - d_{M_2} \overline{M_2} = 0 \implies \mathcal{A}_{M_0} = 1.08 \times 10^6 \text{ (cell/cm}^3\text{)} \text{ day}^{-1}.$$

Using values from [45], and considering (3.4.25) and (3.4.26) at steady state, leads to the equations

$$\begin{aligned} \mathcal{A}_{M_0} - \frac{\lambda_{M_1 I_\alpha} \overline{M_0}}{2} - \frac{\lambda_{M_1 I_\gamma} \overline{M_0}}{2} - \frac{\lambda_{M_2 I_{10}} \overline{M_0}}{2} - \frac{\lambda_{M_2 I_\beta} \overline{M_0}}{2} - d_{M_0} \overline{M_0} &= 0, \\ \frac{\lambda_{M_1 I_\alpha} \overline{M_0}}{2} + \frac{\lambda_{M_1 I_\gamma} \overline{M_0}}{2} - d_{M_1} \overline{M_1} &= 0, \\ \frac{\lambda_{M_1 I_\alpha}}{2 \times 10.77} &= \frac{\lambda_{M_1 I_\gamma}}{2 \times 12.54}, \\ \frac{\lambda_{M_2 I_{10}}}{2 \times 6.81} &= \frac{\lambda_{M_2 I_\beta}}{2 \times 7.63}. \end{aligned}$$

Solving these simultaneously leads to

$$\lambda_{M_1 I_\alpha} = 3.77 \times 10^{-1} \text{ day}^{-1},$$

$$\begin{aligned}\lambda_{M_1 I_\gamma} &= 4.39 \times 10^{-1} \text{ day}^{-1}, \\ \lambda_{M_2 I_{10}} &= 2.09 \times 10^{-1} \text{ day}^{-1}, \\ \lambda_{M_2 I_\beta} &= 2.34 \times 10^{-1} \text{ day}^{-1}.\end{aligned}$$

B.4.3 Estimates for K_0 and K

To estimate NK cell production parameters, we do a similar process to macrophages. Adding (3.4.28) and (3.4.29) at steady state, leads to

$$\mathcal{A}_{K_0} - d_{K_0} \overline{K_0} - d_K \overline{K} = 0 \implies \mathcal{A}_{K_0} = 2.82 \times 10^5 \text{ (cell/cm}^3\text{) day}^{-1}.$$

Considering (3.4.29) at steady state leads to

$$\frac{1}{2} \left(\frac{\lambda_{K I_2} \overline{K_0}}{2} + \frac{\lambda_{K D} \overline{K_0}}{2} \right) - d_K \overline{K} = 0.$$

We finally assume that DC-mediated NK-cell activation is twice as potent as cytokine-induced activation at steady state, so that

$$\frac{\lambda_{K D}/2}{2} = \frac{\lambda_{K I_2}/2}{1}.$$

Solving these simultaneously leads to

$$\begin{aligned}\lambda_{K I_2} &= 4.62 \times 10^{-3} \text{ day}^{-1}, \\ \lambda_{K D} &= 9.24 \times 10^{-3} \text{ day}^{-1}.\end{aligned}$$

B.5 T Cell Parameters and Estimates

B.5.1 Estimates for T_0^8 , T_A^8 , T_8 and T_{ex}

Considering (3.4.9) at steady state leads to

$$\mathcal{A}_{T_0^8} - \overline{R^8} - d_{T_0^8} \overline{T_0^8} = 0,$$

and in particular,

$$\overline{R^8} = \frac{\lambda_{T_0^8 T_A^8} \overline{D^{\text{LN}}} \overline{T_0^8}}{4}.$$

Considering (3.4.11) at steady state leads to

$$\frac{2^{n_{\text{max}}^8} e^{-d_{T_0^8} \tau_{T_A^8}} \overline{R^8}}{4} - \lambda_{T_A^8 T_8} \overline{T_A^8} - d_{T_8} \overline{T_A^8} = 0.$$

We first consider the case where no pembrolizumab is present. Considering (3.4.13) and (3.4.14) at steady state leads to

$$\begin{aligned}\frac{V_{\text{LN}}}{V_{\text{TS}}} \lambda_{T_A^8 T_8} \overline{T_A^8} - \frac{\lambda_{T_8 C} \overline{T_8}}{2} - \frac{d_{T_8} \overline{T_8}}{2} &= 0, \\ \frac{\lambda_{T_8 C} \overline{T_8}}{2} - \frac{d_{T_{\text{ex}}} \overline{T_{\text{ex}}}}{2} &= 0.\end{aligned}$$

To determine $\lambda_{T_{\text{ex}}A_1}$, we assume that when pembrolizumab is present, at steady state, 20% of exhausted CD8+ T cells are reinvigorated. That is, we assume that

$$\frac{\lambda_{T_{\text{ex}}A_1}\overline{T_{\text{ex}}}/2}{0.2} = \frac{d_{T_{\text{ex}}}\overline{T_{\text{ex}}}/2}{0.8}.$$

Solving these equations simultaneously leads to

$$\begin{aligned}\mathcal{A}_{T_0^8} &= 3.76 \times 10^5 \text{ (cell/cm}^3\text{) day}^{-1}, \\ \lambda_{T_0^8 T_A^8} &= 2.69 \times 10^{-11} \text{ (cell/cm}^3\text{)}^{-1} \text{ day}^{-1}, \\ \overline{R^8} &= 2.18 \times 10^3 \text{ (cell/cm}^3\text{) day}^{-1}, \\ \lambda_{T_A^8 T_8} &= 6.64 \times 10^{-1} \text{ day}^{-1}, \\ \lambda_{T_8 C} &= 6.31 \times 10^{-3} \text{ day}^{-1}, \\ \lambda_{T_{\text{ex}}A_1} &= 2.25 \times 10^{-3} \text{ day}^{-1}.\end{aligned}$$

B.5.2 Estimates for T_0^4 , T_A^1 , and T_1

Considering (3.4.15) at steady state leads to

$$\mathcal{A}_{T_0^4} - \overline{R^1} - d_{T_0^4}\overline{T_0^4} = 0,$$

where

$$\overline{R^1} = \frac{\lambda_{T_0^4 T_A^1} \overline{D^{\text{LN}} T_0^4}}{4}.$$

Considering (3.4.17) at steady state leads to

$$\frac{2^{n_{\text{max}}^1} e^{-d_{T_0^4} \tau_{T_A^1}} \overline{R^1}}{4} - \lambda_{T_A^1 T_1} \overline{T_A^1} - d_{T_1} \overline{T_A^1} = 0.$$

Based on murine data from [46], we assume that at steady state, 20% of Th1 cells are converted to Tregs. That is, we assume that

$$\frac{\lambda_{T_1 T_r} \overline{T_1}/2}{0.2} = \frac{d_{T_1} \overline{T_1}}{0.8}.$$

Finally, considering (3.4.19) at steady state leads to

$$\frac{V_{\text{LN}}}{V_{\text{TS}}} \lambda_{T_A^1 T_1} \overline{T_A^1} - \frac{\lambda_{T_1 T_r} \overline{T_1}}{2} - d_{T_1} \overline{T_1} = 0.$$

Solving these equations simultaneously leads to

$$\begin{aligned}\mathcal{A}_{T_0^4} &= 2.76 \times 10^5 \text{ (cell/cm}^3\text{) day}^{-1}, \\ \lambda_{T_0^4 T_A^1} &= 8.12 \times 10^{-11} \text{ (cell/cm}^3\text{)}^{-1} \text{ day}^{-1}, \\ \overline{R^1} &= 3.79 \times 10^3 \text{ (cell/cm}^3\text{) day}^{-1}, \\ \lambda_{T_A^1 T_1} &= 6.48 \times 10^{-2} \text{ day}^{-1}, \\ \lambda_{T_1 T_r} &= 4.00 \times 10^{-3} \text{ day}^{-1}.\end{aligned}$$

B.5.3 Estimates for T_0^r , T_A^r , and T_r

Considering (3.4.20) at steady state leads to

$$\mathcal{A}_{T_0^r} - \overline{R^r} - d_{T_0^r} \overline{T_0^r} = 0,$$

where

$$\overline{R^r} = \lambda_{T_0^r T_A^r} \overline{D^{\text{LN}} T_0^r}.$$

Considering (3.4.22) at steady state leads to

$$2^{n_{\max}^r} e^{-d_{T_0^r} \tau_{T_A^r}} \overline{R^r} - \lambda_{T_A^r T_r} \overline{T_A^r} - d_{T_r} \overline{T_A^r} = 0.$$

Finally, considering (3.4.24) at steady state leads to

$$\frac{V_{\text{LN}}}{V_{\text{TS}}} \lambda_{T_A^r T_r} \overline{T_A^r} + \frac{\lambda_{T_1 T_r} \overline{T_1}}{2} - d_{T_r} \overline{T_r} = 0.$$

Solving these equations simultaneously leads to

$$\begin{aligned} \mathcal{A}_{T_0^r} &= 1.15 \times 10^5 \text{ (cell/cm}^3\text{) day}^{-1}, \\ \lambda_{T_0^r T_A^r} &= 1.06 \times 10^{-8} \text{ (cell/cm}^3\text{)}^{-1} \text{ day}^{-1}, \\ \overline{R^r} &= 1.12 \times 10^5 \text{ (cell/cm}^3\text{) day}^{-1}, \\ \lambda_{T_A^r T_r} &= 4.79 \text{ day}^{-1}. \end{aligned}$$

B.6 Estimates for Cancer Cells

Considering (3.4.1) at steady state leads to

$$\lambda_C \left(1 - \frac{\overline{C}}{C_0}\right) - \frac{\lambda_{CT_8}}{4} \overline{T_8} - \frac{\lambda_{CK}}{4} \overline{K} - \frac{\lambda_{CI_\alpha}}{2} = 0.$$

We assume that CD8+ T cells and NK cells kill cancer cells with similar potency, so we approximate

$$\lambda_{CK}/4 = \lambda_{CT_8}/4 \implies \lambda_{CK} = \lambda_{CT_8}.$$

Considering (3.4.2) at steady state leads to the equation

$$\frac{\lambda_{CI_\alpha} \overline{C}}{2} - d_{N_c} \overline{N_c} = 0.$$

Solving these simultaneously, and using the same λ_C , λ_{CT_8} , and C_0 as the full model, leads to

$$\begin{aligned} \lambda_C &= 5.25 \times 10^{-2} \text{ day}^{-1}, \\ \lambda_{CT_8} &= 8.01 \times 10^{-8} \text{ (cell/cm}^3\text{)}^{-1} \text{ day}^{-1}, \\ C_0 &= 8.89 \times 10^7 \text{ cell/cm}^3, \\ \lambda_{CK} &= 8.01 \times 10^{-8} \text{ (cell/cm}^3\text{)}^{-1} \text{ day}^{-1}, \\ \lambda_{CI_\alpha} &= 7.23 \times 10^{-3} \text{ day}^{-1}, \\ d_{N_c} &= 6.88 \times 10^{-2} \text{ day}^{-1}. \end{aligned}$$

B.7 Estimates for Immune Checkpoint-Associated Components in the TS

B.7.1 Estimates for Synthesis Rates and Steady States

We first denote $\rho_{P_D^{T_8}}$, $\rho_{P_D^{T_1}}$, and $\rho_{P_D^K}$ as the number of PD-1 molecules expressed on the surface of CD8+ T cells, Th1 cells, and activated NK cells in the TS, respectively. To determine these parameters, we used the baseline data collected in [47] on 5 advanced cancer patients before their pembrolizumab infusions. The net number of PD-1 molecules on the surface of CD4+ T cells was 2053 molec/cell, and so we set $\rho_{P_D^{T_1}} = 2.05 \times 10^3$ molec/cell. The net number of PD-1 molecules on the surface of CD8+ T cells was 2761 molec/cell, and so we set $\rho_{P_D^{T_8}} = 2.76 \times 10^3$ molec/cell. Despite the net number of PD-1 molecules on the surface of NK cells being below the lower limit of quantification in [47], NK cells substantially express PD-1 [48] in CRC, and so we set $\rho_{P_D^K} = \rho_{P_D^{T_8}}/5 = 5.52 \times 10^2$ molec/cell.

We next denote $\rho_{P_L C}$ and $\rho_{P_L M_2}$ as the number of PD-L1 molecules expressed on cancer cells and M2 macrophages, respectively. In their quantitative systems pharmacology model of colorectal cancer, Anbari et al. estimated the baseline numbers of PD-L1 molecules per cancer cell and per APC to be 180,000 molec/cell and 266,666 molec/cell, respectively [49]. This makes sense, noting that PD-L1 expression in macrophages is stronger and more continuous than that in cancer cells [50]. As such, we set $\rho_{P_L C} = 1.8 \times 10^5$ molec/cell and $\rho_{P_L M_2} = 2.67 \times 10^5$ molec/cell.

Considering (3.4.39) – (3.4.41), and (3.4.46) – (3.4.49) at steady state in the absence of pembrolizumab leads to

$$\begin{aligned}\lambda_{P_D^{T_8}} \overline{T_8} - d_{P_D} \overline{P_D^{T_8}} &= 0, \\ \lambda_{P_D^{T_1}} \overline{T_1} - d_{P_D} \overline{P_D^{T_1}} &= 0, \\ \lambda_{P_D^K} \overline{K} - d_{P_D} \overline{P_D^K} &= 0, \\ \lambda_{P_L C} \overline{C} + \lambda_{P_L M_2} \overline{M_2} - d_{P_L} \overline{P_L} &= 0, \\ \overline{Q^{T_8}} - \frac{\lambda_{P_D P_L}}{\lambda_Q} \overline{P_D^{T_8}} \overline{P_L} &= 0, \\ \overline{Q^{T_1}} - \frac{\lambda_{P_D P_L}}{\lambda_Q} \overline{P_D^{T_1}} \overline{P_L} &= 0, \\ \overline{Q^K} - \frac{\lambda_{P_D P_L}}{\lambda_Q} \overline{P_D^K} \overline{P_L} &= 0.\end{aligned}$$

By considering the total number of PD-1 receptors expressed on each PD-1-expressing cell at steady state, we expect in the absence of pembrolizumab that

$$\begin{aligned}\overline{P_D^{T_8}} + \overline{Q^{T_8}} &= \rho_{P_D^{T_8}} \overline{T_8}, \\ \overline{P_D^{T_1}} + \overline{Q^{T_1}} &= \rho_{P_D^{T_1}} \overline{T_1}, \\ \overline{P_D^K} + \overline{Q^K} &= \rho_{P_D^K} \overline{K}.\end{aligned}$$

We can also consider the total number of PD-L1 ligands at steady state so that

$$\overline{P_L} + \overline{Q^{T_8}} + \overline{Q^{T_1}} + \overline{Q^K} = \rho_{P_L C} \overline{C} + \rho_{P_L M_2} \overline{M_2}.$$

Finally, we expect the synthesis rates of PD-1 and PD-L1 to be proportional to the total number of PD-1 molecules expressed per PD-1- and PD-L1-expressing cell, so that

$$\frac{\lambda_{P_D^{T_8}}}{\rho_{P_D^{T_8}}} = \frac{\lambda_{P_D^{T_1}}}{\rho_{P_D^{T_1}}} = \frac{\lambda_{P_D^K}}{\rho_{P_D^K}},$$

$$\frac{\lambda_{P_L C}}{\rho_{P_L C}} = \frac{\lambda_{P_L M_2}}{\rho_{P_L M_2}}.$$

Solving these simultaneously and ensuring all model parameters are positive leads to

$$\begin{aligned}\lambda_{P_D^{T_8}} &= 9.25 \times 10^2 \text{ (molec/cell) day}^{-1}, \\ \lambda_{P_D^{T_1}} &= 6.87 \times 10^2 \text{ (molec/cell) day}^{-1}, \\ \lambda_{P_D^K} &= 1.85 \times 10^2 \text{ (molec/cell) day}^{-1}, \\ \lambda_{P_L C} &= 2.50 \times 10^5 \text{ (molec/cell) day}^{-1}, \\ \lambda_{P_L M_2} &= 3.71 \times 10^5 \text{ (molec/cell) day}^{-1}.\end{aligned}$$

This leads to

$$\begin{aligned}\overline{P_D^{T_8}} &= 4.87 \times 10^8 \text{ molec/cm}^3, \\ \overline{P_D^{T_1}} &= 2.17 \times 10^8 \text{ molec/cm}^3, \\ \overline{P_D^K} &= 1.07 \times 10^8 \text{ molec/cm}^3, \\ \overline{P_L} &= 1.30 \times 10^{13} \text{ molec/cm}^3, \\ \overline{Q^{T_8}} &= 1.35 \times 10^6 \text{ molec/cm}^3, \\ \overline{Q^{T_1}} &= 5.99 \times 10^5 \text{ molec/cm}^3, \\ \overline{Q^K} &= 2.95 \times 10^5 \text{ molec/cm}^3.\end{aligned}$$

B.7.2 Estimates for Initial Conditions

To determine the relevant initial conditions, we can simply consider the total number of PD-1 receptors on each PD-1-expressing cell and PD-L1 ligands in the absence of pembrolizumab so that

$$\begin{aligned}P_D^{T_8}(0) + Q^{T_8}(0) &= \rho_{P_D^{T_8}} T_8(0), \\ P_D^{T_1}(0) + Q^{T_1}(0) &= \rho_{P_D^{T_1}} T_1(0), \\ P_D^K(0) + Q^K(0) &= \rho_{P_D^K} K(0), \\ P_L(0) + Q^{T_8}(0) + Q^{T_1}(0) + Q^K(0) &= \rho_{P_L C} C(0) + \rho_{P_L M_2} M_2(0).\end{aligned}$$

We can also consider (3.4.47) – (3.4.49) initially, so that

$$\begin{aligned}Q^{T_8}(0) - \frac{\lambda_{P_D P_L}}{\lambda_Q} P_D^{T_8}(0) P_L(0) &= 0, \\ Q^{T_1}(0) - \frac{\lambda_{P_D P_L}}{\lambda_Q} P_D^{T_1}(0) P_L(0) &= 0,\end{aligned}$$

$$Q^K(0) - \frac{\lambda_{P_D P_L}}{\lambda_Q} P_D^K(0) P_L(0) = 0.$$

Solving these simultaneously leads to

$$\begin{aligned} P_D^{T_8}(0) &= 4.44 \times 10^8 \text{ molec/cm}^3, \\ P_D^{T_1}(0) &= 2.07 \times 10^8 \text{ molec/cm}^3, \\ P_D^K(0) &= 2.46 \times 10^8 \text{ molec/cm}^3, \\ P_L(0) &= 7.36 \times 10^{12} \text{ molec/cm}^3, \\ Q^{T_8}(0) &= 6.96 \times 10^5 \text{ molec/cm}^3, \\ Q^{T_1}(0) &= 3.24 \times 10^5 \text{ molec/cm}^3, \\ Q^K(0) &= 3.86 \times 10^5 \text{ molec/cm}^3. \end{aligned}$$

We note that excluding bound PD-1 receptors when considering the total number of PD-1 receptors on PD-1-expressing cells does not affect the parameter estimates, steady states, or initial conditions at this level of precision, since the number of unbound PD-1 receptors is several orders of magnitude larger than the number of bound PD-1 receptors on PD-1-expressing cells. Furthermore, this also applies when considering the total number of PD-L1 ligands.

B.8 Estimates for Immune Checkpoint-Associated Components in the TDLN

B.8.1 Estimates for Synthesis Rates and Steady States

For simplicity, we assume that the total number of PD-1 receptors on cells in the TDLN is equal to the number on the corresponding cells in the TS. Thus, denoting $\rho_{P_D^{8LN}}$ and $\rho_{P_D^{1LN}}$ as the number of PD-1 molecules expressed on the surface of CD8+ T cells and Th1 cells in the TDLN, respectively, we have that $\rho_{P_D^{8LN}} = \rho_{P_D^{T_8}}$ and $\rho_{P_D^{1LN}} = \rho_{P_D^{T_1}}$.

We denote $\rho_{P_L^{LN} D^{LN}}$ and $\rho_{P_L^{LN} T_A^1}$ as the number of PD-L1 molecules expressed on mature DCs, and effector Th1 cells in the TDLN, respectively. It was found in [4] that the PD-L1 expression on activated CD3+ PD-L1+ T cells was 9282 molec/cell, whilst the PD-L1 expression on mature DCs was 80,372 molec/cell. However, amongst advanced CRC patients, only 22.4% of CD4+ T cells were PD-L1+ [51]. Moreover, only 22% of colonic DCs were PD-L1+ in [52]. We thus assumed that $\rho_{P_L^{LN} T_A^1} = 2.08 \times 10^3$ molec/cell, and $\rho_{P_L^{LN} D^{LN}} = 1.77 \times 10^4$ molec/cell.

The procedure for estimating parameters, steady states, and initial conditions for PD-1, PD-L1, and the PD-1/PD-L1 complex in the TDLN is the same as in the TS. Considering (3.4.50) – (3.4.51) and (3.4.55) – (3.4.57) at steady state in the absence of pembrolizumab, and making the same assumptions for estimation as in the TS, we obtain

$$\begin{aligned} \lambda_{P_D^{8LN}} \overline{P_D^{8LN}} - d_{P_D} \overline{P_D^{8LN}} &= 0, \\ \lambda_{P_D^{1LN}} \overline{P_D^{1LN}} - d_{P_D} \overline{P_D^{1LN}} &= 0, \\ \lambda_{P_L^{LN} D^{LN}} \overline{D^{LN}} + \lambda_{P_L^{LN} T_A^1} \overline{T_A^1} - d_{P_L} \overline{P_L^{LN}} &= 0, \\ \overline{Q^{8LN}} - \frac{\lambda_{P_D P_L}}{\lambda_Q} \overline{P_D^{8LN}} \overline{P_L^{LN}} &= 0, \end{aligned}$$

$$\begin{aligned}
\overline{Q^{1\text{LN}}} - \frac{\lambda_{P_D P_L}}{\lambda_Q} \overline{P_D^{1\text{LN}}} \overline{P_L^{1\text{LN}}} &= 0, \\
\overline{P_D^{8\text{LN}}} + \overline{Q^{8\text{LN}}} &= \rho_{P_D^{8\text{LN}}} \overline{T_A^8}, \\
\overline{P_D^{1\text{LN}}} + \overline{Q^{1\text{LN}}} &= \rho_{P_D^{1\text{LN}}} \overline{T_A^1}, \\
\overline{P_L^{1\text{LN}}} + \overline{Q^{8\text{LN}}} + \overline{Q^{1\text{LN}}} &= \rho_{P_L^{1\text{LN}} D^{\text{LN}}} \overline{D^{\text{LN}}} + \rho_{P_L^{1\text{LN}} T_A^1} \overline{T_A^1}, \\
\frac{\lambda_{P_D^{8\text{LN}}}}{\rho_{P_D^{8\text{LN}}}} &= \frac{\lambda_{P_D^{1\text{LN}}}}{\rho_{P_D^{1\text{LN}}}}, \\
\frac{\lambda_{P_L D^{\text{LN}}}}{\rho_{P_L D^{\text{LN}}}} &= \frac{\lambda_{P_L T_A^1}}{\rho_{P_L T_A^1}}.
\end{aligned}$$

Solving these simultaneously and ensuring all model parameters are positive leads to

$$\begin{aligned}
\lambda_{P_D^{8\text{LN}}} &= 9.27 \times 10^2 \text{ (molec/cell) day}^{-1}, \\
\lambda_{P_D^{1\text{LN}}} &= 6.89 \times 10^2 \text{ (molec/cell) day}^{-1}, \\
\lambda_{P_L^{1\text{LN}} D^{\text{LN}}} &= 2.46 \times 10^4 \text{ (molec/cell) day}^{-1}, \\
\lambda_{P_L^{1\text{LN}} T_A^1} &= 2.89 \times 10^3 \text{ (molec/cell) day}^{-1}.
\end{aligned}$$

This leads to

$$\begin{aligned}
\overline{P_D^{8\text{LN}}} &= 2.29 \times 10^9 \text{ molec/cm}^3, \\
\overline{P_D^{1\text{LN}}} &= 1.37 \times 10^{10} \text{ molec/cm}^3, \\
\overline{P_L^{1\text{LN}}} &= 5.94 \times 10^{11} \text{ molec/cm}^3, \\
\overline{Q^{8\text{LN}}} &= 2.90 \times 10^5 \text{ molec/cm}^3, \\
\overline{Q^{1\text{LN}}} &= 1.73 \times 10^6 \text{ molec/cm}^3.
\end{aligned}$$

B.8.2 Estimates for Initial Conditions

To determine the relevant immune checkpoint initial conditions, we can simply consider the total number of PD-1 receptors on each PD-1-expressing cell and PD-L1 ligands in the absence of pembrolizumab, so that

$$\begin{aligned}
P_D^{8\text{LN}}(0) + Q^{8\text{LN}}(0) &= \rho_{P_D^{8\text{LN}}} T_A^8(0), \\
P_D^{1\text{LN}}(0) + Q^{1\text{LN}}(0) &= \rho_{P_D^{1\text{LN}}} T_A^1(0), \\
P_L^{1\text{LN}}(0) + Q^{8\text{LN}}(0) + Q^{1\text{LN}}(0) &= \rho_{P_L^{1\text{LN}} D^{\text{LN}}} D^{\text{LN}}(0) + \rho_{P_L^{1\text{LN}} T_A^1} T_A^1(0).
\end{aligned}$$

We can also consider (3.4.56) and (3.4.57) initially, so that

$$\begin{aligned}
Q^{8\text{LN}}(0) - \frac{\lambda_{P_D P_L}}{\lambda_Q} P_D^{8\text{LN}}(0) P_L^{1\text{LN}}(0) &= 0, \\
Q^{1\text{LN}}(0) - \frac{\lambda_{P_D P_L}}{\lambda_Q} P_D^{1\text{LN}}(0) P_L^{1\text{LN}}(0) &= 0.
\end{aligned}$$

Solving these simultaneously leads to

$$\begin{aligned}
P_D^{8LN}(0) &= 2.37 \times 10^9 \text{ molec/cm}^3, \\
P_D^{1LN}(0) &= 1.59 \times 10^{10} \text{ molec/cm}^3, \\
P_L^{LN}(0) &= 3.31 \times 10^{11} \text{ molec/cm}^3, \\
Q^{8LN}(0) &= 1.67 \times 10^5 \text{ molec/cm}^3, \\
Q^{1LN}(0) &= 1.12 \times 10^6 \text{ molec/cm}^3.
\end{aligned}$$

We note again that excluding bound PD-1 receptors when considering the total number of PD-1 receptors on PD-1-expressing cells does not affect the parameter estimates, steady states, or initial conditions at this level of precision, since the number of unbound PD-1 receptors is several orders of magnitude larger than the number of bound PD-1 receptors on PD-1-expressing cells. Furthermore, this also applies when considering the total number of PD-L1 ligands.

C Model Parameters for the Reduced Model

The model parameter values are estimated in [Appendix B](#) and are listed in [Table C.1](#).

Table C.1: Parameter values for the reduced model. TDLN denotes the tumour-draining lymph node, whilst TS denotes the tumour site. est. denotes estimated parameters.

Parameter	Description	Value	Unit	References
f_{pembro}	A_1/A_1^{LN} dose scaling factor	1.17×10^{12}	(molec/cm ³) /mg	est.
f_C	C to V_{TS} scaling factor	1.17×10^6	cell/(cm ³) ²	est.
f_{N_c}	N_c to V_{TS} scaling factor	6.16×10^4	cell/(cm ³) ²	est.
\mathcal{A}_{D_0}	Source of D_0	1.18×10^6	(cell/cm ³) day ⁻¹	est.
$\mathcal{A}_{T_0^8}$	Source of T_0^8	3.76×10^5	(cell/cm ³) day ⁻¹	est.
$\mathcal{A}_{T_0^4}$	Source of T_0^4	2.76×10^5	(cell/cm ³) day ⁻¹	est.
$\mathcal{A}_{T_0^r}$	Source of T_0^r	1.15×10^5	(cell/cm ³) day ⁻¹	est.
\mathcal{A}_{M_0}	Source of M_0	1.08×10^6	(cell/cm ³) day ⁻¹	est.
\mathcal{A}_{K_0}	Source of K_0	2.82×10^5	(cell/cm ³) day ⁻¹	est.
λ_C	Growth rate of C	5.25×10^{-2}	day ⁻¹	fitted
λ_{CT_8}	Elimination rate of C by T_8	8.01×10^{-8}	(cell/cm ³) ⁻¹ day ⁻¹	fitted
λ_{CK}	Elimination rate of C by K	8.01×10^{-8}	(cell/cm ³) ⁻¹ day ⁻¹	est.
λ_{CI_α}	Necrosis rate of C by I_α	7.23×10^{-3}	day ⁻¹	est.
λ_{HN_c}	Production rate of H by N_c	2.92×10^{-14}	(g/cell) day ⁻¹	est.
λ_{SN_c}	Production rate of S by N_c	1.70×10^{-14}	(g/cell) day ⁻¹	est.
λ_{DH}	Maturation rate of D_0 by H	1.33	day ⁻¹	est.
λ_{D_0K}	Killing rate of D_0 by K	5.49×10^{-6}	(cell/cm ³) ⁻¹ day ⁻¹	est.
$\lambda_{DD^{\text{LN}}}$	Migration rate of D to TDLN	1.68×10^{-2}	day ⁻¹	est.
$\lambda_{T_0^8 T_A^8}$	Kinetic rate constant for T_0^8 activation	2.69×10^{-11}	(cell/cm ³) ⁻¹ day ⁻¹	est.
$\lambda_{T_A^8 T_8}$	Kinetic rate constant for T_A^8 migration to the TS	6.64×10^{-1}	day ⁻¹	est.

$\lambda_{T_8 C}$	Exhaustion rate of T_8 due to C exposure	6.31×10^{-3}	day^{-1}	est.
$\lambda_{T_{\text{ex}} A_1}$	Reinvigoration rate of T_{ex} by A_1	2.25×10^{-3}	day^{-1}	est.
$\lambda_{T_0^4 T_A^1}$	Kinetic rate constant for T_0^4 activation into T_A^1	8.12×10^{-11}	$(\text{cell}/\text{cm}^3)^{-1} \text{day}^{-1}$	est.
$\lambda_{T_A^1 T_1}$	Kinetic rate constant for T_A^1 migration to the TS	6.48×10^{-2}	day^{-1}	est.
$\lambda_{T_1 T_r}$	Conversion rate of T_1 to T_r by Q^{T_1}	4.00×10^{-3}	day^{-1}	est.
$\lambda_{T_0^r T_A^r}$	Kinetic rate constant for T_0^r activation into T_A^r	1.06×10^{-8}	$(\text{cell}/\text{cm}^3)^{-1} \text{day}^{-1}$	est.
$\lambda_{T_A^r T_r}$	Kinetic rate constant for T_A^r migration to the TS	4.79	day^{-1}	est.
$\lambda_{M_1 I_\alpha}$	Polarisation rate of M_0 to M_1 by I_α	3.77×10^{-1}	day^{-1}	est.
$\lambda_{M_1 I_\gamma}$	Polarisation rate of M_0 to M_1 by I_γ	4.39×10^{-1}	day^{-1}	est.
$\lambda_{M_2 I_{10}}$	Polarisation rate of M_0 to M_2 by I_{10}	2.09×10^{-1}	day^{-1}	est.
$\lambda_{M_2 I_\beta}$	Polarisation rate of M_0 to M_2 by I_β	2.34×10^{-1}	day^{-1}	est.
$\lambda_{K I_2}$	Maturation rate of K_0 by I_2	4.62×10^{-3}	day^{-1}	est.
$\lambda_{K D}$	Maturation rate of K_0 by D	9.24×10^{-3}	day^{-1}	est.
$\lambda_{I_2 T_8}$	Production rate of I_2 by T_8	5.95×10^{-16}	$(\text{g}/\text{cell}) \text{day}^{-1}$	est.
$\lambda_{I_2 T_1}$	Production rate of I_2 by T_1	1.74×10^{-15}	$(\text{g}/\text{cell}) \text{day}^{-1}$	est.
$\lambda_{I_\gamma K}$	Production rate of I_γ by K	8.46×10^{-15}	$(\text{g}/\text{cell}) \text{day}^{-1}$	est.
$\lambda_{I_\alpha T_8}$	Production rate of I_α by T_8	5.55×10^{-15}	$(\text{g}/\text{cell}) \text{day}^{-1}$	est.
$\lambda_{I_\alpha T_1}$	Production rate of I_α by T_1	9.17×10^{-15}	$(\text{g}/\text{cell}) \text{day}^{-1}$	est.
$\lambda_{I_\alpha M_1}$	Production rate of I_α by M_1	3.36×10^{-15}	$(\text{g}/\text{cell}) \text{day}^{-1}$	est.
$\lambda_{I_\alpha K}$	Production rate of I_α by K	9.68×10^{-15}	$(\text{g}/\text{cell}) \text{day}^{-1}$	est.
$\lambda_{I_\beta C}$	Production rate of I_β by C	7.42×10^{-12}	$(\text{g}/\text{cell}) \text{day}^{-1}$	est.
$\lambda_{I_\beta T_r}$	Production rate of I_β by T_r	4.30×10^{-11}	$(\text{g}/\text{cell}) \text{day}^{-1}$	est.
$\lambda_{I_\beta M_2}$	Production rate of I_β by M_2	5.34×10^{-11}	$(\text{g}/\text{cell}) \text{day}^{-1}$	est.
$\lambda_{I_{10} C}$	Production rate of I_{10} by C	1.56×10^{-17}	$(\text{g}/\text{cell}) \text{day}^{-1}$	est.
$\lambda_{I_{10} M_2}$	Production rate of I_{10} by M_2	3.11×10^{-17}	$(\text{g}/\text{cell}) \text{day}^{-1}$	est.
$\lambda_{P_D^{T_8}}$	Synthesis rate of $P_D^{T_8}$	9.25×10^2	$(\text{molec}/\text{cell}) \text{day}^{-1}$	est.
λ_{Q_A}	Dissociation rate of the PD-1/pembrolizumab complex	2.6	day^{-1}	[3]
λ_Q	Dissociation rate of the PD-1/PD-L1 complex	1.24×10^5	$(\text{molec}/\text{cell}) \text{day}^{-1}$	[4]
$\lambda_{P_D A_1}$	Formation rate of the PD-1/pembrolizumab complex	4.63×10^{-13}	$(\text{molec}/\text{cm}^3)^{-1} \text{day}^{-1}$	fitted
$\lambda_{P_D P_L}$	Formation rate of the PD-1/PD-L1 complex	2.64×10^{-11}	$(\text{molec}/\text{cm}^3)^{-1} \text{day}^{-1}$	[4]
$\lambda_{P_D^{T_1}}$	Synthesis rate of $P_D^{T_1}$	6.87×10^2	$(\text{molec}/\text{cell}) \text{day}^{-1}$	est.
$\lambda_{P_D^K}$	Synthesis rate of P_D^K	1.85×10^2	$(\text{molec}/\text{cell}) \text{day}^{-1}$	est.
$\lambda_{P_L C}$	Synthesis rate of P_L by C	2.50×10^5	$(\text{molec}/\text{cell}) \text{day}^{-1}$	est.

$\lambda_{P_L M_2}$	Synthesis rate of P_L by M_2	3.71×10^5	(molec/cell) day ⁻¹	est.
$\lambda_{P_D^{8LN}}$	Synthesis rate of P_D^{8LN}	9.27×10^2	(molec/cell) day ⁻¹	est.
$\lambda_{P_D^{1LN}}$	Synthesis rate of P_D^{1LN}	6.89×10^2	(molec/cell) day ⁻¹	est.
$\lambda_{P_L^{LN} D^{LN}}$	Synthesis rate of P_L^{LN} by D^{LN}	2.46×10^4	(molec/cell) day ⁻¹	est.
$\lambda_{P_L^{LN} T_A^1}$	Synthesis rate of P_L^{LN} by T_A^1	2.89×10^3	(molec/cell) day ⁻¹	est.
K_{CI_α}	Half-saturation constant of I_α for C	9.00×10^{-11}	g/cm ³	est.
K_{DH}	Half-saturation constant of H for D	1.94×10^{-8}	g/cm ³	est.
$K_{T_8 C}$	Half-saturation constant T_8 exhaustion due to C exposure	7.02×10^7	cell/cm ³	est.
$K_{T_{ex} A_1}$	Half-saturation constant of T_{ex} reinvigoration by A_1	2.05×10^{14}	molec/cm ³	est.
$K_{T_1 T_r}$	Half-saturation constant of T_1 conversion to T_r by Q^{T_1}	5.99×10^5	molec/cm ³	est.
$K_{M_1 I_\alpha}$	Half-saturation constant of I_α for M_1	9.00×10^{-11}	g/cm ³	est.
$K_{M_1 I_\gamma}$	Half-saturation constant of I_γ for M_1	4.93×10^{-11}	g/cm ³	est.
$K_{M_2 I_{10}}$	Half-saturation constant of I_{10} for M_2	1.84×10^{-10}	g/cm ³	est.
$K_{M_2 I_\beta}$	Half-saturation constant of I_β for M_2	1.51×10^{-6}	g/cm ³	est.
$K_{K I_2}$	Half-saturation constant of I_2 for K	2.00×10^{-12}	g/cm ³	est.
K_{KD}	Half-saturation constant of D for K	1.91×10^6	cell/cm ³	est.
C_0	Carrying capacity of C	8.89×10^7	cell/cm ³	fitted
$K_{C I_\beta}$	Inhibition constant of T_8 and K elimination of C by I_β	1.51×10^{-6}	g/cm ³	est.
$K_{C Q^{T_8}}$	Inhibition constant of T_8 elimination of C by Q^{T_8}	1.35×10^6	molec/cm ³	est.
$K_{C Q^K}$	Inhibition constant of K elimination of C by Q^K	2.95×10^5	molec/cm ³	est.
$K_{D_0 I_\beta}$	Inhibition constant of K elimination of D_0 by I_β	1.51×10^{-6}	g/cm ³	est.
V_{LN}	Volume of the TDLN	1.47×10^{-1}	cm ³	[5] est.
$K_{T_0^8 T_A^r}$	Inhibition constant of T_0^8 activation by T_A^r	1.47×10^6	cell/cm ³	est.
$K_{T_0^8 Q^{8LN}}$	Inhibition constant of T_0^8 activation by Q^{8LN}	2.90×10^5	(molec/cm ³) day	est.
$K_{T_A^8 T_A^r}$	Inhibition constant of T_A^8 activation by T_A^r	1.47×10^6	cell/cm ³	est.
$K_{T_A^8 Q^{8LN}}$	Inhibition constant of T_A^8 proliferation by Q^{8LN}	2.90×10^5	(molec/cm ³) day	est.
$K_{T_8 I_{10}}$	Inhibition constant of T_8 death by I_{10}	1.84×10^{-10}	g/cm ³	est.

$K_{T_{\text{ex}}I_{10}}$	Inhibition constant of T_{ex} death by I_{10}	1.84×10^{-10}	g/cm^3	est.
$K_{T_0^4 T_A^r}$	Inhibition constant of T_0^4 activation by T_A^r	1.47×10^6	cell/cm^3	est.
$K_{T_0^4 Q^{1\text{LN}}}$	Inhibition constant of T_0^4 activation by $Q^{1\text{LN}}$	1.73×10^6	molec/cm^3	est.
$K_{T_A^1 T_A^r}$	Inhibition constant of T_A^1 proliferation by T_A^r	1.47×10^6	cell/cm^3	est.
$K_{T_A^1 Q^{1\text{LN}}}$	Inhibition constant of T_A^1 proliferation by $Q^{1\text{LN}}$	1.73×10^6	molec/cm^3	est.
K_{KI_β}	Inhibition constant of NK cell activation by I_β	1.51×10^{-6}	g/cm^3	est.
d_{N_c}	Removal rate of N_c	6.88×10^{-2}	day^{-1}	est.
d_H	Degradation rate of H	5.55	day^{-1}	[6] est.
d_S	Degradation rate of S	1.39	day^{-1}	[7, 8] est.
d_{D_0}	Death rate of D_0	3.57×10^{-2}	day^{-1}	[9] est.
d_D	Death rate of D	3.15×10^{-1}	day^{-1}	[10] est.
$d_{T_0^8}$	Death rate of T_0^8	3.22×10^{-2}	day^{-1}	[11] est.
d_{T_8}	Death rate of T_8	9×10^{-3}	day^{-1}	[12]
$d_{T_{\text{ex}}}$	Death rate of T_{ex}	9×10^{-3}	day^{-1}	[12]
$d_{T_0^4}$	Death rate of T_0^4	4.03×10^{-2}	day^{-1}	[11] est.
d_{T_1}	Death rate of T_1	8×10^{-3}	day^{-1}	[12]
$d_{T_0^r}$	Death rate of T_0^r	2.2×10^{-3}	day^{-1}	[13]
d_{T_r}	Death rate of T_r	6.30×10^{-2}	day^{-1}	[14] est.
d_{M_0}	Death rate of M_0	0.73	day^{-1}	[15]
d_{M_1}	Death rate of M_1	0.99	day^{-1}	[15]
d_{M_2}	Death rate of M_2	1.35×10^{-1}	day^{-1}	[15]
d_{K_0}	Death rate of K_0	6.93×10^{-2}	day^{-1}	[16–18] est.
d_K	Death rate of K	6.93×10^{-2}	day^{-1}	[16–18] est.
d_{I_2}	Degradation rate of I_2	1.45×10^2	day^{-1}	[19] est.
d_{I_γ}	Degradation rate of I_γ	3.33×10^1	day^{-1}	[20] est.
d_{I_α}	Degradation rate of I_α	5.48×10^1	day^{-1}	[21, 22] est.
d_{I_β}	Degradation rate of I_β	3.99×10^2	day^{-1}	[23] est.
$d_{I_{10}}$	Degradation rate of I_{10}	6.16	day^{-1}	[24] est.
d_{P_D}	Degradation rate of unbound PD-1 receptors	3.36×10^{-1}	day^{-1}	[25]
d_{Q_A}	Internalisation rate of the PD-1/pembrolizumab complex	0.43	day^{-1}	[3]
d_{A_1}	Elimination rate of $A_1/A_1^{1\text{LN}}$	2.92×10^{-2}	day^{-1}	[26–28] est.
d_{P_L}	Degradation rate of unbound PD-L1	1.39	day^{-1}	[29]
τ_m	DC migration time from TDLN to the TS	0.75	day	[30] est.
Δ_8^0	Time taken for first CTL division	1.63	day	[32]
n_{max}^8	Maximal number of CTL divisions in the TDLN	10	dimensionless	[33, 34] est.

Δ_8	Time taken for successive CTL divisions	0.36	day	[33]
$\tau_{T_A^8}$	Time taken for CTL division program	4.87	day	est.
Δ_1^0	Time taken for first Th1 cell division	0.77	day	[38] est.
n_{\max}^1	Maximal number of Th1 cell divisions in the TDLN	9	dimensionless	[39] est.
Δ_1	Time taken for successive Th1 cell divisions	0.42	day	[38] est.
$\tau_{T_A^1}$	Time taken for Th1 cell division program	4.13	day	est.
Δ_r^0	Time taken for first Treg division	0.77	day	[38] est.
n_{\max}^r	Maximal number of Treg divisions in the TDLN	6	dimensionless	[40] est.
Δ_r	Time taken for successive Treg divisions	0.42	day	[38] est.
$\tau_{T_A^r}$	Time taken for Treg division program	2.87	day	est.

D Minimal Model Parameter Estimation

We estimate all parameters, where possible, under the assumption that no pembrolizumab has/will be administered. The exception to this is the parameters directly related to pembrolizumab treatment, for which the assumptions are explicitly stated during estimation. Many of the assumptions and techniques in this section are adopted from [1] and [41].

For the sake of brevity, we present parameter estimation only for those parameters that differ between the reduced and the minimal model. The absence of a parameter in this section implies that its value and derivation are identical to those provided in [Appendix B](#) and [Table C.1](#).

D.1 Half-Saturation Constants

Using (B.1), we have that

$$\begin{aligned}
K_{T_8 T_{\text{ex}}} &= \overline{C} = 7.02 \times 10^7 \text{ cell/cm}^3, \\
K_{DN_c} &= \overline{N_c} = 3.69 \times 10^6 \text{ cell/cm}^3, \\
K_{KT_8} &= \overline{T_8} = 1.77 \times 10^5 \text{ cell/cm}^3.
\end{aligned}$$

D.2 Inhibition Constants

Using (B.2), we have that

$$K_{CQT_8} = \overline{Q^{T_8}} = 1.31 \times 10^6 \text{ molec/cm}^3,$$

$$\begin{aligned}
K_{CQ^K} &= \overline{Q^K} = 2.87 \times 10^6 \text{ molec/cm}^3, \\
K_{T_0^8 T_A^r} &= K_{T_A^8 T_A^r} = \overline{T_A^r} = 1.47 \times 10^6 \text{ cell/cm}^3, \\
K_{T_8 C} &= K_{T_{\text{ex}} C} = \overline{C} = 7.02 \times 10^7 \text{ cell/cm}^3, \\
K_{T_0^8 Q^{8\text{LN}}} &= K_{T_A^8 Q^{8\text{LN}}} = \overline{Q^{8\text{LN}}} = 2.83 \times 10^5 \text{ molec/cm}^3.
\end{aligned}$$

D.3 Cytokine Production Parameters

To estimate the cytokine production constants, we consider (3.5.21) and (3.5.23) at steady state and use the data from [45]. For each immune cell, we assume that each cytokine's corresponding gene expression is proportional to its production rate by that cell.

D.3.1 Estimates for I_α

Using values from [45] and considering (3.5.21) at steady state, or equivalently considering (3.5.22), leads to the equations

$$\frac{\lambda_{I_\alpha T_8}}{0.0654443776961264} = \frac{\lambda_{I_\alpha K}}{0.114108294134927},$$

and

$$\lambda_{I_\alpha T_8} \overline{T_8} + \lambda_{I_\alpha K} \overline{K} - d_{I_\alpha} \overline{I_\alpha} = 0.$$

Solving these simultaneously leads to

$$\begin{aligned}
\lambda_{I_\alpha T_8} &= 9.57 \times 10^{-15} \text{ (g/cell) day}^{-1}, \\
\lambda_{I_\alpha K} &= 1.67 \times 10^{-14} \text{ (g/cell) day}^{-1}.
\end{aligned}$$

Consequently, considering (3.5.22), we have that

$$I_\alpha(0) = \frac{1}{d_{I_\alpha}} (\lambda_{I_\alpha T_8} T_8(0) + \lambda_{I_\alpha K} K(0)) = 1.64 \times 10^{-10} \text{ g/cm}^3.$$

D.3.2 Estimates for I_β

Estimating the production constants for TGF- β is slightly more complicated compared to other cytokines. We assume that the results for fibroblastic reticular cells in [53] translate directly to results for cancer-associated fibroblasts (CAFs), which are considered to be all fibroblasts found in the TME [53]. We assume that at steady state, CAFs produce twice as much TGF- β as cancer cells in the TME, and denote the production rate of TGF- β by CAFs as $\lambda_{I_\beta C_F}$. This, in conjunction with values from [45], and considering (3.5.23) at steady state, or equivalently considering (3.5.24), leads to the equations

$$\frac{\lambda_{I_\beta C_F}}{2} = \frac{\lambda_{I_\beta C}}{1},$$

and

$$\frac{\lambda_{I_\beta C_F}}{0.175283003265127} = \frac{\lambda_{I_\beta T_r}}{0.507677682409403},$$

and

$$\lambda_{I_\beta C} \overline{C} + \lambda_{I_\beta T_r} \overline{T_r} - d_{I_\beta} \overline{I_\beta} = 0.$$

Solving these simultaneously leads to

$$\begin{aligned}\lambda_{I_\beta C} &= 8.39 \times 10^{-12} \text{ (g/cell) day}^{-1}, \\ \lambda_{I_\beta T_r} &= 4.86 \times 10^{-11} \text{ (g/cell) day}^{-1}.\end{aligned}$$

Consequently, considering (3.5.24), we have that

$$I_\beta(0) = \frac{1}{d_{I_\beta}} (\lambda_{I_\beta C} C(0) + \lambda_{I_\beta T_r} T_r(0)) = 8.45 \times 10^{-7} \text{ g/cm}^3.$$

D.4 Parameters for DCs and NK Cells

D.4.1 Estimates for D_0 and D

Using the values from Appendix B.4.1, as well as substituting $\lambda_{DN_c} = \lambda_{DH}$, we get that

$$\begin{aligned}\mathcal{A}_{D_0} &= 1.18 \times 10^6 \text{ (cell/cm}^3\text{) day}^{-1}, \\ \lambda_{DN_c} &= 1.33 \text{ day}^{-1}, \\ \lambda_{DD^{LN}} &= 1.68 \times 10^{-2} \text{ day}^{-1}.\end{aligned}$$

D.4.2 Estimates for K

Using the values from Appendix B.4.3, and applying the transformations $\lambda_{KI_2} \overline{K_0} \mapsto \lambda_{KI_2}$, and $\lambda_{KD} \overline{K_0} \mapsto \lambda_{KD}$, where $\overline{K_0}$ is as in both the full and reduced models, leads to

$$\begin{aligned}\lambda_{KT_8} &= 1.79 \times 10^4 \text{ (cell/cm}^3\text{) day}^{-1}, \\ \lambda_{KD} &= 3.59 \times 10^4 \text{ (cell/cm}^3\text{) day}^{-1}.\end{aligned}$$

D.5 T Cell Parameters and Estimates

D.5.1 Estimates for T_A^8 , T_8 and T_{ex}

Using the values from Appendix B.5.1, and applying the transformation $\lambda_{T_0^8 T_A^8} \overline{T_0^8} \mapsto \lambda_{T_0^8 T_A^8}$, where $\overline{T_0^8}$ is as in both the full and reduced models, leads to

$$\begin{aligned}\lambda_{T_0^8 T_A^8} &= 3.12 \times 10^{-4} \text{ day}^{-1}, \\ \overline{R^8} &= 2.55 \times 10^3 \text{ (cell/cm}^3\text{) day}^{-1}, \\ \lambda_{T_A^8 T_8} &= 6.64 \times 10^{-1} \text{ day}^{-1}, \\ \lambda_{T_8 C} &= 6.31 \times 10^{-3} \text{ day}^{-1}, \\ \lambda_{T_{\text{ex}} A_1} &= 2.25 \times 10^{-3} \text{ day}^{-1}.\end{aligned}$$

D.5.2 Estimates for T_0^r , T_A^r , and T_r

Considering (3.5.15) at steady state leads to

$$\mathcal{A}_{T_0^r} - \overline{R^r} - d_{T_0^r} \overline{T_0^r} = 0,$$

where

$$\overline{R^r} = \lambda_{T_0^r T_A^r} \overline{D^{\text{LN}} T_0^r}.$$

Considering (3.5.17) at steady state leads to

$$2^{n_{\max}^r} e^{-d_{T_0^r} \tau_{T_A^r}} \overline{R^r} - \lambda_{T_A^r T_r} \overline{T_A^r} - d_{T_r} \overline{T_A^r} = 0.$$

Finally, considering (3.5.19) at steady state leads to

$$\frac{V_{\text{LN}}}{V_{\text{TS}}} \lambda_{T_A^r T_r} \overline{T_A^r} - d_{T_r} \overline{T_r} = 0.$$

Solving these equations simultaneously leads to

$$\begin{aligned} \mathcal{A}_{T_0^r} &= 1.14 \times 10^5 \text{ (cell/cm}^3\text{) day}^{-1}, \\ \lambda_{T_0^r T_A^r} &= 1.07 \times 10^{-8} \text{ (cell/cm}^3\text{)}^{-1} \text{ day}^{-1}, \\ \overline{R^r} &= 1.14 \times 10^5 \text{ (cell/cm}^3\text{) day}^{-1}, \\ \lambda_{T_A^r T_r} &= 4.85 \text{ day}^{-1}. \end{aligned}$$

D.6 Estimates for Immune Checkpoint-Associated Components in the TS

D.6.1 Estimates for Synthesis Rates and Steady States

As in Appendix B.7, we denote $\rho_{P_D^{T_8}}$ and $\rho_{P_D^K}$ as the number of PD-1 molecules expressed on the surface of CD8+ T cells and activated NK cells in the TS, respectively, with $\rho_{P_D^{T_8}} = 2.76 \times 10^3$ molec/cell and $\rho_{P_D^K} = 5.52 \times 10^2$ molec/cell. Similarly, we denote $\rho_{P_L^C}$ as the number of PD-L1 molecules expressed on cancer cells with $\rho_{P_L^C} = 1.8 \times 10^5$ molec/cell.

Considering (3.5.25) – (3.5.26), and (3.5.30) – (3.5.32) at steady state in the absence of pembrolizumab leads to

$$\begin{aligned} \lambda_{P_D^{T_8}} \overline{T_8} - d_{P_D} \overline{P_D^{T_8}} &= 0, \\ \lambda_{P_D^K} \overline{K} - d_{P_D} \overline{P_D^K} &= 0, \\ \lambda_{P_L^C} \overline{C} - d_{P_L} \overline{P_L} &= 0, \\ \overline{Q^{T_8}} - \frac{\lambda_{P_D P_L}}{\lambda_Q} \overline{P_D^{T_8}} \overline{P_L} &= 0, \\ \overline{Q^K} - \frac{\lambda_{P_D P_L}}{\lambda_Q} \overline{P_D^K} \overline{P_L} &= 0. \end{aligned}$$

By considering the total number of PD-1 receptors expressed on each PD-1-expressing cell at steady state, we expect in the absence of pembrolizumab that

$$\begin{aligned} \overline{P_D^{T_8}} + \overline{Q^{T_8}} &= \rho_{P_D^{T_8}} \overline{T_8}, \\ \overline{P_D^K} + \overline{Q^K} &= \rho_{P_D^K} \overline{K}. \end{aligned}$$

We can also consider the total number of PD-L1 ligands at steady state so that

$$\overline{P_L} + \overline{Q^{T_8}} + \overline{Q^K} = \rho_{P_L C} \overline{C}.$$

Finally, we expect the synthesis rates of PD-1 to be proportional to the total number of PD-1 molecules expressed per PD-1-expressing cell so that

$$\frac{\lambda_{P_D^{T_8}}}{\rho_{P_D^{T_8}}} = \frac{\lambda_{P_D^K}}{\rho_{P_D^K}}.$$

Solving these simultaneously and ensuring all model parameters are positive leads to

$$\begin{aligned}\lambda_{P_D^{T_8}} &= 9.25 \times 10^2 \text{ (molec/cell) day}^{-1}, \\ \lambda_{P_D^K} &= 1.85 \times 10^2 \text{ (molec/cell) day}^{-1}, \\ \lambda_{P_L C} &= 2.50 \times 10^5 \text{ (molec/cell) day}^{-1}.\end{aligned}$$

This leads to

$$\begin{aligned}\overline{P_D^{T_8}} &= 4.87 \times 10^8 \text{ molec/cm}^3, \\ \overline{P_D^K} &= 1.07 \times 10^8 \text{ molec/cm}^3, \\ \overline{P_L} &= 1.26 \times 10^{13} \text{ molec/cm}^3, \\ \overline{Q^{T_8}} &= 1.31 \times 10^6 \text{ molec/cm}^3, \\ \overline{Q^K} &= 2.87 \times 10^5 \text{ molec/cm}^3.\end{aligned}$$

D.6.2 Estimates for Initial Conditions

To determine the relevant initial conditions, we can simply consider the total number of PD-1 receptors on each PD-1-expressing cell and PD-L1 ligands in the absence of pembrolizumab so that

$$\begin{aligned}P_D^{T_8}(0) + Q^{T_8}(0) &= \rho_{P_D^{T_8}} T_8(0), \\ P_D^K(0) + Q^K(0) &= \rho_{P_D^K} K(0), \\ P_L(0) + Q^{T_8}(0) + Q^K(0) &= \rho_{P_L C} C(0).\end{aligned}$$

We can also consider (3.5.31) – (3.5.32) initially, so that

$$\begin{aligned}Q^{T_8}(0) - \frac{\lambda_{P_D P_L}}{\lambda_Q} P_D^{T_8}(0) P_L(0) &= 0, \\ Q^K(0) - \frac{\lambda_{P_D P_L}}{\lambda_Q} P_D^K(0) P_L(0) &= 0.\end{aligned}$$

Solving these simultaneously leads to

$$\begin{aligned}P_D^{T_8}(0) &= 4.44 \times 10^8 \text{ molec/cm}^3, \\ P_D^K(0) &= 2.46 \times 10^8 \text{ molec/cm}^3, \\ P_L(0) &= 7.02 \times 10^{12} \text{ molec/cm}^3,\end{aligned}$$

$$Q^{T_8}(0) = 6.63 \times 10^5 \text{ molec/cm}^3,$$

$$Q^K(0) = 3.68 \times 10^5 \text{ molec/cm}^3.$$

We note that excluding bound PD-1 receptors when considering the total number of PD-1 receptors on PD-1-expressing cells does not affect the parameter estimates, steady states, or initial conditions at this level of precision, since the number of unbound PD-1 receptors is several orders of magnitude larger than the number of bound PD-1 receptors on PD-1-expressing cells. Furthermore, this also applies when considering the total number of PD-L1 ligands.

D.7 Estimates for Immune Checkpoint-Associated Components in the TDLN

D.7.1 Estimates for Synthesis Rates and Steady States

Again, for simplicity, we assume that the total number of PD-1 receptors on cells in the TDLN is equal to the number on the corresponding cells in the TS. Thus, denoting $\rho_{P_D^{8LN}}$ as the number of PD-1 molecules expressed on the surface of CD8+ T cells in the TDLN, we have that $\rho_{P_D^{8LN}} = \rho_{P_D^{T_8}} = 2.76 \times 10^3 \text{ molec/cell}$. Similarly, as in [Appendix B.8](#), we denote $\rho_{P_L^{LN} D^{LN}}$ as the number of PD-L1 molecules expressed on the surface of mature DCs in the TDLN, with $\rho_{P_L^{LN} D^{LN}} = 1.77 \times 10^4 \text{ molec/cell}$.

Considering (3.5.33) and (3.5.36) – (3.5.37) at steady state in the absence of pembrolizumab, and making the same assumptions for estimation as in the TS, we obtain

$$\begin{aligned} \lambda_{P_D^{8LN}} \overline{P_D^{8LN}} - d_{P_D} \overline{P_D^{8LN}} &= 0, \\ \lambda_{P_L^{LN} D^{LN}} \overline{D^{LN}} - d_{P_L} \overline{P_L^{LN}} &= 0, \\ \overline{Q^{8LN}} - \frac{\lambda_{P_D P_L}}{\lambda_Q} \overline{P_D^{8LN} P_L^{LN}} &= 0, \\ \overline{P_D^{8LN}} + \overline{Q^{8LN}} &= \rho_{P_D^{8LN}} \overline{T_A^8}, \\ \overline{P_L^{LN}} + \overline{Q^{8LN}} &= \rho_{P_L^{LN} D^{LN}} \overline{D^{LN}}. \end{aligned}$$

Solving these simultaneously and ensuring all model parameters are positive leads to

$$\begin{aligned} \lambda_{P_D^{8LN}} &= 9.27 \times 10^2 \text{ (molec/cell) day}^{-1}, \\ \lambda_{P_L^{LN} D^{LN}} &= 2.46 \times 10^4 \text{ (molec/cell) day}^{-1}. \end{aligned}$$

This leads to

$$\begin{aligned} \overline{P_D^{8LN}} &= 2.29 \times 10^9 \text{ molec/cm}^3, \\ \overline{P_L^{LN}} &= 5.81 \times 10^{11} \text{ molec/cm}^3, \\ \overline{Q^{8LN}} &= 2.83 \times 10^5 \text{ molec/cm}^3. \end{aligned}$$

D.7.2 Estimates for Initial Conditions

To determine the relevant immune checkpoint initial conditions, we can simply consider the total number of PD-1 receptors on each PD-1-expressing cell and PD-L1 ligands in the absence of pem-

brolizumab, so that

$$\begin{aligned} P_D^{8\text{LN}}(0) + Q^{8\text{LN}}(0) &= \rho_{P_D^{8\text{LN}}} T_A^8(0), \\ P_L^{\text{LN}}(0) + Q^{8\text{LN}}(0) &= \rho_{P_L^{\text{LN}} D^{\text{LN}}} D^{\text{LN}}(0). \end{aligned}$$

We can also consider (3.5.37) initially so that

$$Q^{8\text{LN}}(0) - \frac{\lambda_{P_D P_L}}{\lambda_Q} P_D^{8\text{LN}}(0) P_L^{\text{LN}}(0) = 0.$$

Solving these simultaneously leads to

$$\begin{aligned} P_D^{8\text{LN}}(0) &= 2.37 \times 10^9 \text{ molec/cm}^3, \\ P_L^{\text{LN}}(0) &= 3.15 \times 10^{11} \text{ molec/cm}^3, \\ Q^{8\text{LN}}(0) &= 1.59 \times 10^5 \text{ molec/cm}^3. \end{aligned}$$

We note again that excluding bound PD-1 receptors when considering the total number of PD-1 receptors on PD-1-expressing cells does not affect the parameter estimates, steady states, or initial conditions at this level of precision, since the number of unbound PD-1 receptors is several orders of magnitude larger than the number of bound PD-1 receptors on PD-1-expressing cells. Furthermore, this also applies when considering the total number of PD-L1 ligands.

E Model Parameters for the Minimal Model

The model parameter values are estimated in [Appendix D](#) and are listed in [Table E.1](#).

Table E.1: Parameter values for the minimal model. TDLN denotes the tumour-draining lymph node, whilst TS denotes the tumour site. est. denotes estimated parameters.

Parameter	Description	Value	Unit	References
f_{pembro}	A_1/A_1^{LN} dose scaling factor	1.17×10^{12}	(molec/cm ³) /mg	est.
f_C	C to V_{TS} scaling factor	1.17×10^6	cell/(cm ³) ²	est.
f_{N_c}	N_c to V_{TS} scaling factor	6.16×10^4	cell/(cm ³) ²	est.
\mathcal{A}_{D_0}	Source of D_0	1.18×10^6	(cell/cm ³) day ⁻¹	est.
$\mathcal{A}_{T_0^r}$	Source of T_0^r	1.14×10^5	(cell/cm ³) day ⁻¹	est.
λ_C	Growth rate of C	5.25×10^{-2}	day ⁻¹	fitted
λ_{CT_8}	Elimination rate of C by T_8	8.01×10^{-8}	(cell/cm ³) ⁻¹ day ⁻¹	fitted
λ_{CK}	Elimination rate of C by K	8.01×10^{-8}	(cell/cm ³) ⁻¹ day ⁻¹	est.
λ_{CI_α}	Necrosis rate of C by I_α	7.23×10^{-3}	day ⁻¹	est.
$\lambda_{D_{N_c}}$	Maturation rate of D_0 by DAMPs	1.33	day ⁻¹	est.
$\lambda_{D_0 K}$	Killing rate of D_0 by K	5.49×10^{-6}	(cell/cm ³) ⁻¹ day ⁻¹	est.
$\lambda_{D D^{\text{LN}}}$	Migration rate of D to TDLN	1.68×10^{-2}	day ⁻¹	est.
$\lambda_{T_0^8 T_A^8}$	Kinetic rate constant for naive CD8+ T cell activation	3.12×10^{-4}	day ⁻¹	est.

$\lambda_{T_A^8 T_8}$	Kinetic rate constant for T_A^8 migration to the TS	6.64×10^{-1}	day^{-1}	est.
$\lambda_{T_8 C}$	Exhaustion rate of T_8 due to C exposure	6.31×10^{-3}	day^{-1}	est.
$\lambda_{T_{\text{ex}} A_1}$	Reinvigoration rate of T_{ex} by A_1	2.25×10^{-3}	day^{-1}	est.
$\lambda_{T_0^r T_A^r}$	Kinetic rate constant for T_0^r activation into T_A^r	1.07×10^{-8}	$(\text{cell}/\text{cm}^3)^{-1} \text{day}^{-1}$	est.
$\lambda_{T_A^r T_r}$	Kinetic rate constant for T_A^r migration to the TS	4.85	day^{-1}	est.
$\lambda_{K T_8}$	Maturation rate of K_0 by I_2	1.79×10^4	$(\text{cell}/\text{cm}^3) \text{day}^{-1}$	est.
$\lambda_{K D}$	Maturation rate of K_0 by D	3.59×10^4	$(\text{cell}/\text{cm}^3) \text{day}^{-1}$	est.
$\lambda_{I_\alpha T_8}$	Production rate of I_α by T_8	9.57×10^{-15}	$(\text{g}/\text{cell}) \text{day}^{-1}$	est.
$\lambda_{I_\alpha K}$	Production rate of I_α by K	1.67×10^{-14}	$(\text{g}/\text{cell}) \text{day}^{-1}$	est.
$\lambda_{I_\beta C}$	Production rate of I_β by C	8.39×10^{-12}	$(\text{g}/\text{cell}) \text{day}^{-1}$	est.
$\lambda_{I_\beta T_r}$	Production rate of I_β by T_r	4.86×10^{-11}	$(\text{g}/\text{cell}) \text{day}^{-1}$	est.
$\lambda_{P_D^{T_8}}$	Synthesis rate of $P_D^{T_8}$	9.25×10^2	$(\text{molec}/\text{cell}) \text{day}^{-1}$	est.
λ_{Q_A}	Dissociation rate of the PD-1/pembrolizumab complex	2.6	day^{-1}	[3]
λ_Q	Dissociation rate of the PD-1/PD-L1 complex	1.24×10^5	$(\text{molec}/\text{cell}) \text{day}^{-1}$	[4]
$\lambda_{P_D A_1}$	Formation rate of the PD-1/pembrolizumab complex	4.63×10^{-13}	$(\text{molec}/\text{cm}^3)^{-1} \text{day}^{-1}$	fitted
$\lambda_{P_D P_L}$	Formation rate of the PD-1/PD-L1 complex	2.64×10^{-11}	$(\text{molec}/\text{cm}^3)^{-1} \text{day}^{-1}$	[4]
$\lambda_{P_D^K}$	Synthesis rate of P_D^K	1.85×10^2	$(\text{molec}/\text{cell}) \text{day}^{-1}$	est.
$\lambda_{P_L C}$	Synthesis rate of P_L by C	2.50×10^5	$(\text{molec}/\text{cell}) \text{day}^{-1}$	est.
$\lambda_{P_D^{8\text{LN}}}$	Synthesis rate of $P_D^{8\text{LN}}$	9.27×10^2	$(\text{molec}/\text{cell}) \text{day}^{-1}$	est.
$\lambda_{P_L^{\text{LN}} D^{\text{LN}}}$	Synthesis rate of P_L^{LN} by D^{LN}	2.46×10^4	$(\text{molec}/\text{cell}) \text{day}^{-1}$	est.
$K_{C I_\alpha}$	Half-saturation constant of I_α for C	9.00×10^{-11}	g/cm^3	est.
$K_{D N_c}$	Half-saturation constant of N_c for D	3.69×10^6	cell/cm^3	est.
$K_{T_8 T_{\text{ex}}}$	Half-saturation constant T_8 exhaustion due to C exposure	7.02×10^7	cell/cm^3	est.
$K_{T_{\text{ex}} A_1}$	Half-saturation constant of T_{ex} reinvigoration by A_1	2.05×10^{14}	molec/cm^3	est.
$K_{K T_8}$	Half-saturation constant of T_8 for K	1.77×10^5	cell/cm^3	est.
$K_{K D}$	Half-saturation constant of D for K	1.91×10^6	cell/cm^3	est.
C_0	Carrying capacity of C	8.89×10^7	cell/cm^3	fitted
$K_{C I_\beta}$	Inhibition constant of T_8 and K elimination of C by I_β	1.51×10^{-6}	g/cm^3	est.
$K_{C Q^{T_8}}$	Inhibition constant of T_8 elimination of C by Q^{T_8}	1.31×10^6	molec/cm^3	est.
$K_{C Q^K}$	Inhibition constant of K elimination of C by Q^K	2.87×10^5	molec/cm^3	est.

$K_{D_0 I_\beta}$	Inhibition constant of K elimination of D_0 by I_β	1.51×10^{-6}	g/cm^3	est.
V_{LN}	Volume of the TDLN	1.47×10^{-1}	cm^3	[5] est.
$K_{T_0^8 T_A^r}$	Inhibition constant of T_0^8 activation by T_A^r	1.47×10^6	cell/cm^3	est.
$K_{T_0^8 Q^{\text{SLN}}}$	Inhibition constant of T_0^8 activation by Q^{SLN}	2.83×10^5	$(\text{molec}/\text{cm}^3) \text{ day}$	est.
$K_{T_A^8 T_A^r}$	Inhibition constant of T_A^8 activation by T_A^r	1.47×10^6	cell/cm^3	est.
$K_{T_A^8 Q^{\text{SLN}}}$	Inhibition constant of T_A^8 proliferation by Q^{SLN}	2.83×10^5	$(\text{molec}/\text{cm}^3) \text{ day}$	est.
$K_{T_8 C}$	Inhibition constant of T_8 death by IL-10	7.02×10^7	cell/cm^3	est.
$K_{T_{\text{ex}} C}$	Inhibition constant of T_{ex} death by IL-10	7.02×10^7	cell/cm^3	est.
$K_{K I_\beta}$	Inhibition constant of NK cell activation by I_β	1.51×10^{-6}	g/cm^3	est.
d_{N_c}	Removal rate of N_c	6.88×10^{-2}	day^{-1}	est.
d_{D_0}	Death rate of D_0	3.57×10^{-2}	day^{-1}	[9] est.
d_D	Death rate of D	3.15×10^{-1}	day^{-1}	[10] est.
$d_{T_0^8}$	Death rate of naive CD8+ T cells	3.22×10^{-2}	day^{-1}	[11] est.
d_{T_8}	Death rate of T_8	9×10^{-3}	day^{-1}	[12]
$d_{T_{\text{ex}}}$	Death rate of T_{ex}	9×10^{-3}	day^{-1}	[12]
$d_{T_0^r}$	Death rate of T_0^r	2.2×10^{-3}	day^{-1}	[13]
d_{T_r}	Death rate of T_r	6.30×10^{-2}	day^{-1}	[14] est.
d_K	Death rate of K	6.93×10^{-2}	day^{-1}	[16–18] est.
d_{I_α}	Degradation rate of I_α	5.48×10^1	day^{-1}	[21, 22] est.
d_{I_β}	Degradation rate of I_β	3.99×10^2	day^{-1}	[23] est.
d_{P_D}	Degradation rate of unbound PD-1 receptors	3.36×10^{-1}	day^{-1}	[25]
d_{Q_A}	Internalisation rate of the PD-1/pembrolizumab complex	0.43	day^{-1}	[3]
d_{A_1}	Elimination rate of A_1/A_1^{LN}	2.92×10^{-2}	day^{-1}	[26–28] est.
d_{P_L}	Degradation rate of unbound PD-L1	1.39	day^{-1}	[29]
τ_m	DC migration time from TDLN to the TS	0.75	day	[30] est.
Δ_8^0	Time taken for first CTL division	1.63	day	[32]
n_{max}^8	Maximal number of CTL divisions in the TDLN	10	dimensionless	[33, 34] est.
Δ_8	Time taken for successive CTL divisions	0.36	day	[33]
$\tau_{T_A^8}$	Time taken for CTL division program	4.87	day	est.

Δ_r^0	Time taken for first Treg division	0.77	day	[38] est.
n_{\max}^r	Maximal number of Treg divisions in the TDLN	6	dimensionless	[40] est.
Δ_r	Time taken for successive Treg divisions	0.42	day	[38] est.
$\tau_{T_A}^r$	Time taken for Treg division program	2.87	day	est.

F Full Model Sensitivity Analysis Indices

Table F.1: Maximum first-order indices (S_i) and total-order indices (S_{Ti}) for the RMSRE of variables in the full model at 180.9 days under the standard regimen, along with the indices associated with the RMSRE of V_{TS} — the primary tumour volume.

Param	Max S_i	Max S_{Ti}	S_i for V_{TS}	S_{Ti} for V_{TS}	Param	Max S_i	Max S_{Ti}	S_i for V_{TS}	S_{Ti} for V_{TS}
f_{pembro}	0.196455	0.781830	0.000142	0.030835	f_C	0.154395	0.689673	0.154395	0.468892
f_{N_c}	0.000572	0.286282	0.000572	0.028513	\mathcal{A}_{D_0}	0.098118	0.361952	0.000924	0.032853
$\mathcal{A}_{T_0^8}$	0.098988	0.745633	0.000013	0.026813	$\mathcal{A}_{T_0^4}$	0.113653	0.867688	0.000033	0.029270
$\mathcal{A}_{T_0^6}$	0.053728	0.868902	0.000023	0.033829	\mathcal{A}_{M_0}	0.240664	0.836605	0.000052	0.024638
\mathcal{A}_{K_0}	0.111575	0.841465	0.001600	0.051894	λ_C	0.045830	0.756570	0.044835	0.312093
λ_{CT_8}	0.020103	0.487583	0.001134	0.063549	λ_{CK}	0.013353	0.826863	0.003405	0.084351
λ_{CI_α}	0.039973	0.581582	0.000587	0.036730	λ_{CI_γ}	0.001039	0.527882	0.000025	0.031523
λ_{HN_c}	0.053316	0.696267	0.000025	0.029590	λ_{SN_c}	0.051485	0.557700	0.000011	0.025580
λ_{DH}	0.007218	0.428341	0.000022	0.030887	λ_{DS}	0.000717	0.821022	0.000016	0.030449
λ_{D_0K}	0.010631	0.803754	0.000049	0.028679	$\lambda_{DD^{LN}}$	0.016469	0.440553	0.000095	0.032598
$\lambda_{T_0^8T_A^8}$	0.009913	0.815172	0.000031	0.038289	$\lambda_{T_A^8T_8}$	0.025050	0.683439	0.000005	0.025455
$\lambda_{T_8I_2}$	0.000398	0.693214	0.000009	0.023958	λ_{T_8C}	0.002766	0.715876	0.000102	0.028300
$\lambda_{T_{\text{ex}}A_1}$	0.000595	0.686386	0.000022	0.031097	$\lambda_{T_0^4T_A^1}$	0.008659	0.611239	0.000006	0.030416
$\lambda_{T_A^1T_1}$	0.006964	0.867024	0.000005	0.024661	$\lambda_{T_1I_2}$	0.000277	0.367976	0.000025	0.031124
$\lambda_{T_1T_r}$	0.000419	0.549419	0.000006	0.026430	$\lambda_{T_0^rT_A^r}$	0.011332	0.529358	0.000002	0.025710
$\lambda_{T_A^rT_r}$	0.037037	0.694783	0.000098	0.034798	$\lambda_{M_1I_\alpha}$	0.005957	0.383106	0.000036	0.029591
$\lambda_{M_1I_\gamma}$	0.006690	0.544117	0.000008	0.023943	$\lambda_{M_2I_{10}}$	0.012403	0.528181	0.000009	0.027346
$\lambda_{M_2I_\beta}$	0.015300	0.443515	0.000018	0.025119	λ_{MI_γ}	0.000516	0.626537	0.000015	0.028707
λ_{MI_α}	0.000453	0.425568	0.000008	0.022884	λ_{MI_β}	0.000508	0.654224	0.000008	0.028281
λ_{KI_2}	0.019479	0.379776	0.000115	0.033761	λ_{KD_0}	0.000408	0.587977	0.000036	0.025974
λ_{KD}	0.002305	0.477241	0.000489	0.033624	$\lambda_{I_2T_8}$	0.000498	0.640375	0.000022	0.028599
$\lambda_{I_2T_1}$	0.000511	0.621754	0.000053	0.029137	$\lambda_{I_\gamma T_8}$	0.002761	0.505682	0.000008	0.027038
$\lambda_{I_\gamma T_1}$	0.000435	0.549770	0.000012	0.023860	$\lambda_{I_\gamma K}$	0.006003	0.709358	0.000017	0.031138
$\lambda_{I_\alpha T_8}$	0.000473	0.592204	0.000007	0.029306	$\lambda_{I_\alpha T_1}$	0.000619	0.538387	0.000025	0.024793
$\lambda_{I_\alpha M_1}$	0.000474	0.585327	0.000012	0.026705	$\lambda_{I_\alpha K}$	0.000667	0.560243	0.000044	0.025397
$\lambda_{I_\beta C}$	0.009754	0.519025	0.004696	0.050936	$\lambda_{I_\beta T_r}$	0.001067	0.418672	0.000016	0.023998
$\lambda_{I_\beta M_2}$	0.000497	0.628144	0.000080	0.027637	$\lambda_{I_{10}C}$	0.002527	0.535806	0.000109	0.022529
$\lambda_{I_{10}M_2}$	0.000316	0.438253	0.000009	0.021582	$\lambda_{I_{10}T_r}$	0.000871	0.471220	0.000009	0.024644
$\lambda_{I_{10}I_2}$	0.000289	0.393170	0.000012	0.029589	$\lambda_{P_D^{T_8}}$	0.002471	0.395530	0.000016	0.029102

λ_{QA}	0.025001	0.710132	0.000012	0.027026	λ_Q	0.018023	0.588070	0.000009	0.028938
$\lambda_{PD A_1}$	0.060459	0.572133	0.000013	0.023879	$\lambda_{PD PL}$	0.017739	0.678943	0.000063	0.024731
$\lambda_{PD T_1}$	0.000676	0.520618	0.000013	0.026382	$\lambda_{PD K}$	0.049163	0.563250	0.000030	0.023153
$\lambda_{PL C}$	0.009473	0.380163	0.000027	0.028253	$\lambda_{PL D}$	0.000349	0.476055	0.000010	0.022271
$\lambda_{PL T_8}$	0.000285	0.422810	0.000014	0.024339	$\lambda_{PL T_1}$	0.000479	0.605555	0.000019	0.027530
$\lambda_{PL T_r}$	0.000416	0.558997	0.000018	0.024703	$\lambda_{PL M_2}$	0.000253	0.492355	0.000020	0.027700
$\lambda_{PD^{8LN}}$	0.016826	0.373082	0.000015	0.028454	$\lambda_{PD^{1LN}}$	0.009439	0.350992	0.000013	0.024811
$\lambda_{PL^{LN} D^{LN}}$	0.018080	0.550259	0.000011	0.026725	$\lambda_{PL^{LN} T_A^8}$	0.000469	0.606482	0.000028	0.025046
$\lambda_{PL^{LN} T_A^1}$	0.000423	0.558748	0.000023	0.023104	$\lambda_{PL^{LN} T_A^r}$	0.000224	0.344181	0.000018	0.027921
K_{CI_α}	0.007051	0.571664	0.000069	0.024656	K_{CI_γ}	0.000331	0.502299	0.000007	0.027936
K_{DH}	0.001836	0.536396	0.000028	0.025420	K_{DS}	0.000297	0.435087	0.000024	0.023824
$K_{T_8 I_2}$	0.000450	0.482466	0.000026	0.023693	$K_{T_8 C}$	0.001754	0.352477	0.000073	0.029270
$K_{T_{ex} A_1}$	0.000355	0.489704	0.000055	0.023480	$K_{T_1 I_2}$	0.000275	0.523019	0.000012	0.029960
$K_{T_1 T_r}$	0.000471	0.594317	0.000021	0.027960	$K_{M_1 I_\alpha}$	0.000603	0.335303	0.000007	0.029736
$K_{M_1 I_\gamma}$	0.000815	0.503111	0.000024	0.028087	$K_{M_2 I_{10}}$	0.004164	0.562269	0.000011	0.029065
$K_{M_2 I_\beta}$	0.002805	0.385447	0.000021	0.025002	K_{MI_γ}	0.000314	0.443723	0.000022	0.023068
K_{MI_α}	0.000196	0.334591	0.000016	0.029593	K_{MI_β}	0.000363	0.517795	0.000009	0.029048
K_{KI_2}	0.000389	0.386053	0.000047	0.026070	K_{KD_0}	0.000261	0.397275	0.000006	0.028063
K_{KD}	0.001280	0.532152	0.000094	0.026022	$K_{I_{10} I_2}$	0.000222	0.375698	0.000011	0.028945
C_0	0.216866	0.663083	0.141903	0.449168	K_{CI_β}	0.006226	0.397751	0.004442	0.064300
$K_{CQ T_8}$	0.000393	0.526433	0.000019	0.025382	$K_{CQ K}$	0.000254	0.390986	0.000025	0.028895
$K_{D_0 I_\beta}$	0.002976	0.372823	0.000036	0.026400	V_{LN}	0.032220	0.761538	0.000011	0.035396
$K_{T_0^8 T_A^r}$	0.001215	0.360980	0.000058	0.029030	$K_{T_0^8 Q^{8LN}}$	0.000647	0.353112	0.000020	0.028440
$K_{T_A^8 T_A^r}$	0.000978	0.507490	0.000015	0.032324	$K_{T_A^8 Q^{8LN}}$	0.000543	0.590254	0.000013	0.031324
$K_{T_8 T_r}$	0.000327	0.440936	0.000010	0.026860	$K_{T_8 I_{10}}$	0.000221	0.361707	0.000109	0.027530
$K_{T_{ex} I_{10}}$	0.000386	0.515569	0.000003	0.025007	$K_{T_0^4 T_A^r}$	0.000906	0.416674	0.000013	0.027251
$K_{T_0^4 Q^{1LN}}$	0.000607	0.601432	0.000017	0.027814	$K_{T_A^1 T_A^r}$	0.001141	0.390313	0.000013	0.027740
$K_{T_A^1 Q^{1LN}}$	0.000659	0.663544	0.000003	0.028727	$K_{T_1 T_r}$	0.000358	0.483177	0.000013	0.025290
K_{KI_β}	0.003117	0.367399	0.000659	0.033125	$K_{I_\gamma T_r}$	0.001390	0.547457	0.000007	0.025100
d_{N_c}	0.091396	0.868058	0.000264	0.024513	d_H	0.091265	0.449674	0.000004	0.026243
d_S	0.076757	0.567976	0.000005	0.025488	d_{D_0}	0.000779	0.598566	0.000005	0.023806
d_D	0.147321	0.776825	0.000978	0.045696	$d_{T_0^8}$	0.250308	0.896970	0.000010	0.036000
d_{T_8}	0.001293	0.486334	0.000195	0.025046	$d_{T_{ex}}$	0.000777	0.524852	0.000009	0.029467
$d_{T_0^4}$	0.242511	0.882519	0.000010	0.027031	d_{T_1}	0.000718	0.657060	0.000023	0.022276
$d_{T_0^r}$	0.000798	0.540833	0.000013	0.026578	d_{T_r}	0.003225	0.534336	0.000023	0.025321
d_{M_0}	0.055325	0.586456	0.000029	0.028598	d_{M_1}	0.226859	0.644728	0.000023	0.026919
d_{M_2}	0.125127	0.460048	0.000069	0.030346	d_{K_0}	0.264315	0.882659	0.001545	0.051803
d_K	0.095537	0.514093	0.003873	0.068345	d_{I_2}	0.000631	0.437762	0.000063	0.024649
d_{I_γ}	0.034021	0.601873	0.000043	0.026979	d_{I_α}	0.006243	0.611070	0.000176	0.027942
d_{I_β}	0.019153	0.509755	0.007105	0.079089	$d_{I_{10}}$	0.016709	0.602077	0.000054	0.026421
d_{PD}	0.000559	0.501914	0.000007	0.025763	d_{Q_A}	0.095190	0.522846	0.000045	0.026934
d_{A_1}	0.217898	0.800762	0.000073	0.027830	d_{PL}	0.118656	0.751497	0.000022	0.029878
τ_m	0.000804	0.724374	0.000017	0.027370	τ_8^{act}	0.001235	0.713127	0.000059	0.027581
Δ_8^0	0.000563	0.669466	0.000037	0.026410	n_{max}^8	0.342734	0.873702	0.004335	0.287343
Δ_8	0.000841	0.608572	0.000032	0.024798	τ_a	0.000816	0.774151	0.000017	0.025973
τ_l	0.020278	0.644328	0.000062	0.025358	τ_4^{act}	0.000787	0.756608	0.000016	0.025606
Δ_1^0	0.000723	0.766798	0.000025	0.027289	n_{max}^1	0.245710	0.786345	0.000248	0.028258
Δ_1	0.001106	0.767379	0.000011	0.026659	τ_r^{act}	0.000608	0.689967	0.000025	0.024408
Δ_r^0	0.000549	0.700840	0.000026	0.025698	n_{max}^r	0.455148	0.872521	0.001873	0.123402

Δ_r	0.000208	0.296629	0.000014	0.026179					
------------	----------	----------	----------	----------	--	--	--	--	--

G Reduced Model Sensitivity Analysis Indices

Table G.1: Maximum first-order indices (S_i) and total-order indices (S_{Ti}) for the RMSRE of variables in the reduced model at 180.9 days under the standard regimen, along with the indices associated with the RMSRE of V_{TS} — the primary tumour volume.

Param	Max S_i	Max S_{Ti}	S_i for V_{TS}	S_{Ti} for V_{TS}	Param	Max S_i	Max S_{Ti}	S_i for V_{TS}	S_{Ti} for V_{TS}
f_{pembro}	0.196699	0.782368	0.000018	0.028101	f_C	0.156199	0.865079	0.156199	0.479742
f_{N_c}	0.000394	0.463306	0.000394	0.031755	\mathcal{A}_{D_0}	0.074493	0.511470	0.000396	0.038541
$\mathcal{A}_{T_0^8}$	0.097871	0.834404	0.000070	0.031580	$\mathcal{A}_{T_0^4}$	0.110457	0.750074	0.000039	0.029241
$\mathcal{A}_{T_0^r}$	0.054063	0.609495	0.000258	0.038541	\mathcal{A}_{M_0}	0.255852	0.847846	0.000108	0.029145
\mathcal{A}_{K_0}	0.112343	0.726756	0.001923	0.049679	λ_C	0.043134	0.457370	0.042920	0.300684
λ_{CT_8}	0.016052	0.625139	0.001379	0.066753	λ_{CK}	0.010201	0.578997	0.003086	0.077898
λ_{CI_α}	0.044683	0.645409	0.000704	0.037197	λ_{HN_c}	0.042463	0.594310	0.000017	0.029839
λ_{SN_c}	0.054364	0.730376	0.000006	0.026103	λ_{DH}	0.009758	0.492553	0.000063	0.030330
λ_{D_0K}	0.018260	0.789082	0.000037	0.029910	$\lambda_{DD^{LN}}$	0.013301	0.533852	0.000061	0.030025
$\lambda_{T_0^8T_A^8}$	0.009162	0.567546	0.000013	0.037923	$\lambda_{T_A^8T_8}$	0.020333	0.626416	0.000035	0.029267
λ_{T_8C}	0.010465	0.533543	0.000185	0.031121	$\lambda_{T_{ex}A_1}$	0.000618	0.727339	0.000080	0.032953
$\lambda_{T_0^4T_A^1}$	0.006429	0.843575	0.000081	0.032684	$\lambda_{T_A^1T_1}$	0.010808	0.860397	0.000009	0.028221
$\lambda_{T_1T_r}$	0.000201	0.413099	0.000005	0.028087	$\lambda_{T_0^rT_A^r}$	0.010996	0.438753	0.000015	0.030774
$\lambda_{T_A^rT_r}$	0.046559	0.543385	0.000053	0.033947	$\lambda_{M_1I_\alpha}$	0.007544	0.505262	0.000016	0.028446
$\lambda_{M_1I_\gamma}$	0.005616	0.673982	0.000016	0.027777	$\lambda_{M_2I_{10}}$	0.012041	0.564238	0.000017	0.027264
$\lambda_{M_2I_\beta}$	0.015363	0.711958	0.000008	0.027330	λ_{KI_2}	0.012993	0.434006	0.000167	0.035123
λ_{KD}	0.004344	0.530308	0.000986	0.037752	$\lambda_{I_2T_8}$	0.000346	0.437036	0.000021	0.030972
$\lambda_{I_2T_1}$	0.000505	0.470982	0.000015	0.031061	$\lambda_{I_\gamma K}$	0.047020	0.469126	0.000022	0.030584
$\lambda_{I_\alpha T_8}$	0.000358	0.483409	0.000015	0.032958	$\lambda_{I_\alpha T_1}$	0.000577	0.609750	0.000019	0.026065
$\lambda_{I_\alpha M_1}$	0.000272	0.448167	0.000013	0.027329	$\lambda_{I_\alpha K}$	0.000744	0.587610	0.000011	0.026171
$\lambda_{I_\beta C}$	0.009140	0.476749	0.005372	0.065933	$\lambda_{I_\beta T_r}$	0.001208	0.582373	0.000009	0.027140
$\lambda_{I_\beta M_2}$	0.000482	0.470403	0.000111	0.034241	$\lambda_{I_{10}C}$	0.070524	0.653060	0.000028	0.025077
$\lambda_{I_{10}M_2}$	0.000420	0.469329	0.000010	0.033561	$\lambda_{P_D^{T_8}}$	0.001438	0.364811	0.000026	0.027597
λ_{Q_A}	0.033563	0.533773	0.000037	0.033103	λ_Q	0.023865	0.550601	0.000021	0.030076
$\lambda_{P_D A_1}$	0.065135	0.449660	0.000093	0.032422	$\lambda_{P_D P_L}$	0.029281	0.714233	0.000068	0.034821
$\lambda_{P_D^{T_1}}$	0.000702	0.443972	0.000009	0.031971	$\lambda_{P_D^K}$	0.048038	0.365372	0.000022	0.031603
$\lambda_{P_L C}$	0.072411	0.394143	0.000033	0.027409	$\lambda_{P_L M_2}$	0.000299	0.462689	0.000007	0.032642
$\lambda_{P_D^{LN}}$	0.020138	0.416773	0.000019	0.034631	$\lambda_{P_D^{LN}}$	0.008002	0.558867	0.000007	0.031067
$\lambda_{P_L^{LN} D^{LN}}$	0.018164	0.654417	0.000011	0.030028	$\lambda_{P_L^{LN} T_A^1}$	0.000198	0.380404	0.000012	0.027096
K_{CI_α}	0.008810	0.384462	0.000181	0.027225	K_{DH}	0.002113	0.528954	0.000023	0.030381
K_{T_8C}	0.004342	0.616622	0.000008	0.027834	$K_{T_{ex}A_1}$	0.000512	0.617239	0.000034	0.027696
$K_{T_1T_r}$	0.000550	0.627109	0.000013	0.031656	$K_{M_1I_\alpha}$	0.000714	0.599344	0.000014	0.028523
$K_{M_1I_\gamma}$	0.000974	0.406854	0.000019	0.029125	$K_{M_2I_{10}}$	0.002916	0.492126	0.000013	0.032249
$K_{M_2I_\beta}$	0.002589	0.380563	0.000012	0.030998	K_{KI_2}	0.000460	0.568078	0.000047	0.032673
K_{KD}	0.002210	0.535704	0.000190	0.035304	C_0	0.216418	0.659926	0.134699	0.438727
K_{CI_β}	0.006842	0.413199	0.005062	0.071254	$K_{CQ^{T_8}}$	0.000264	0.402001	0.000011	0.031511

K_{CQ^K}	0.000451	0.559173	0.000002	0.031582	$K_{D_0 I_\beta}$	0.002991	0.542746	0.000048	0.028396
V_{LN}	0.031432	0.491612	0.000034	0.037856	$K_{T_0^s T_A^r}$	0.001054	0.419920	0.000010	0.031579
$K_{T_0^s Q^{sLN}}$	0.000495	0.666322	0.000009	0.028865	$K_{T_A^s T_A^r}$	0.001104	0.440874	0.000017	0.025948
$K_{T_A^s Q^{sLN}}$	0.000647	0.756078	0.000006	0.027987	$K_{T_8 I_{10}}$	0.000205	0.352087	0.000074	0.030958
$K_{T_{ex} I_{10}}$	0.000451	0.624676	0.000007	0.029233	$K_{T_0^4 T_A^r}$	0.000717	0.534408	0.000034	0.032599
$K_{T_0^4 Q^{1LN}}$	0.000567	0.609289	0.000008	0.029015	$K_{T_A^1 T_A^r}$	0.000968	0.464576	0.000026	0.028965
$K_{T_A^1 Q^{1LN}}$	0.000707	0.557800	0.000018	0.031212	K_{KI_β}	0.002623	0.436641	0.000541	0.036278
d_{N_c}	0.072744	0.872253	0.000139	0.033711	d_H	0.074184	0.512795	0.000003	0.029891
d_S	0.074398	0.598835	0.000018	0.031017	d_{D_0}	0.000585	0.572300	0.000026	0.030700
d_D	0.106839	0.443295	0.001198	0.061665	$d_{T_0^s}$	0.252751	0.900001	0.000015	0.034062
d_{T_8}	0.000577	0.355399	0.000213	0.032954	$d_{T_{ex}}$	0.021297	0.399114	0.000014	0.033962
$d_{T_0^4}$	0.240662	0.881627	0.000017	0.033046	d_{T_1}	0.000397	0.363997	0.000011	0.032331
$d_{T_0^r}$	0.000822	0.479558	0.000019	0.034144	d_{T_r}	0.000768	0.461821	0.000009	0.029399
d_{M_0}	0.074767	0.547764	0.000007	0.032210	d_{M_1}	0.220101	0.671529	0.000009	0.033616
d_{M_2}	0.142668	0.514810	0.000058	0.029554	d_{K_0}	0.268048	0.882146	0.001720	0.043581
d_K	0.083896	0.508186	0.002192	0.066429	d_{I_2}	0.000554	0.393571	0.000077	0.033173
d_{I_γ}	0.100467	0.455116	0.000013	0.023677	d_{I_α}	0.010932	0.465299	0.000106	0.024842
d_{I_β}	0.020297	0.454115	0.007799	0.083064	$d_{I_{10}}$	0.129228	0.422049	0.000133	0.030982
d_{P_D}	0.000295	0.369661	0.000011	0.032970	d_{Q_A}	0.080240	0.386906	0.000012	0.032232
d_{A_1}	0.217378	0.800610	0.000037	0.027867	d_{P_L}	0.142276	0.535291	0.000053	0.035635
τ_m	0.000950	0.406262	0.000021	0.023889	Δ_0^8	0.000140	0.324964	0.000017	0.030383
n_{\max}^8	0.341779	0.865224	0.005149	0.312416	Δ_8	0.000211	0.324558	0.000015	0.038173
Δ_1^0	0.000129	0.432236	0.000018	0.038985	n_{\max}^1	0.259140	0.761432	0.000279	0.039751
Δ_1	0.000230	0.332084	0.000006	0.026368	Δ_r^0	0.000199	0.478516	0.000021	0.037171
n_{\max}^r	0.537028	0.885371	0.002362	0.140304	Δ_r	0.000116	0.274462	0.000030	0.023804

H Minimal Model Sensitivity Analysis Indices

Table H.1: Maximum first-order indices (S_i) and total-order indices (S_{Ti}) for the RMSRE of variables in the minimal model at 180.9 days under the standard regimen, along with the indices associated with the RMSRE of V_{TS} — the primary tumour volume.

Param	Max S_i	Max S_{Ti}	S_i for V_{TS}	S_{Ti} for V_{TS}	Param	Max S_i	Max S_{Ti}	S_i for V_{TS}	S_{Ti} for V_{TS}
f_{pembro}	0.196714	0.781397	0.000053	0.029181	f_C	0.155495	0.477257	0.155495	0.466771
f_{N_c}	0.000802	0.230561	0.000513	0.034046	\mathcal{A}_{D_0}	0.080313	0.353478	0.000795	0.044875
$\mathcal{A}_{T_0^r}$	0.052635	0.405867	0.000072	0.029519	λ_C	0.045353	0.358603	0.045353	0.290649
λ_{CT_8}	0.018126	0.266294	0.001267	0.069703	λ_{CK}	0.008360	0.289387	0.003218	0.064299
λ_{CI_α}	0.036782	0.334747	0.000788	0.038577	λ_{DN_c}	0.008558	0.295177	0.000127	0.031737
$\lambda_{D_0 K}$	0.019602	0.288701	0.000070	0.029169	$\lambda_{DD^{LN}}$	0.011157	0.381432	0.000080	0.029407
$\lambda_{T_0^s T_A^s}$	0.008600	0.505163	0.000020	0.038178	$\lambda_{T_A^s T_8}$	0.024229	0.369096	0.000002	0.026556
$\lambda_{T_8 C}$	0.003473	0.328211	0.000182	0.027518	$\lambda_{T_{ex} A_1}$	0.001145	0.332576	0.000028	0.025827
$\lambda_{T_0^r T_A^r}$	0.010304	0.310825	0.000057	0.028596	$\lambda_{T_A^r T_r}$	0.046368	0.355147	0.000009	0.037796
λ_{KT_8}	0.011316	0.343820	0.000199	0.029113	λ_{KD}	0.007381	0.462180	0.001108	0.037246
$\lambda_{I_\alpha T_8}$	0.002358	0.364446	0.000016	0.025512	$\lambda_{I_\alpha K}$	0.002799	0.285920	0.000096	0.029224
$\lambda_{I_\beta C}$	0.013157	0.240479	0.005137	0.063172	$\lambda_{I_\beta T_r}$	0.001449	0.405260	0.000025	0.029763

$\lambda_{P_D^{T_8}}$	0.014701	0.299428	0.000022	0.027847	λ_{Q_A}	0.029650	0.285242	0.000027	0.028960
λ_Q	0.027488	0.400916	0.000044	0.029495	$\lambda_{P_{DA_1}}$	0.062137	0.348826	0.000006	0.026113
$\lambda_{P_D P_L}$	0.015567	0.326772	0.000048	0.029725	$\lambda_{P_D^K}$	0.046745	0.407042	0.000006	0.026605
$\lambda_{P_L C}$	0.078813	0.366148	0.000029	0.025288	$\lambda_{P^{SLN}_D}$	0.019039	0.374169	0.000014	0.025930
$\lambda_{P^{LN}_D^{LN}}$	0.015530	0.356287	0.000005	0.026136	K_{CI_α}	0.009615	0.319686	0.000210	0.034703
K_{DN_c}	0.002715	0.307489	0.000077	0.030232	$K_{T_8 T_{ex}}$	0.002102	0.311059	0.000034	0.033769
$K_{T_{ex} A_1}$	0.000490	0.240533	0.000021	0.029109	K_{KT_8}	0.001318	0.338152	0.000106	0.027441
K_{KD}	0.002650	0.327721	0.000186	0.030883	C_0	0.239215	0.669053	0.146308	0.447836
K_{CI_β}	0.005655	0.319877	0.003165	0.050119	$K_{CQ^{T_8}}$	0.001067	0.345712	0.000031	0.028128
K_{CQ^K}	0.000720	0.306517	0.000032	0.031147	$K_{D_0 I_\beta}$	0.003973	0.314481	0.000058	0.028029
V_{LN}	0.035060	0.458468	0.000025	0.033560	$K_{T_0^s T_A^r}$	0.002032	0.501240	0.000033	0.030690
$K_{T_0^s Q^{SLN}}$	0.000644	0.317083	0.000027	0.032202	$K_{T_A^s T_A^r}$	0.001591	0.409334	0.000050	0.029279
$K_{T_A^s Q^{SLN}}$	0.000545	0.285883	0.000021	0.031257	$K_{T_8 C}$	0.000763	0.307931	0.000143	0.030565
$K_{T_{ex} C}$	0.000644	0.263686	0.000021	0.027768	K_{KI_β}	0.004027	0.289919	0.000639	0.033093
d_{N_c}	0.074221	0.789225	0.000226	0.031497	d_{D_0}	0.000524	0.315449	0.000007	0.027834
d_D	0.108263	0.423138	0.000884	0.054999	$d_{T_0^s}$	0.000541	0.522774	0.000008	0.026585
d_{T_8}	0.000626	0.447007	0.000372	0.031383	$d_{T_{ex}}$	0.034663	0.369677	0.000012	0.029355
$d_{T_0^r}$	0.000937	0.458592	0.000049	0.026591	d_{T_r}	0.001711	0.384029	0.000011	0.030659
d_K	0.109494	0.721891	0.002838	0.055667	d_{I_α}	0.009238	0.431077	0.000228	0.027491
d_{I_β}	0.023981	0.468133	0.007949	0.078904	d_{P_D}	0.000298	0.508645	0.000006	0.026462
d_{Q_A}	0.107907	0.522369	0.000024	0.028929	d_{A_1}	0.218158	0.801259	0.000054	0.027654
d_{P_L}	0.125013	0.425971	0.000047	0.031199	τ_m	0.000586	0.379641	0.000021	0.030613
Δ_8^0	0.000207	0.340482	0.000006	0.028781	n_{\max}^8	0.366052	0.842425	0.008491	0.361357
Δ_8	0.000365	0.391673	0.000030	0.032536	Δ_r^0	0.000203	0.319411	0.000036	0.031947
n_{\max}^r	0.561872	0.894193	0.002088	0.132968	Δ_r	0.000199	0.279566	0.000006	0.028821

References

- [1] Hawi G, Kim PS, Lee PP. Optimisation of pembrolizumab therapy for de novo metastatic MSI-H/dMMR colorectal cancer using data-driven delay integro-differential equations. bioRxiv. 2025. Available from: <https://www.biorxiv.org/content/early/2025/05/24/2025.05.23.655752>.
- [2] Lo WC, Arsenescu V, Arsenescu RI, Friedman A. Inflammatory Bowel Disease: How Effective Is TNF- α Suppression? PLOS ONE. 2016 Nov;11(11):e0165782. Available from: <https://doi.org/10.1371/journal.pone.0165782>.
- [3] Li TR, Chatterjee M, Lala M, Abraham AK, Freshwater T, Jain L, et al. Pivotal Dose of Pembrolizumab: A Dose-Finding Strategy for Immuno-Oncology. Clinical Pharmacology & Therapeutics. 2021 Mar;110(1):200–209. Available from: <https://doi.org/10.1002/cpt.2170>.
- [4] Cheng X, Veverka V, Radhakrishnan A, Waters LC, Muskett FW, Morgan SH, et al. Structure and Interactions of the Human Programmed Cell Death 1 Receptor. Journal of Biological Chemistry. 2013 Apr;288(17):11771–11785. Available from: <https://doi.org/10.1074/jbc.M112.448126>.
- [5] Rössler O, Betge J, Harbaum L, Mrak K, Tschmelitsch J, Langner C. Tumor size, tumor location, and antitumor inflammatory response are associated with lymph node size in colorectal cancer

- patients. *Modern Pathology*. 2017 Jun;30(6):897–904. Available from: <https://doi.org/10.1038/modpathol.2016.227>.
- [6] Zandarashvili L, Sahu D, Lee K, Lee YS, Singh P, Rajarathnam K, et al. Real-time Kinetics of High-mobility Group Box 1 (HMGB1) Oxidation in Extracellular Fluids Studied by in Situ Protein NMR Spectroscopy. *Journal of Biological Chemistry*. 2013 Apr;288(17):11621–11627. Available from: <https://doi.org/10.1074/jbc.M113.449942>.
 - [7] Goicoechea SM, Murphy-Ullrich JE. In: *Cell Surface Calreticulin: Role in Signaling Thrombospondin Anti-Adhesive Activity*. Springer US; 2003. p. 193–204. Available from: https://doi.org/10.1007/978-1-4419-9258-1_18.
 - [8] Zhang Y, Thangam R, You SH, Sultonova RD, Venu A, Min JJ, et al. Engineering Calreticulin-Targeting Monobodies to Detect Immunogenic Cell Death in Cancer Chemotherapy. *Cancers*. 2021 Jun;13(11):2801. Available from: <https://doi.org/10.3390/cancers13112801>.
 - [9] Ruedl C, Koebel P, Bachmann M, Hess M, Karjalainen K. Anatomical Origin of Dendritic Cells Determines Their Life Span in Peripheral Lymph Nodes. *The Journal of Immunology*. 2000 Nov;165(9):4910–4916. Available from: <https://doi.org/10.4049/jimmunol.165.9.4910>.
 - [10] Kamath AT, Henri S, Battye F, Tough DF, Shortman K. Developmental kinetics and lifespan of dendritic cells in mouse lymphoid organs. *Blood*. 2002 Sep;100(5):1734–1741. Available from: https://doi.org/10.1182/blood.V100.5.1734.h81702001734_1734_1741.
 - [11] Takada K, Jameson SC. Self-class I MHC molecules support survival of naive CD8 T cells, but depress their functional sensitivity through regulation of CD8 expression levels. *Journal of Experimental Medicine*. 2009 Sep;206(10):2253–2269. Available from: <https://doi.org/10.1084/jem.20082553>.
 - [12] Hellerstein M, Hanley MB, Cesar D, Siler S, Papageorgopoulos C, Wieder E, et al. Directly measured kinetics of circulating T lymphocytes in normal and HIV-1-infected humans. *Nature Medicine*. 1999 Jan;5(1):83–89. Available from: <https://doi.org/10.1038/4772>.
 - [13] Kumbhari A, Egelston CA, Lee PP, Kim PS. Mature Dendritic Cells May Promote High-Avidity Tuning of Vaccine T Cell Responses. *Frontiers in Immunology*. 2020 Oct;11. Available from: <https://doi.org/10.3389/fimmu.2020.584680>.
 - [14] Vukmanovic-Stejić M, Zhang Y, Cook JE, Fletcher JM, McQuaid A, Masters JE, et al. Human CD4⁺ CD25^{hi} Foxp3⁺ regulatory T cells are derived by rapid turnover of memory populations in vivo. *Journal of Clinical Investigation*. 2006 Sep;116(9):2423–2433. Available from: <https://doi.org/10.1172/JCI28941>.
 - [15] Patel AA, Zhang Y, Fullerton JN, Boelen L, Rongvaux A, Maini AA, et al. The fate and lifespan of human monocyte subsets in steady state and systemic inflammation. *Journal of Experimental Medicine*. 2017 Jun;214(7):1913–1923. Available from: <https://doi.org/10.1084/jem.20170355>.
 - [16] Wu SY, Fu T, Jiang YZ, Shao ZM. Natural killer cells in cancer biology and therapy. *Molecular Cancer*. 2020 Aug;19(1). Available from: <https://doi.org/10.1186/s12943-020-01238-x>.
 - [17] Vivier E, Tomasello E, Baratin M, Walzer T, Ugolini S. Functions of natural killer cells. *Nature Immunology*. 2008 Apr;9(5):503–510. Available from: <https://doi.org/10.1038/ni1582>.

- [18] Lowry LE, Zehring WA. Potentiation of Natural Killer Cells for Cancer Immunotherapy: A Review of Literature. *Frontiers in Immunology*. 2017 Sep;8. Available from: <https://doi.org/10.3389/fimmu.2017.01061>.
- [19] Lotze MT, Matory YL, Ettinghausen SE, Rayner AA, Sharrow SO, Seipp CA, et al. In vivo administration of purified human interleukin 2. II. Half life, immunologic effects, and expansion of peripheral lymphoid cells in vivo with recombinant IL 2. *The Journal of Immunology*. 1985 Oct;135(4):2865–2875. Available from: <https://doi.org/10.4049/jimmunol.135.4.2865>.
- [20] Balachandran S, Adams GP. Interferon- γ -Induced Necrosis: An Antitumor Biotherapeutic Perspective. *Journal of Interferon & Cytokine Research*. 2013 Apr;33(4):171–180. Available from: <https://doi.org/10.1089/jir.2012.0087>.
- [21] Ma Y, Zhao S, Shen S, Fang S, Ye Z, Shi Z, et al. A novel recombinant slow-release TNF α -derived peptide effectively inhibits tumor growth and angiogenesis. *Scientific Reports*. 2015 Sep;5(1). Available from: <https://doi.org/10.1038/srep13595>.
- [22] Oliver J, Bland L, Oettinger C, Arduino M, McAllister S, Aguero S, et al. Cytokine kinetics in an in vitro whole blood model following an endotoxin challenge. *Lymphokine and cytokine research*. 1993 April;12(2):115—120. Available from: <https://pubmed.ncbi.nlm.nih.gov/8324076/>.
- [23] Tirado-Rodriguez B, Ortega E, Segura-Medina P, Huerta-Yepez S. TGF- β : An Important Mediator of Allergic Disease and a Molecule with Dual Activity in Cancer Development. *Journal of Immunology Research*. 2014;2014:1–15. Available from: <https://doi.org/10.1155/2014/318481>.
- [24] Huhn RD, Radwanski E, Gallo J, Affrime MB, Sabo R, Gonyo G, et al. Pharmacodynamics of subcutaneous recombinant human interleukin-10 in healthy volunteers. *Clinical Pharmacology & Therapeutics*. 1997 Aug;62(2):171–180. Available from: [https://doi.org/10.1016/S0009-9236\(97\)90065-5](https://doi.org/10.1016/S0009-9236(97)90065-5).
- [25] Lassman ME, Chappell DL, McAvoy T, Cheng A, de Alwis DP, Pruitt SK, et al. Experimental Medicine Study to Measure Immune Checkpoint Receptors PD-1 and GITR Turnover Rates In Vivo in Humans. *Clinical Pharmacology & Therapeutics*. 2021 Feb;109(6):1575–1582. Available from: <https://doi.org/10.1002/cpt.2129>.
- [26] Li H, Yu J, Liu C, Liu J, Subramaniam S, Zhao H, et al. Time dependent pharmacokinetics of pembrolizumab in patients with solid tumor and its correlation with best overall response. *Journal of Pharmacokinetics and Pharmacodynamics*. 2017 Jun;44(5):403–414. Available from: <https://doi.org/10.1007/s10928-017-9528-y>.
- [27] Li H, Sun Y, Yu J, Liu C, Liu J, Wang Y. Semimechanistically Based Modeling of Pembrolizumab Time-Varying Clearance Using 4 Longitudinal Covariates in Patients With Non-Small Cell Lung Cancer. *Journal of Pharmaceutical Sciences*. 2019 Jan;108(1):692–700. Available from: <https://doi.org/10.1016/j.xphs.2018.10.064>.
- [28] Ahamadi M, Freshwater T, Prohn M, Li C, de Alwis D, de Greef R, et al. Model-Based Characterization of the Pharmacokinetics of Pembrolizumab: A Humanized Anti-PD-1 Monoclonal Antibody in Advanced Solid Tumors. *CPT: Pharmacometrics & Systems Pharmacology*. 2016 Nov;6(1):49–57. Available from: <https://doi.org/10.1002/psp4.12139>.

- [29] Cha JH, Chan LC, Li CW, Hsu JL, Hung MC. Mechanisms Controlling PD-L1 Expression in Cancer. *Molecular Cell*. 2019 Nov;76(3):359–370. Available from: <https://doi.org/10.1016/j.molcel.2019.09.030>.
- [30] Catron DM, Itano AA, Pape KA, Mueller DL, Jenkins MK. Visualizing the First 50 Hr of the Primary Immune Response to a Soluble Antigen. *Immunity*. 2004 Sep;21(3):341–347. Available from: <https://doi.org/10.1016/j.immuni.2004.08.007>.
- [31] Kinjyo I, Qin J, Tan SY, Wellard CJ, Mrass P, Ritchie W, et al. Real-time tracking of cell cycle progression during CD8+ effector and memory T-cell differentiation. *Nature Communications*. 2015 Feb;6(1). Available from: <https://doi.org/10.1038/ncomms7301>.
- [32] Plambeck M, Kazeroonian A, Loeffler D, Kretschmer L, Salinno C, Schroeder T, et al. Heritable changes in division speed accompany the diversification of single T cell fate. *Proceedings of the National Academy of Sciences*. 2022 Feb;119(9). Available from: <https://doi.org/10.1073/pnas.2116260119>.
- [33] Kaech SM, Ahmed R. Memory CD8+ T cell differentiation: initial antigen encounter triggers a developmental program in naïve cells. *Nature Immunology*. 2001 May;2(5):415–422. Available from: <https://doi.org/10.1038/87720>.
- [34] Masopust D, Murali-Krishna K, Ahmed R. Quantitating the Magnitude of the Lymphocytic Choriomeningitis Virus-Specific CD8 T-Cell Response: It Is Even Bigger than We Thought. *Journal of Virology*. 2007 Feb;81(4):2002–2011. Available from: <https://doi.org/10.1128/jvi.01459-06>.
- [35] Blank CU, Haining WN, Held W, Hogan PG, Kallies A, Lugli E, et al. Defining ‘T cell exhaustion’. *Nature Reviews Immunology*. 2019 Sep;19(11):665–674. Available from: <https://doi.org/10.1038/s41577-019-0221-9>.
- [36] McLane LM, Abdel-Hakeem MS, Wherry EJ. CD8 T Cell Exhaustion During Chronic Viral Infection and Cancer. *Annual Review of Immunology*. 2019 Apr;37(1):457–495. Available from: <https://doi.org/10.1146/annurev-immunol-041015-055318>.
- [37] Jelley-Gibbs DM, Lepak NM, Yen M, Swain SL. Two Distinct Stages in the Transition from Naïve CD4 T Cells to Effectors, Early Antigen-Dependent and Late Cytokine-Driven Expansion and Differentiation. *The Journal of Immunology*. 2000 Nov;165(9):5017–5026. Available from: <https://doi.org/10.4049/jimmunol.165.9.5017>.
- [38] Kaech SM, Wherry EJ, Ahmed R. Effector and memory T-cell differentiation: implications for vaccine development. *Nature Reviews Immunology*. 2002 Apr;2(4):251–262. Available from: <https://doi.org/10.1038/nri778>.
- [39] Homann D, Teyton L, Oldstone MBA. Differential regulation of antiviral T-cell immunity results in stable CD8+ but declining CD4+ T-cell memory. *Nature Medicine*. 2001 Aug;7(8):913–919. Available from: <https://doi.org/10.1038/90950>.
- [40] Darrasse-Jèze G, Bergot AS, Durgeau A, Billiard F, Salomon BL, Cohen JL, et al. Tumor emergence is sensed by self-specific CD44hi memory Tregs that create a dominant tolerogenic environment for tumors in mice. *Journal of Clinical Investigation*. 2009 Aug. Available from: <https://doi.org/10.1172/JCI36628>.

- [41] Hawi G, Kim PS, Lee PP. Optimisation of neoadjuvant pembrolizumab therapy for locally advanced MSI-H/dMMR colorectal cancer using data-driven delay integro-differential equations; 2025. arXiv:2411.12123 [q-bio.CB]. Available from: <https://doi.org/10.48550/arXiv.2411.12123>.
- [42] Gastl GA, Abrams JS, Nanus DM, Oosterkamp R, Silver J, Liu F, et al. Interleukin-10 production by human carcinoma cell lines and its relationship to interleukin-6 expression. *International Journal of Cancer*. 1993 Aug;55(1):96–101. Available from: <https://doi.org/10.1002/ijc.2910550118>.
- [43] Piccioli D, Sbrana S, Melandri E, Valiante NM. Contact-dependent Stimulation and Inhibition of Dendritic Cells by Natural Killer Cells. *The Journal of Experimental Medicine*. 2002 Feb;195(3):335–341. Available from: <https://doi.org/10.1084/jem.20010934>.
- [44] Verdijk P, Aarntzen EHJG, Lesterhuis WJ, Boullart ACI, Kok E, van Rossum MM, et al. Limited Amounts of Dendritic Cells Migrate into the T-Cell Area of Lymph Nodes but Have High Immune Activating Potential in Melanoma Patients. *Clinical Cancer Research*. 2009 Apr;15(7):2531–2540. Available from: <https://doi.org/10.1158/1078-0432.CCR-08-2729>.
- [45] Cui A, Huang T, Li S, Ma A, Pérez JL, Sander C, et al. Dictionary of immune responses to cytokines at single-cell resolution. *Nature*. 2023 Dec;625(7994):377–384. Available from: <https://doi.org/10.1038/s41586-023-06816-9>.
- [46] Tan SN, Hao J, Ge J, Yang Y, Liu L, Huang J, et al. Regulatory T cells converted from Th1 cells in tumors suppress cancer immunity via CD39. *Journal of Experimental Medicine*. 2025 Feb;222(4). Available from: <https://doi.org/10.1084/jem.20240445>.
- [47] Pluim D, Ros W, Miedema IHC, Beijnen JH, Schellens JHM. Multiparameter Flow Cytometry Assay for Quantification of Immune Cell Subsets, PD-1 Expression Levels and PD-1 Receptor Occupancy by Nivolumab and Pembrolizumab. *Cytometry Part A*. 2019 Aug;95(10):1053–1065. Available from: <https://doi.org/10.1002/cyto.a.23873>.
- [48] Liu Y, Cheng Y, Xu Y, Wang Z, Du X, Li C, et al. Increased expression of programmed cell death protein 1 on NK cells inhibits NK-cell-mediated anti-tumor function and indicates poor prognosis in digestive cancers. *Oncogene*. 2017 Jul;36(44):6143–6153. Available from: <https://doi.org/10.1038/onc.2017.209>.
- [49] Anbari S, Wang H, Zhang Y, Wang J, Pilvankar M, Nickaeen M, et al. Using quantitative systems pharmacology modeling to optimize combination therapy of anti-PD-L1 checkpoint inhibitor and T cell engager. *Frontiers in Pharmacology*. 2023 Jun;14. Available from: <https://doi.org/10.3389/fphar.2023.1163432>.
- [50] Saito Y, Fujiwara Y, Shinchu Y, Mito R, Miura Y, Yamaguchi T, et al. Classification of PD-L1 expression in various cancers and macrophages based on immunohistocytological analysis. *Cancer Science*. 2022 Jun;113(9):3255–3266. Available from: <https://doi.org/10.1111/cas.15442>.
- [51] Saito A, Tojo M, Kumagai Y, Ohzawa H, Yamaguchi H, Miyato H, et al. Flow cytometry detection of cell type-specific expression of programmed death receptor ligand-1 (PD-L1) in colorectal cancer specimens. *Heliyon*. 2021 Jan;7(1):e05880. Available from: <https://doi.org/10.1016/j.heliyon.2020.e05880>.

- [52] Moreira TG, Mangani D, Cox LM, Leibowitz J, Lobo ELC, Oliveira MA, et al. PD-L1+ and XCR1+ dendritic cells are region-specific regulators of gut homeostasis. *Nature Communications*. 2021 Aug;12(1). Available from: <https://doi.org/10.1038/s41467-021-25115-3>.
- [53] Zhang Y, Lv N, Li M, Liu M, Wu C. Cancer-associated fibroblasts: tumor defenders in radiation therapy. *Cell Death & Disease*. 2023 Aug;14(8). Available from: <https://doi.org/10.1038/s41419-023-06060-z>.